3D SEISMIC INTERPRETATION OF THE KB FIELD, OFFSHORE, NIGER DELTA BASIN, SOUTHERN NIGERIA.

BY

KEKU, OLORUNTOBA UCHECHUKWU

18010401004

A RESEARCH PROJECT

SUBMITTED TO

THE DEPARTMENT OF GEOSCIENCES, COLLEGE OF BASIC AND APPLIED SCIENCES, MOUNTAIN TOP UNIVERSITY, PRAYER CITY, IBAFO, OGUN STATE IN PARTIAL FULFILMENT OF THE REQUIREMENTS FOR THE AWARD OF A BACHELOR OF SCIENCE (B.Sc.) DEGREE IN APPLIED GEOPHYSICS.

AUGUST 2022

CERTIFICATION

This is to certify that this research project titled **"3D SEISMIC INTERPRETATION OF THE KB FIELD, OFFSHORE, NIGER DELTA, NIGERIA".** was carried out by KEKU, Oloruntoba Uchechukwu, with matriculation number 18010401004, This project meets the requirements governing the award of Bachelor of Science (B.Sc.) Degree in Applied Geophysics, Geosciences Department of the Mountain Top University, Ogun state, Nigeria and is approved for its contribution to knowledge and literary presentation.

_____ _____

Dr A.E Jonathan Date

Supervisor

_____ _____

Dr. O. B. Balogun Date

Head of Department

DECLARATION

I hereby declare that this project report written under the supervision of Dr. A.E Jonathan, is a product of my own research work. Information derived from various sources have been duly acknowledged in the text and a list of references provided. This research project report has not been previously presented anywhere for the award of any degree or certificate.

_____ _____

KEKU, Oloruntoba U. Date

DEDICATION

I dedicate this project work to God for His gift of life, His never-ending kindness and mercy, His protection, favor and grace all through my journey at Mountain Top University, and for the successful completion of this work. I also dedicate this project work to my Dear parents – Dr Babatunde and Mrs Ebere Keku. I also dedicate this project work to my brothers – Tosin and Timilehin.

ACKNOWLEDGEMENT

My gratitude goes to God Almighty for the gift of Life and Protection and for seeing me through my sojourn in Mountain Top University; it is only by His mercy and grace I have come this far. I also wish to express my sincere gratitude to my dear parents Dr Babatunde and Mrs Ebere Keku for their all-round support throughout this program.

I sincerely appreciate the Vice Chancellor of this great Institution for his unending support from my first year to the completion of this final year project. My profound appreciation goes to my supervisor, Dr A.E Jonathan for his guidance, lecture and advice despite his very busy schedule. Thanks to the Head of Department for his support and advice throughout the time of this research work.

I sincerely appreciate Dr Abiodun Adesanya for granting me the opportunity to have a firsthand experience on seismic data interpretation and giving me the foreknowledge needed for carrying out this research work.

I would like to appreciate my dear brothers – Tosin and Timilehin, for their unending financial, mental and moral support throughout this study.

I also would like to appreciate my colleague - Adeboye Oluwatofunmi - for assisting me during the course of this study.

My gratitude also goes to a few other Persons who also supported me morally, financially and psychologically –Foluwakemi Olorunsogo, Solomon Omishakin, Isaac Oyeniyi, Temitope Obisesan and a countless other who have supported me in one way or the other.

Finally I would like to appreciate the members of staff of the Department of Geosciences, Mountain Top University.

TABLE OF CONTENTS

LIST OF FIGURES

LIST OF TABLES

ABSTRACT

Niger Delta Basin is one of the most prolific oil producing basins in the world made up of complex structural features which if not well understood may hinder maximum exploitation of hydrocarbon. Therefore, understanding the detailed structural relationships between fault networks and stratigraphic stacking patterns of the area for future field development is very necessary. 2D and 3D seismic data associated with drilling data are the unique tools that facilitate study and interpretation of geologic structural subsurface features. 3D seismic, well log and structural interpretation was carried out to evaluate hydrocarbon potentials of the reservoirs using the Petrel 2017 Software.

The seismic dataset which covers an area of about 55,000km^2 is used majorly in the interpretation of faults and horizons. Well data which includes 6 well datasets is used in the identification of reservoirs and for petrophysical evaluation. Prediction of Depositional environment is carried out using the well data. The depositional environment is interpreted to be a coastal environment and prograding marine shelf environment. Faults are interpreted to be normal faults which include growth faults, synthetic faults and antithetic faults. Mapping of six horizons that corresponded to selected well tops after well to seismic tie is carried out. Time and depth structural maps are generated from the mapped horizons which are used for the identification of tested area and prospect area. Isopach maps are also generated.

Petrophysical analysis is conducted on three hydrocarbon bearing reservoirs within the depth range of 9,567.23ft – 11,209.60ft obtaining values of parameters which include an average Porosity value of 0.24, an average water saturation of 0.52 and an average Net to Gross of 0.6. Volumetric estimations are carried out on three hydrocarbon bearing reservoirs. For sand F, the STOIIP for the tested area, prospect 1 and prospect 2 is 21.5mmBBL, 1.6MMbbl and 7.9MMbbl respectively. For sand G, the OGIP for the tested area and prospect is 102.5MMscf and 36.8MMscf while the OOIP for the tested area and prospect is 17.3mmBBL and 4.7MMbbl. For sand H, the STOIIP for the tested area, prospect 1 and prospect 2 is 40.4mmBBL, 4.9MMbbl and 19.4MMbbl respectively. Seismic attributes analysis of the horizon maps are carried out. Amplitude maps are used as direct hydrocarbon indicator for the targeted formations. As a result, bright spots are indicated and used to identify potential reservoirs. The use of structural and attribute maps has aided the identification of prospects in the KB Field. It is recommended that

wells be drilled to target the new prospects which will improve the hydrocarbon recovery in KB Field.

CHAPTER ONE

INTRODUCTION

1.1 PREAMBLE

Niger Delta Basin is one of the most prolific oil producing basins in the world. The basin is made up of complex structural features which if not well understood may hinder maximum exploitation of hydrocarbon. Therefore, understanding the detailed structural relationships between fault networks and stratigraphic stacking patterns of the area for future field development is very necessary. 2D and 3D seismic data associated with drilling data are the unique tools that facilitate study and interpretation of geologic structural subsurface features. 3D seismic datasets gives a more accurate interpretation of structural and stratigraphic details of the subsurface to 2D due to its dense grid of lines (Saeland and Simpson 1982).

Over the years, it has been observed that hydrocarbon exploration is highly dependent on the presence of structural traps. The anticlinal theory, the rollover anticlines in the Niger Delta for instance, has been a successful exploration strategy. In recent times, most of the identified structural closures on the shelf and upper slope have been drilled and hydrocarbon exploration is becoming increasingly difficult and expensive. The conventional large and easy to discover structures have been found. Subtle structures and stratigraphic elements are presently considered. The combination of seismic and well data makes it possible to map subsurface structural elements with a high degree of accuracy. This combined approach will no doubt be an effective exploration tool to delineate structural features such as faults, stratigraphic features such as anticlines, lithofacies, sequences, depositional environment and hydrocarbon reservoirs.

In this study, our focus is to carry out a 3D seismic interpretation of the KB field, Niger delta basin, Nigeria in order to delineate its geologic structures, its seismic sequences and to attempt an interpretation of the petrophysical properties of the field. This would therefore lead to a proper understanding of its tectonic evolution and structural architecture.

This study is aimed at contributing to the previous works done on this field and to improve the understanding of the subsurface geology of the field with distinct attention to its geologic structural features.

Seismic reflection survey has been in existence since the 19th century and is considered the most widely used geophysical technique. It is predominantly applied in hydrocarbon exploration. It is also applied in crustal structure research in which depths of many kilometers is being achieved. Geophysical and geologic studies have discovered many structural hydrocarbon traps in the Niger delta basin.

1.2 LOCATION OF STUDY AREA

The study area is the KB field located offshore of the Niger Delta basin, Nigeria (Figure 1.1). The Niger Delta is situated in the Gulf of Guinea on the west coast of Central Africa. Niger Delta lies between latitudes 4° and 6° N and longitudes 3° and 9° E in the south-south geo-political region of Nigeria.

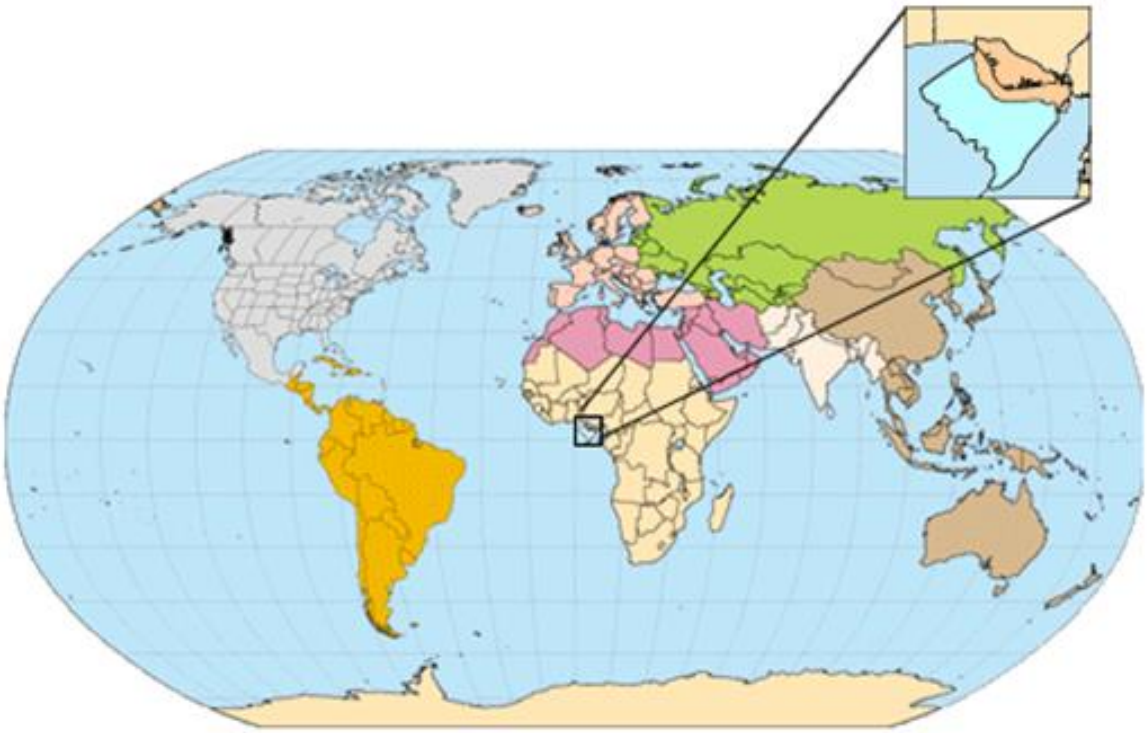

Figure 1.1: Location of the Niger delta basin on the world map (Tuttle et al, 1999[a])

1.3 STATEMENT OF RESEARCH PROBLEM

Poor well performance in many fields of the Niger Delta is a clear evidence of the limited understanding of the structure and stratigraphy of the Basin. From onshore and moving basinwards to the south, the Niger Delta is subdivided into structural domains with various structural styles and implications for stratigraphic development. These structural domains are poorly understood and more studies are required to unravel the complexities in them.

The KB field is within the western margin of the offshore Niger Delta, and has not been fully explored and exploited to its potential. Although, six exploratory wells have been drilled to extract useful information about the field, there is still a level of uncertainty as regards the structure of the reservoir, its geologic architecture, fluid properties and hydrocarbon resources.

1.4 AIM AND OBJECTIVES

The aim of this study is to investigate the subsurface geology of the field, its reservoir structure and structural elements and to extract meaningful information about the field which can be very helpful in the exploration for hydrocarbons. The objectives of the study are to

i. carry out research on the study area by extensively reviewing literatures on the geology, structure, and geologic processes of the study area and on the application of 3D seismic data for structural analysis;
ii. perform a lithostratigraphic correlation along all wells identifying the deposition process of sediments and depositional environments;
iii. calculate for the petrophysical properties of the reservoir rocks;
iv. carry out fault and horizon interpretation on the seismic in-lines and cross-lines;
v. generate time maps, depth maps and thickness maps of the interpreted horizons;
vi. carry out seismic attributes analysis;
vii. identify hydrocarbon traps and new prospect; and
viii. carry out volumetric estimates.

1.5 CONTRIBUTION TO KNOWLEDGE

This study gives detailed information on the structural development, depositional environment and reservoir properties of the study area. It also identified subsurface geologic structures within study area especially structural traps.

1.6 PREVIOUS WORKS

In the past, several authors have carried out seismic data interpretation methods. Some of the studies are reviewed as follows.

Ologe et al. (2013) did a study on 3D seimic structural interpretation of part of the Aloo-field, southwestern Niger Delta, Nigeria. In this study, three horizons were analyzed. This study showed the main structural features of the area which included growth faults trending W-Eand dipping towards the east (with majority of the faults in the northern part trending N-S which are responsible for the high rententive capacity of the reservoirs and hydrocarbon trapping mechanism in the studied area), anticlinal structures, rollover anticlines and crestal faults. They also confirmed the presence of hydrocarbon in two of the studied horizons. One horizon having a gas-water contact (GWC) and the other horizon having an oil-water contact (OWC). The presence of structural highs, growth faults, rollover anticlines and fair reservoir thickness were suggested to be the controlling factor responsible for the economic hydrocarbon accumulation in the area.

Fajana et al. (2018) carried out seismic interpretation and petrophysical analysis for hydrocarbon resource evaluation on the 'Pennay' field, Niger Delta, Nigeria. Four hydrocarbon-bearing sands were delineated along with their various petrophysical parameters. These parameters showed high hydrocarbon saturation 72%, low water saturation 28% and excellent porosity 31% of the two of the sands. Three major faults and two antithetic were identified. Structural closures identified as rollover anticlines and it also describe as four-way dip closure was displayed on the time/depth structure map. The Volume of hydrocarbon in the sands was therefore estimated and results were given thereafter.

Obaje and Okosun. (2013) did a paleoenvironmental interpretation of the Tomboy field, offshore western Niger delta, Nigeria. Foraminifera specimens and lithofacies data were used. The assessed lithofacies and fossil accessories confirmed the paleodepths of inner neritic, middle neritic and outer neritic. It also established paleodepths of inner neritic to outer neritic. Paleoenvironmental interpretation is very useful for determining environments of deposition, which is a valuable cost-effective input into petroleum exploration and development.

Satti et al. (2014) carried out an integrated seismic interpretation, offshore peninsular Malaysia. For his study, he made use of 3D high resolution seismic data for the interpretation of structures which favor the accumulation of hydrocarbons whereas advanced seismic attributes and seismic inversion have been used to map out stratigraphic traps. The implementation of seismic attributes showed the presence of a seismic channel. The morphology of the channel was outlined by the application of the advanced seismic attributes while seismic inversion showed the location of a sand zone in the NE side of the channel morphology. This study showed the importance of seismic interpretation in the delineation of geologic structures such as buried channels.

Etuk et al. (2020) worked on the evaluation of seismic attributes for reservoir characterization over Edi field, Niger delta, Nigeria with the use of 3D seismic data. In this study, four horizons were picked along the in-lines and the cross-lines, five faults were delineated and mapped. The results showed that the area is highly faulted and also depicts the tectonic location of Niger delta. Time structural maps were produced to study the geometry of the structure which contains the accumulated hydrocarbon. Attribute maps such as RMS amplitude, instantaneous phase, gradient magnitude and chaos were extracted to complement the structural maps. The presence of hydrocarbon was indicated by the High amplitude anomalies of bright spots.

CHAPTER TWO

LITERATURE REVIEW

2.1 GEOLOGY OF THE STUDY AREA

The Niger Delta Basin which covers a wide area of about 300,000 km^2 is a passive margin basin located in the Niger Delta at the West African margin of the Gulf of guinea (Fatoke, 2010). It has a sediment fill of about 500,000 km^3 with a sedimentary depth of about 9-12 km (Fatoke, 2010). Three depositional cycles were responsible for the formation of this Passive margin basin; the first cycle was a marine incursion in the middle cretaceous which was terminated by mild folding of sediments during the Santonian time. The second tectonic cycle was majorly the growth of a proto-Niger delta during the Late Cretaceous which ended in a major Paleocene marine transgression. The third cycle was the continuous growth of the main Niger delta, from Eocene to Recent. Figure 2.1(a) shows the geologic map of the Niger Delta Basin.

The Niger Delta Basin is divided into 3 subsurface lithostratigraphic units as seen in Figure 2.1(b) which is comprised of; the Benin Formation which is composed of course-grained, gravelly sandstone (uppermost unit), intervening unit known as the Agbada Formation composed of the intercalation of sandstones and shales and the Akata shales (lowest unit).

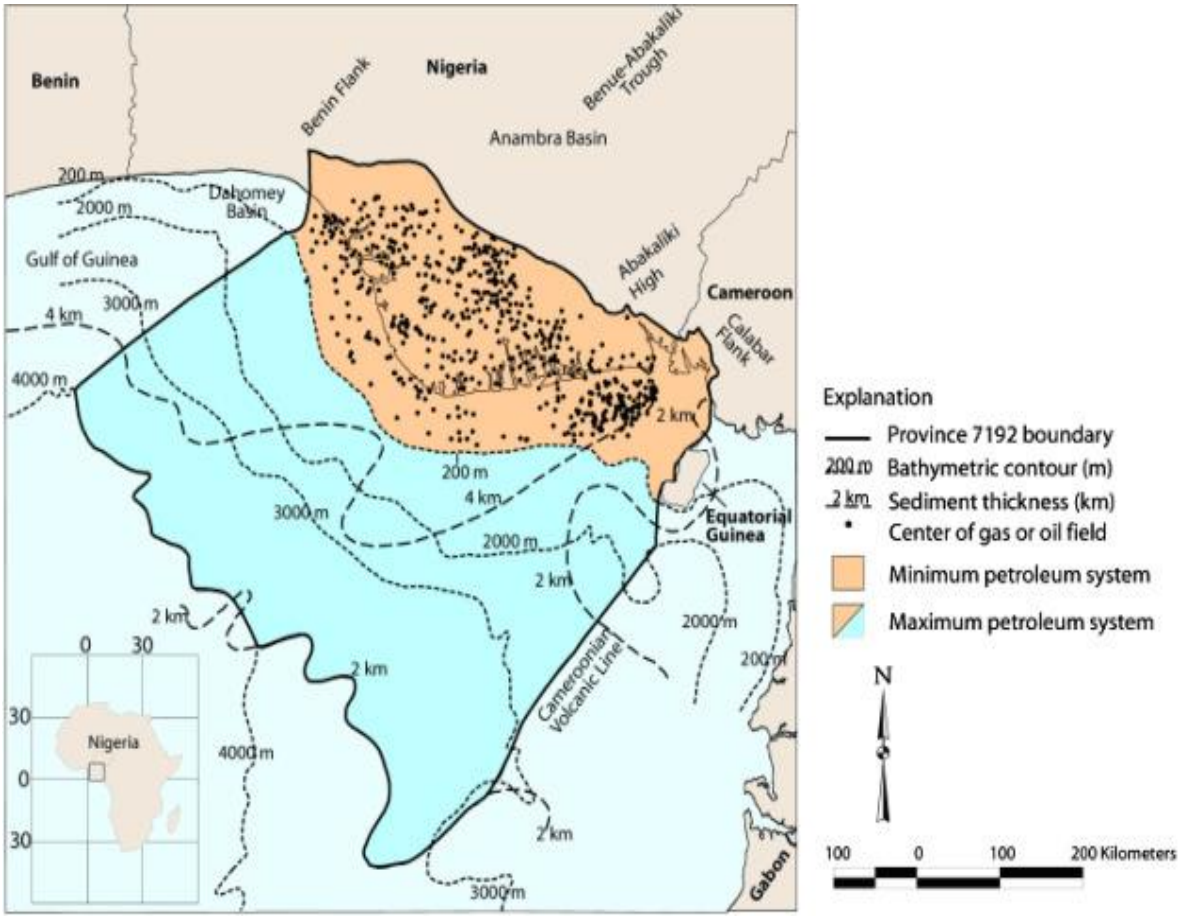

Figure 2.1(a): Geologic map of the Niger Delta Basin (Adegoke, 2017).

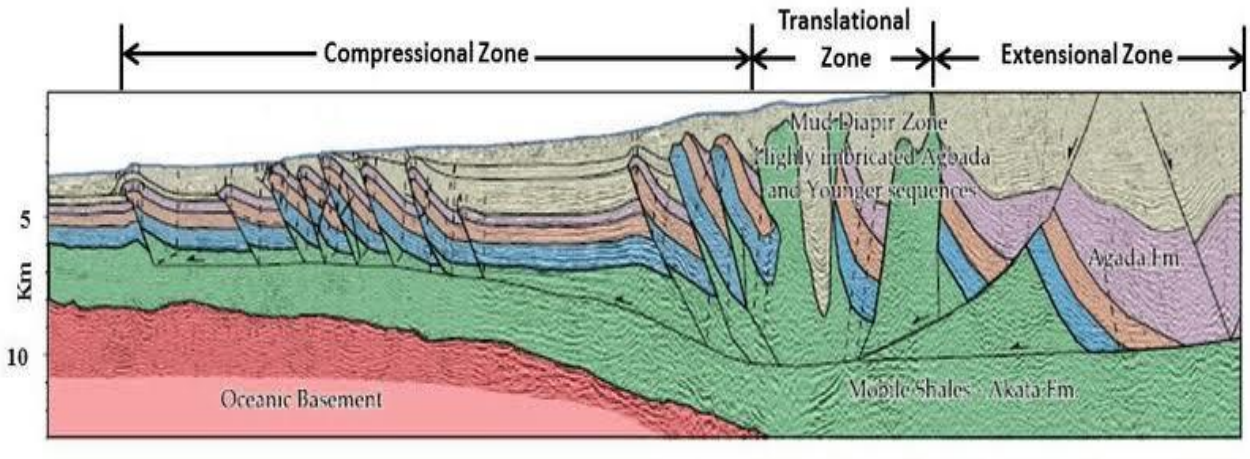

Figure 2.1(b): Regional cross section showing the three structural provinces of the Niger Delta (Corridor et. Al, 2005).

2.2 STRATIGRAPHY OF THE NIGER DELTA BASIN

The Niger Delta Basin comprises of three lithostratigraphic units which include the Benin Formation, Agbada Formation and Akata Formation (Figure 2.2). The Benin Formation was deposited in an alluvial depositional environment extending from the west of the Niger Delta basin to the south beyond the coastline. The Benin Formation is Oligocene and younger in age and has a thickness of about 2000 m (Tuttle et al, 1999[b]). The Agbada Formation was fromed in a Fluvial-deltaic environment and dates back to Eogene in age. It is about 4000m thick (Tuttle et al, 1999[b]). The Akata Formation, the lowest formation, was deposited in a marine environment. This formation outcrops offshore in shale diapers and has a maximum thickness of about 7000 m (Tuttle et al, 1999[b]). The shale diapers form as a result of the squeezing of the ductile shale formations which is rich in clay. The Akata Formation grades vertically into the Agbada Formation with abundant plant remains and micas in the transition zone.

The Niger Delta Basin also comprises of other outcropping units which include the Imo Formation and the Ameki Group (Ameki, Nanka, Nsugbe, and Ogwashi-Asaba Formations). Rollover anticlines in front of growth faults referred to as dip closures is the major trapping system for oil exploration. Stratigraphic traps are very rare in this basin. Hydrocarbons present in the Niger Delta basin is mainly found in sandstone reservoirs of the Agbada Formation.

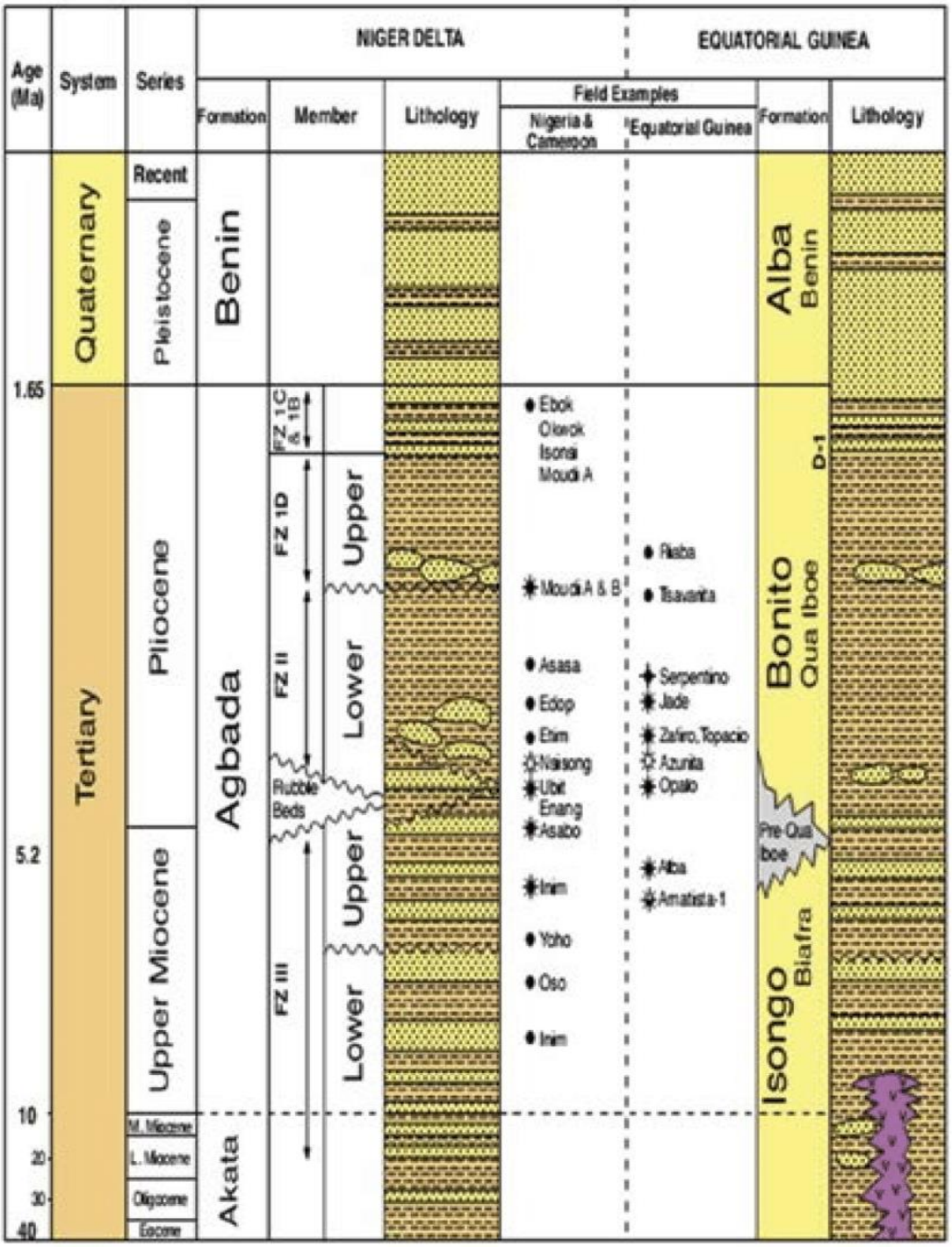

Figure 2.2: Stratigraphy of the Niger Delta basin (Doust and Omashola, 1990)

2.3 DEPOSITIONAL HISTORY OF THE NIGER DELTA BASIN

The Niger Delta Basin was formed by a failed rift junction between the South American plate and the African plate during their separation, as the South Atlantic began to open. Rifting in this basin started in the late Jurassic and ended in the mid Cretaceous. The rifting in this basin lead to the formation of several faults many of which were thrust faults (older rocks being pushed above the younger rocks). The Niger Delta grades upwards from massive and monotonous marine shales into inter-bedded shallow-marine and fluvial sands, silts and clays (Figure 2.3). The basin can be divided into a series of depobelts, separated by major syn-sedimentary fault zones. These depobelts can be thought of as transient basinal areas succeeding one another in space and time as the delta prograded southward (Doust and Omatsola, 1990).

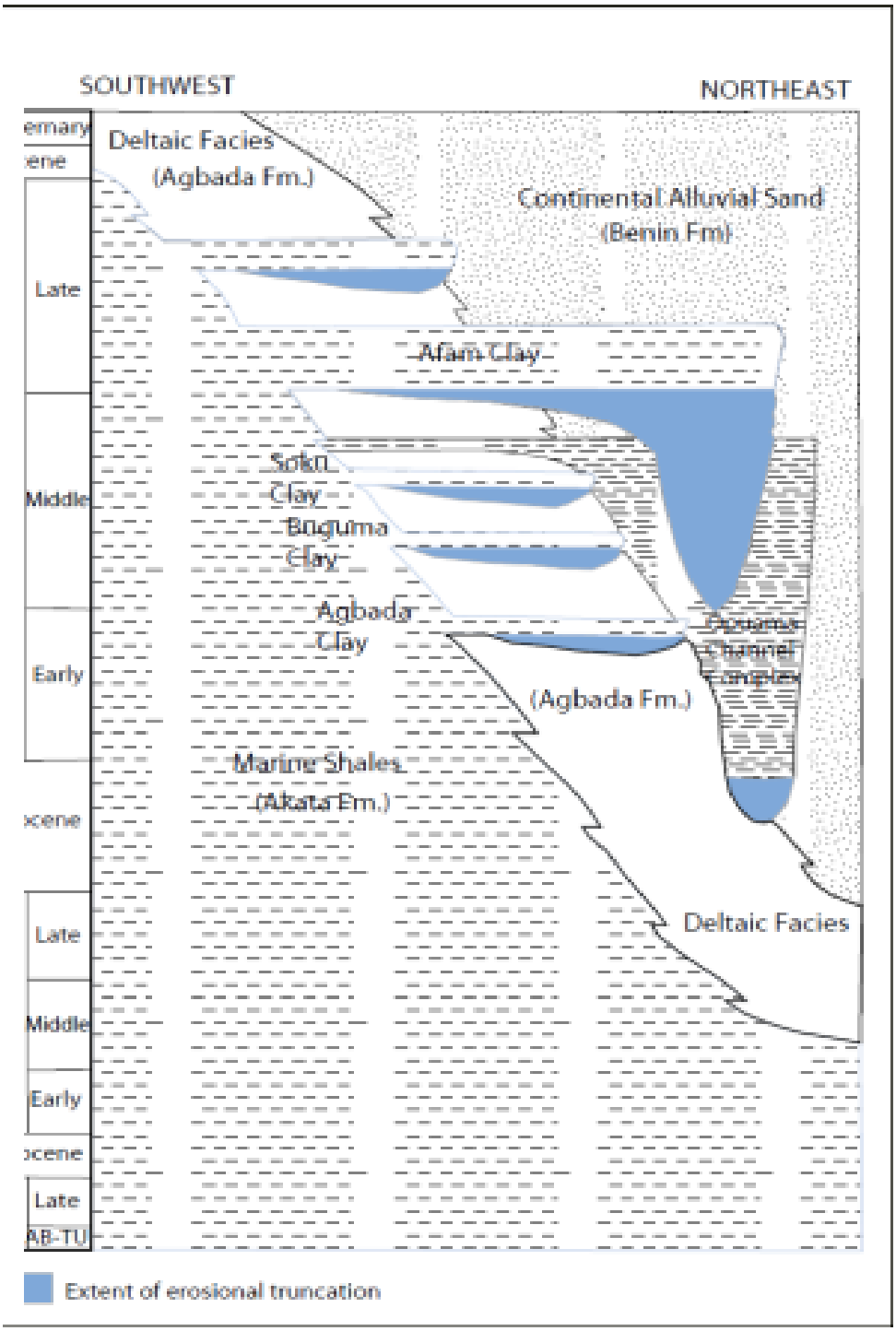

Figure 2.3: Stratigraphic column of the Niger Delta Basin (Doust and Omatsola 1990)

2.4 DEPOBELTS OF THE NIGER DELTA BASIN

Sedimentation in the depobelts is a function of sediment supply and of accommodation space created by basement subsidence and growth faulting. Growth faults are the dominant structural features in the Niger delta which are triggered by a deformation of deltaic sediments generated by rapid sedimentation load and gravitational instability of the Agbada sediment pile accumulating on the mobile undercompacted Akata shales. Toe thrusting at the delta front, lateral flow and extrusion of the Akata pro- delta shales during growth faulting and related extension also account for the diapiric structures on the continental slope of the Niger delta in front of the prograding depocenter with paralic sediments (Doust and Omatsola, 1990; Reijers, 1996).

Three major depositional cycles have been identified within Tertiary Niger Delta deposits (Short and Stauble, 1967; Doust and Omatsola, 1990). The second of these three cycles, starting in late Paleocene to Eocene time, reflects the progradation of a "true" delta, with an arcuate, wave and tide dominated coastline. These sediments range in age from Eocene in the north to Quaternary in the south (Doust and Omatsola, 1990). Deposits of the last depositional cycle have been divided into a series of five depobelts (Doust and Omatsola, 1990) as shown in Figure 2.4.

At a certain stage however, further subsidence and sedimentation could no longer be accommodated and the focus of deposition shifted basin ward to form a new depobelt. Similarly, syn-sedimentary and most post sedimentary faulting ceased with the abandoned depobelt. A depobelt therefore, forms the structurally and depositionally most active portion of the delta at each stage of its development.

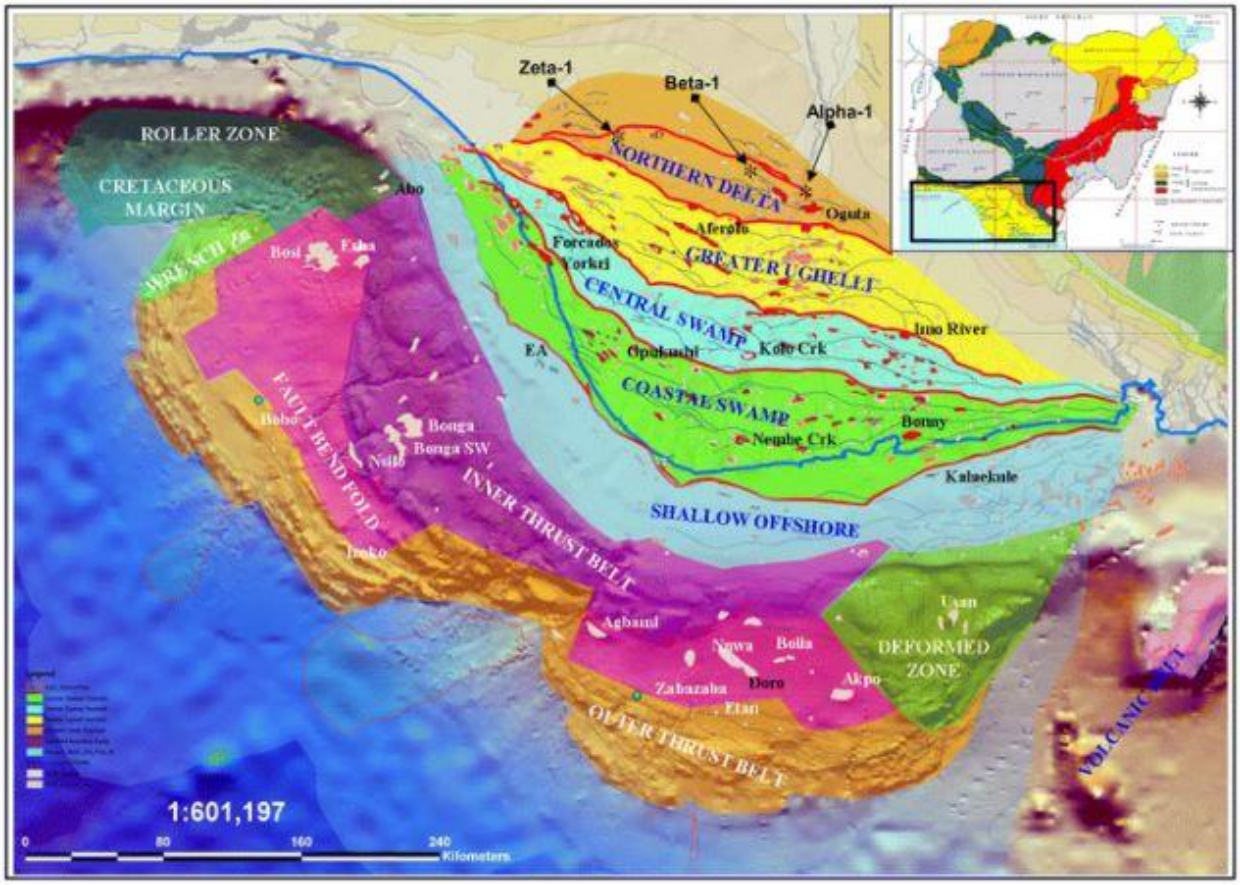

Figure 2.4: Depobelts of the Niger Delta Basin (Ejedavwe et al. 2002)

2.5 BASIC THEORY OF METHODS USED

2.5.1 SEISMIC REFLECTION METHOD

The seismic reflection technique measures the time taken for a seismic wave to travel from a source (at a known location at or near the surface) down into the ground where it is reflected back to the surface and then detected at a receiver, which is also at or near the surface at a known position as shown in Figure 2.5. This time is known as the two way travel time (TWT). The seismic method gives important details on the geometry of structures and physical properties of the materials present in the subsurface.

The seismic method is divided into three processes:

- Data acquisition
- Data processing
- Data Interpretation

Data acquisition: Reflection seismology is directed primarily at finding the depths of reflecting surfaces and the seismic velocities of subsurface rock layers. The Principle involves, a seismic signal e.g. an explosion is produced at a known place and time and the echoes reflected from the boundaries between rock layers with different seismic velocities and densities are recorded and analyzed. Acquisition can be performed on land as shown in Figure 2.6(a) and on water as shown in Figure 2.6(b).

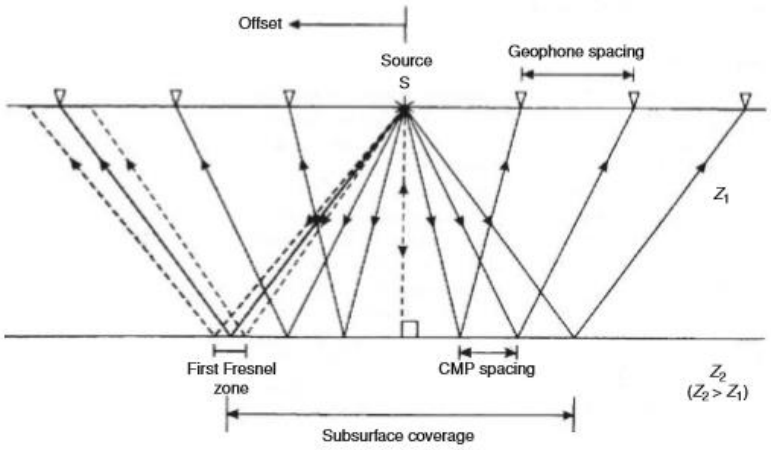

Figure 2.5: Schematic diagram of reflection raypaths over a horizontal interface (Reynolds, 2011)

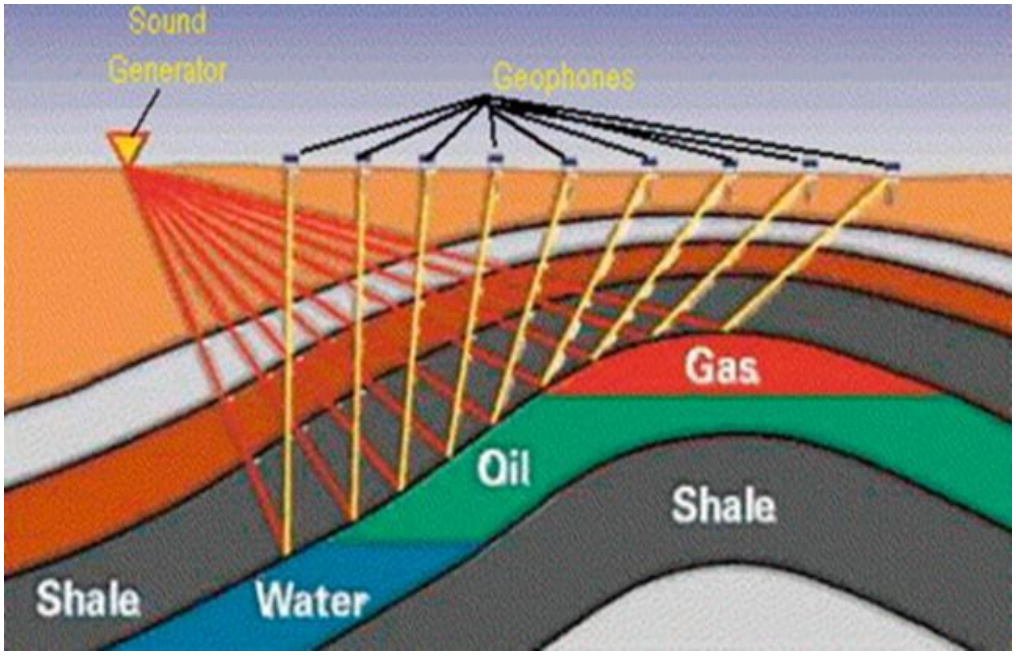

Figure 2.6(a): Seismic data acquisition on land (Aminzadeh and Dasgupta, 2013).

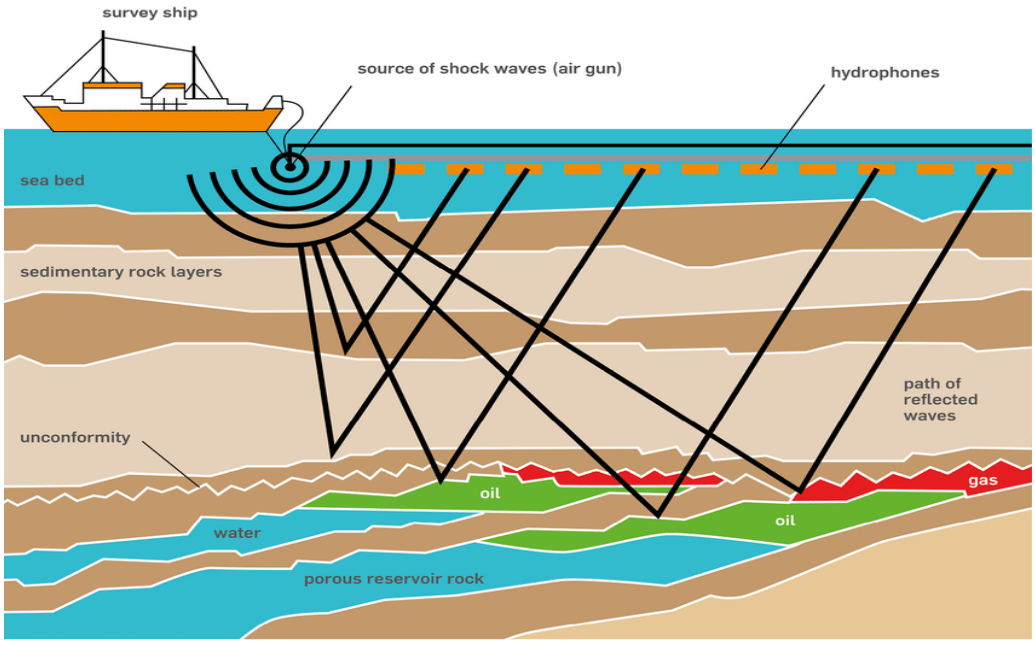

Figure 2.6(b): Seismic data acquisition on water (Kukreja et al, 2017).

Data processing: Seismic data processing is the steps necessary to convert field data into a meaningful format ready for interpretation. Data Processing involves many stages of signal processing and computer summing. The objectives of seismic data processing include:

- To recover and transform the field data
- To reduce noise
- To improve resolution

Data Interpretation: Seismic interpretation aims at extracting all available geologic information from the data including structure, stratigraphy, rock properties and perhaps reservoir fluid changes in space and time. This process will require the best possible acquisition and processing to have been performed, and also knowledge of local geology from outcrop and pre-existing wells. The interpretation may be done by hand on paper sections, but is normally done interactively these days on an interpretation workstation.

2.5.2 WELL LOGS

2.5.2.1 GAMMA RAY LOG

The gamma ray log is a measurement of the radioactivity of the formations (Figure 2.7). In sedimentary formations, the log normally reflects the shale content of the formations. As the shale content in a formation increases the gamma ray log response increases, this is because the radioactive elements tend to concentrate in clays and shales. Clean sandstone (low shale content) usually has a low gamma ray response, unless potassium feldspars, volcanic ash, granite wash, micas, glauconite, or uranium- rich water is present (Schlumberger, 1989).

The GR log can be recorded in cased wells, which makes it very useful as a correlation tool in completion and work over operations. It is frequently used to complement the SP log and as a substitute for the SP curve in wells drilled with salt mud, air, or oil-based muds. Unlike the SP log, the gamma ray log is not affected by Formation water resistivity (Rw) because the GR log responds to the radioactive nature of the Formation rather than the electrical nature (Helander, 1983). Gamma ray log is useful for location of shale and non shaly beds and, most importantly, for general correlation.

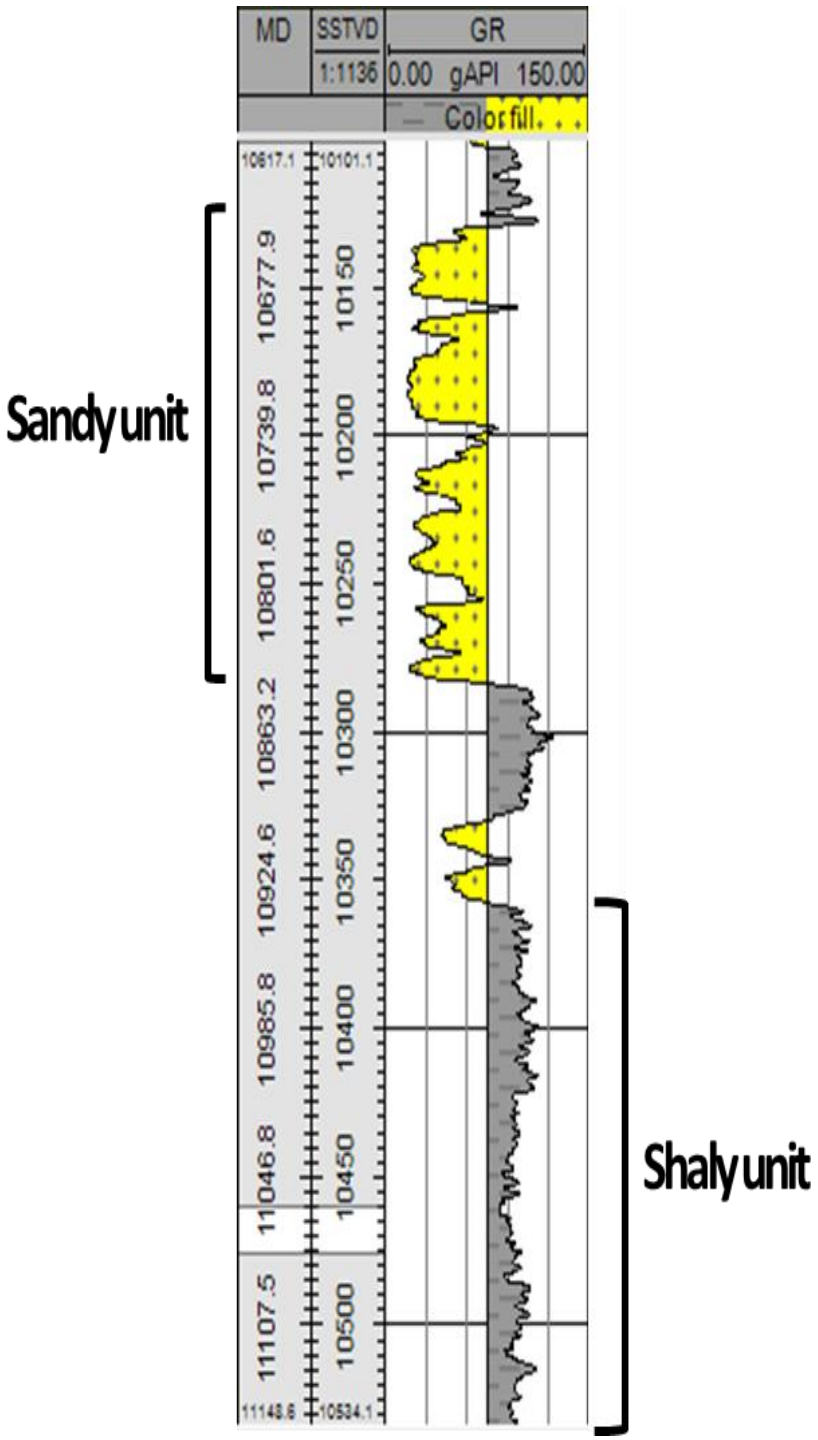

Figure 2.7: Gamma ray log showing difference in the subsurface lithology

2.5.2.2 RESISTIVITY LOG

Resistivity logs can be used to:

- Determine hydrocarbon-bearing versus water bearing zones.
- Indicate permeable zones.
- Determine porosity.

The most important use of resistivity logs is the determination of hydrocarbon bearing versus water-bearing zones (Figure 2.8), this is because the rock's matrix or grains are nonconductive and any hydrocarbons in the pores are also nonconductive, the ability of the rock to transmit a current is entirely a function of water in the pores. As the hydrocarbon saturation of the pores increases, the formation's resistivity increases. As the salinity of the water in the pores decreases the rock's resistivity also increases (Asquith, 1982).

There are two types of resistivity tools: the laterolog and induction log. The laterolog tools are better for resolution of thin beds to moderately thick beds. The tools are available with deep, medium, and shallow depths of investigation. The induction tool was originally designed to measure formation resistivity in boreholes containing oil-base muds and in air-drilled boreholes. Designed for deep investigation, induction logs can be focused in order to minimize the influences of the borehole, the surrounding formations, and the invaded zone (Schlumberger, 1985).

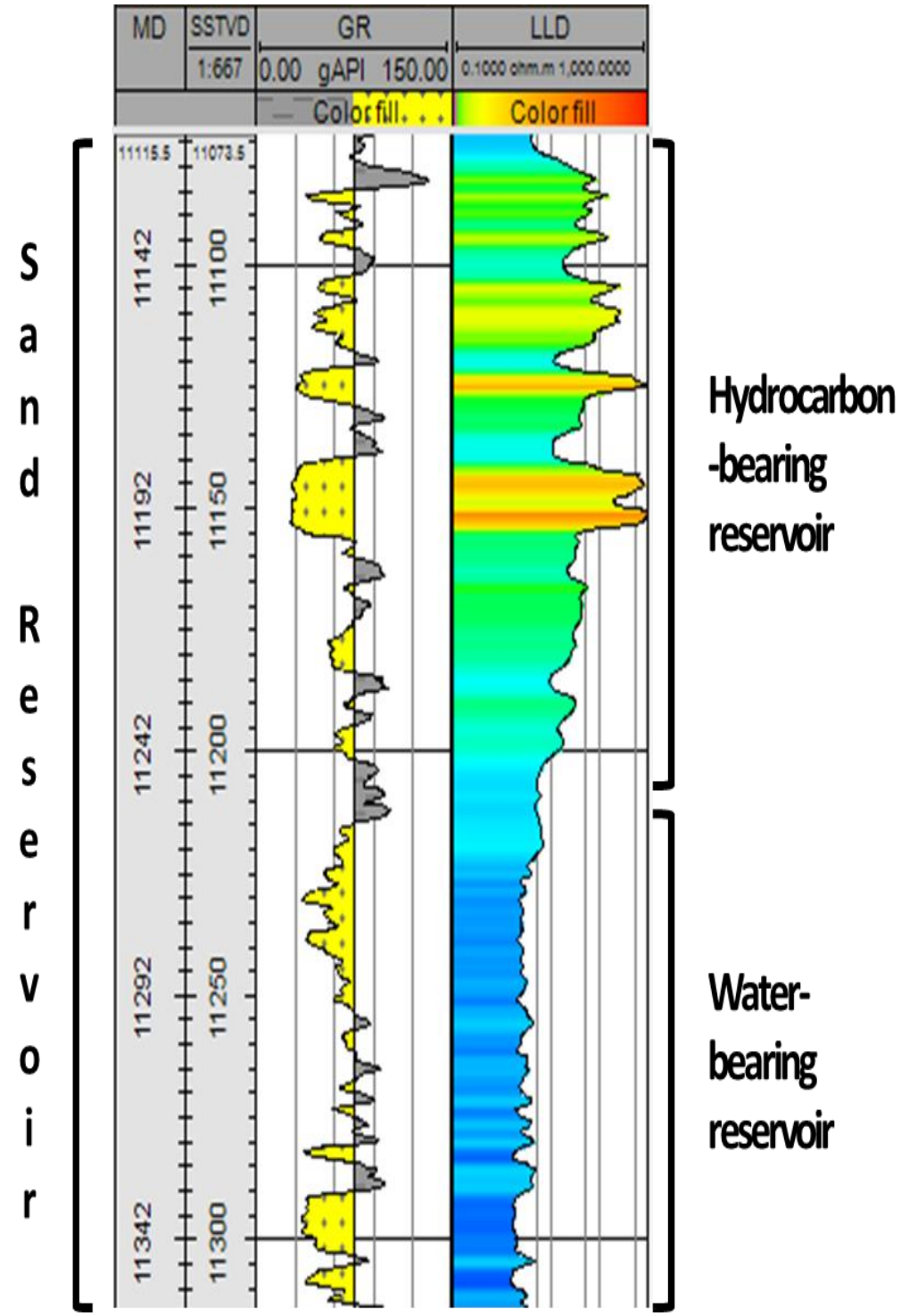

Figure 2.8: Resistivity log showing highlighting the hydrocarbon-bearing zone and the water-bearing zone in a sand reservoir.

2.5.2.3 POROSITY LOGS

The three main types of logs used to determine porosity of formations are the neutron, density and sonic log. The Density and Neutron logs are nuclear measurements while the sonic log uses acoustic measurements. In addition to porosity, these logs are affected by other parameters such as lithology, nature of pore fluids, shaliness and pressure contrast.

2.5.2.4 NEUTRON LOG

The log measures the hydrogen ion concentration in a formation. In a clean formation, the neutron log measures the liquid filled porosity. A combination of neutron log with one or more porosity logs will give better results in porosity estimation. The neutron log is also useful to ascertain the presence of gas and determine mineralogy and shaliness.

2.5.2.5 DENSITY LOG

These tools operate by emitting gamma radiation and detecting the proportion of the radiation that returns to detectors on the tool. The amount of radiation returned is proportional to the electron density of the material bombarded and this is in turn proportional to the overall density of the formation. When pores are filled with gas rather than oil or water, neutron porosity will be lowered; this is as a result of less concentration of hydrogen in gas compared to oil or water.

2.5.2.6 SONIC LOG

The sonic log is a porosity log that measures the travel time (interval transit time) of the compressional sound wave over a unit distance, and hence, a record of the reciprocal of compressional wave velocity (Schlumberger, 1985). The time for acoustic energy to travel a distance through the formation is the desired measurement. The units of such measurements are usually expressed in microseconds per foot (μsec/ft). The interval transit time can be integrated to give the total time travel over the logged interval.

CHAPTER THREE

METHODOLOGY

3.1 INTRODUCTION

This study was carried out using the modern method of seismic interpretation technique which was done using PETREL™ workstation, a schlumberger interpretation tool for visualization of seismic models and reservoir characterization.

3.2 DATA AVAILABILITY

The data made available for this study includes;

- 33 three dimensional Seismic reflection data (21 in-lines and 12 cross-lines)
- The area has 6 wells which includes 4 Vertical wells (KB-1, KB-2, KB-4 and KB-5) and 2 deviated wells (KB-3 and KB-6).
- Well logs were made available for the study.

Other data sets made available base map, check-shot data, directional data for deviated wells and a geological map of the Niger Delta basin used in structural analysis.

3.2.1 3D SEISMIC REFLECTION DATA

The 3D seismic reflection data were acquired in time (it is a time data). It consists of 21 in-lines and 12 cross-lines. The study area as shown in Figure 3.1(c) and Figure 3.1(d) covers an area of approximately 55,000km^2. It provides resolved cross-sectional views along any azimuth within the survey area. The nature and location of geologic features such as structural and stratigraphic features can be determined accurately using the seismic data with the help of the other sets of data provided.

The inline section as shown in Figure 3.1(a) is acquired in the direction of the survey (the shooting direction) while the crossline section as shown in Figure 3.1(b) is acquired in a direction that is perpendicular to the inline direction.

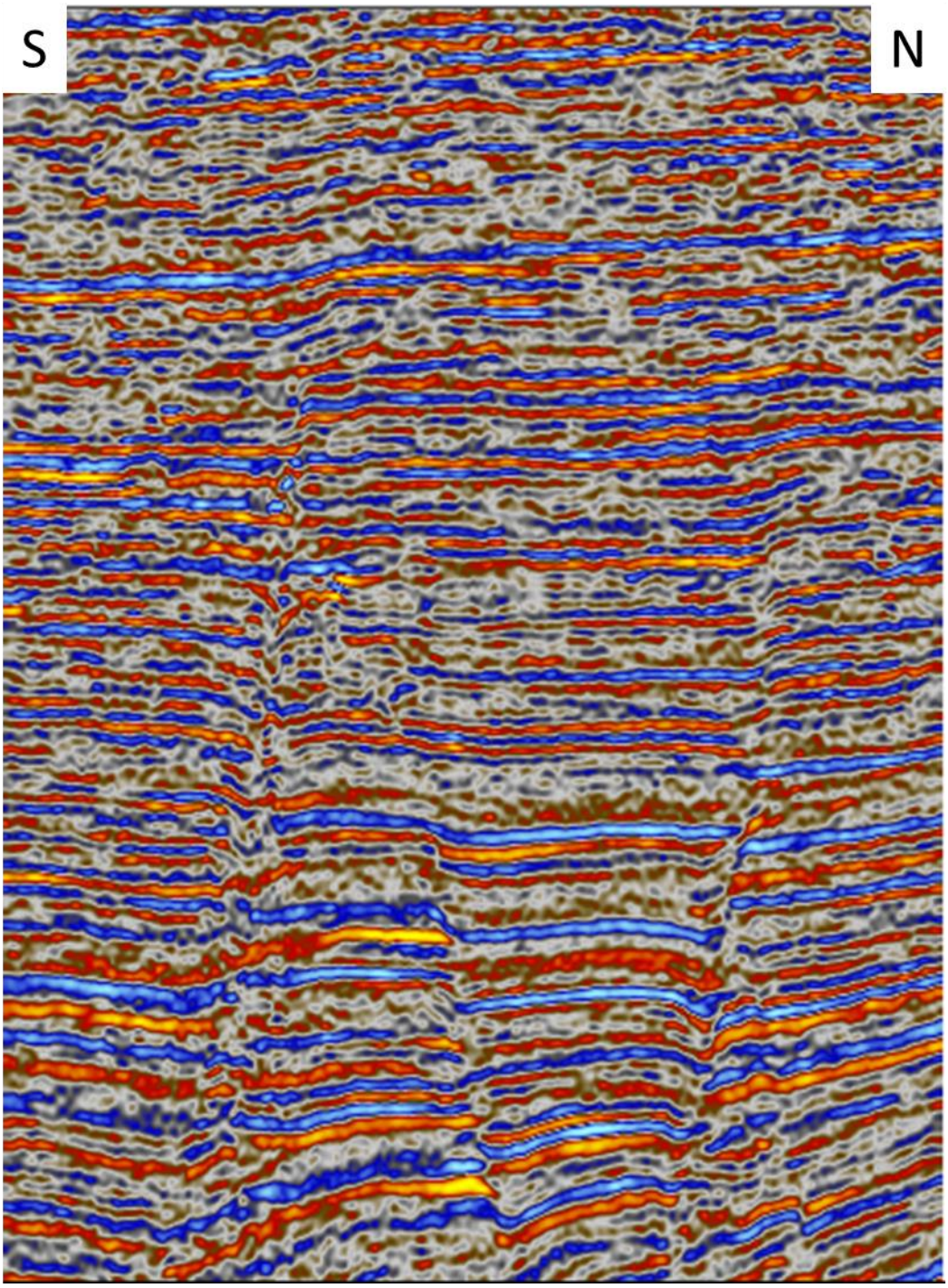

Figure 3.1(a): Inline Seismic data (Inline 5920).

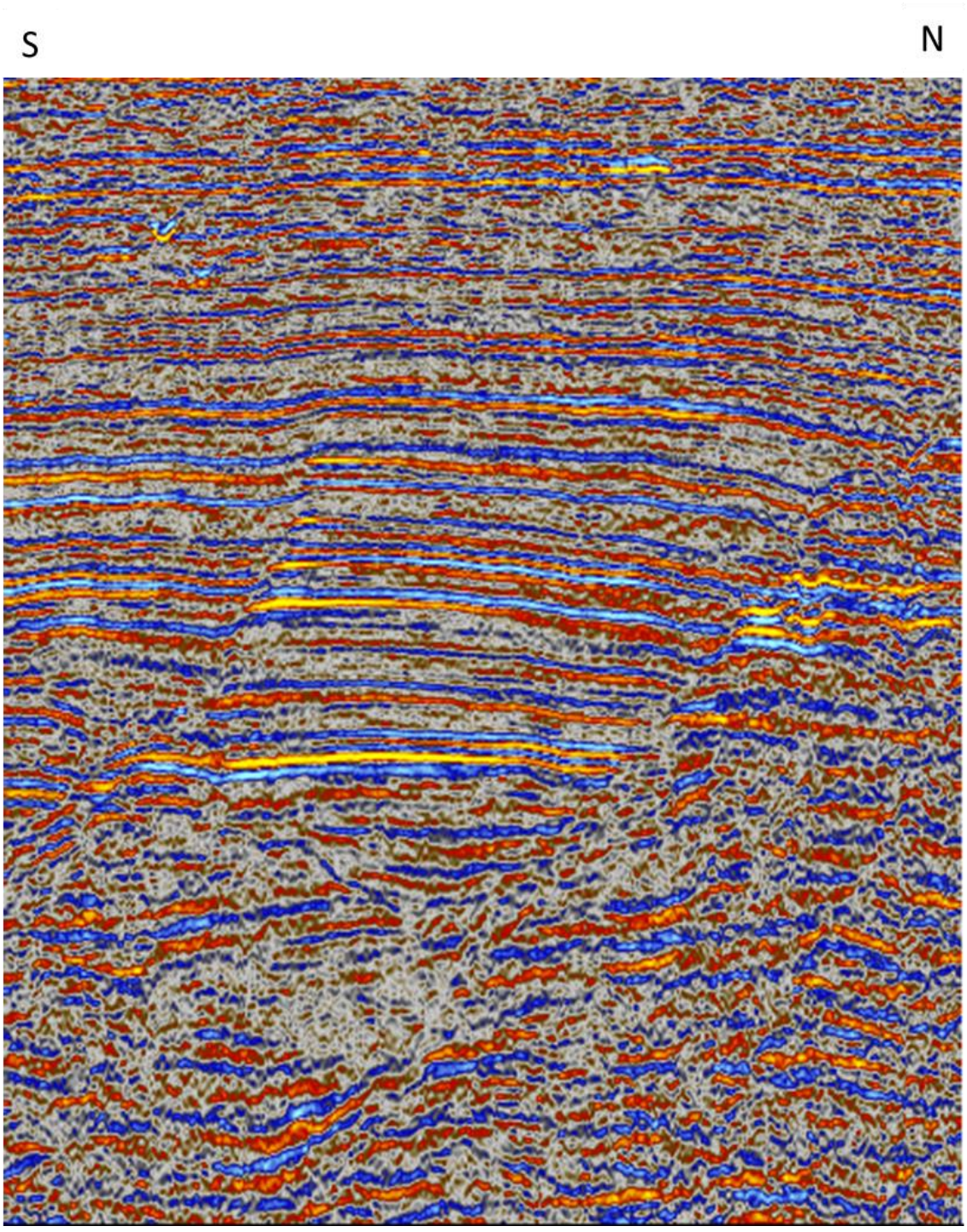

Figure 3.1(b): Crossline Seismic data (Crossline 1590).

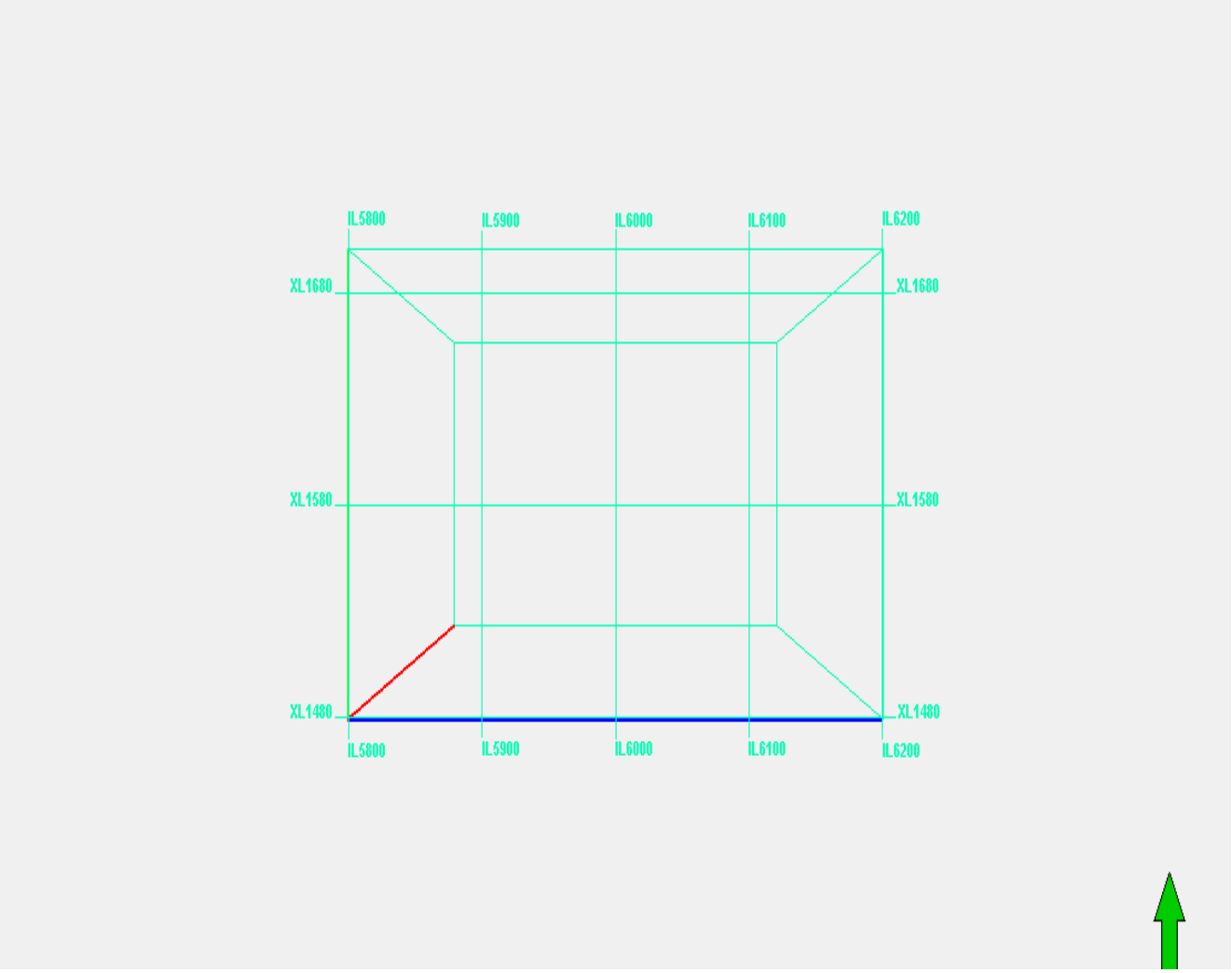

Figure 3.1(c): 3D view of the base Map of Study area.

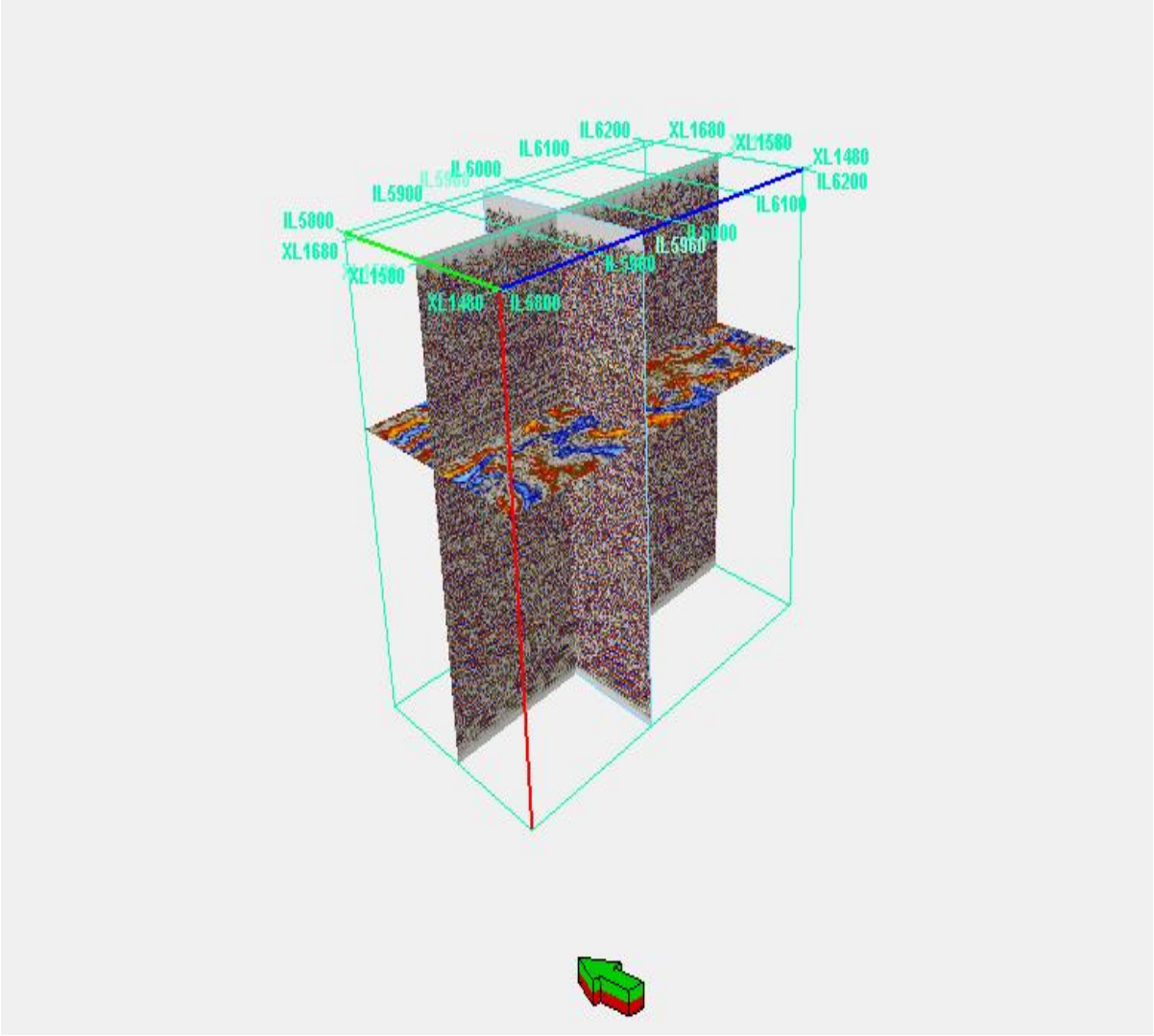

Figure 3.1(d): 3D view of the base Map of Study area showing inline 5960 and crossline 1590.

3.2.2 WELL DATA

Six wells were made available in the data set as seen in Figure 3.2(a) and Figure 3.2(b). 4 of the wells are vertical (KB-1, KB-2, KB-4 and KB-5) while 2 are deviated (KB-3 and KB-6). The wells are presented in Table 1 showing the status of their various well logs.

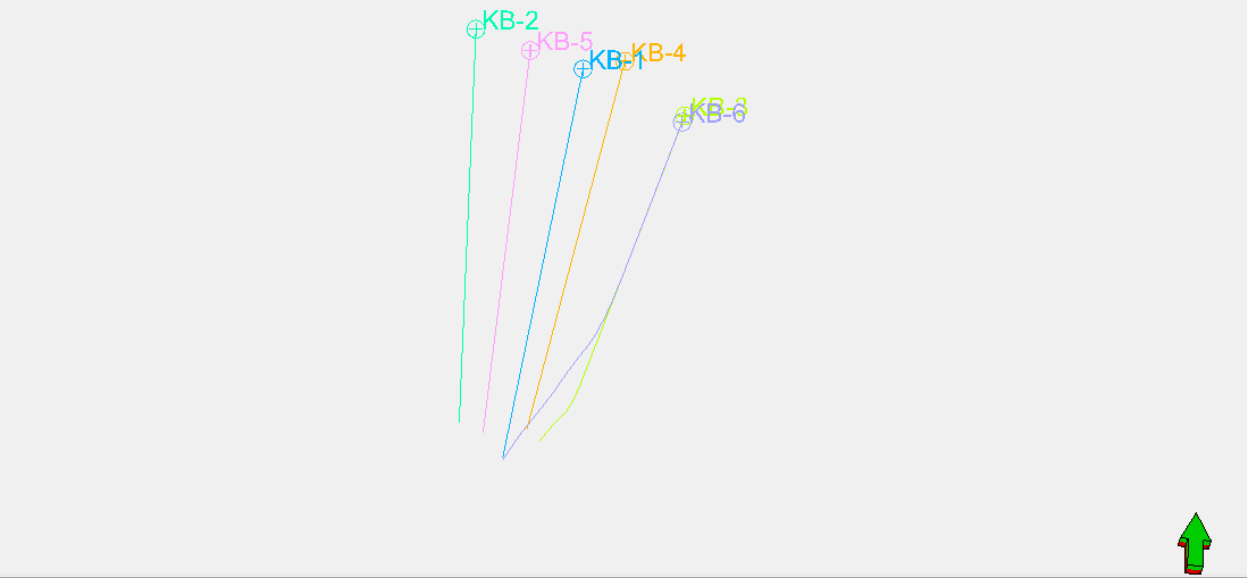

Figure 3.2(a): Cross section of the six wells available.

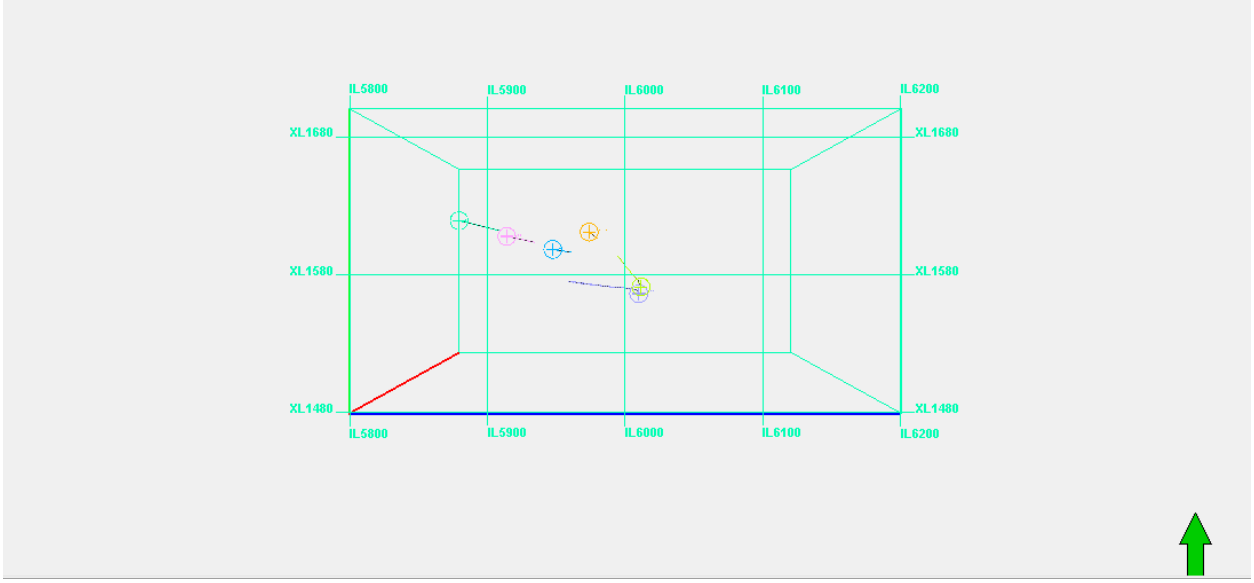

Figure 3.2(b): 3D Base map of the study area showing the location of the six wells.

Table 1: Summary of well logs in the study area

Well Name/ Log type	Gamma	Resistivity	S.P	Sonic	Neutron	Density	Porosity	Caliper
KB-1	✓	✓	✓	✗	✗	✗	✓	✓
KB-2	✓	✓	✓	✓	✗	✗	✗	✗
KB-3	✓	✓	✓	✗	✓	✗	✓	✓
KB-4	✓	✓	✓	✓	✓	✓	✓	✓
KB-5	✓	✓	✓	✓	✓	✓	✓	✓
KB-6	✓	✗	✓	✗	✓	✓	✓	✓

✓ - Available

✗ - Not available

3.3 WORKFLOW

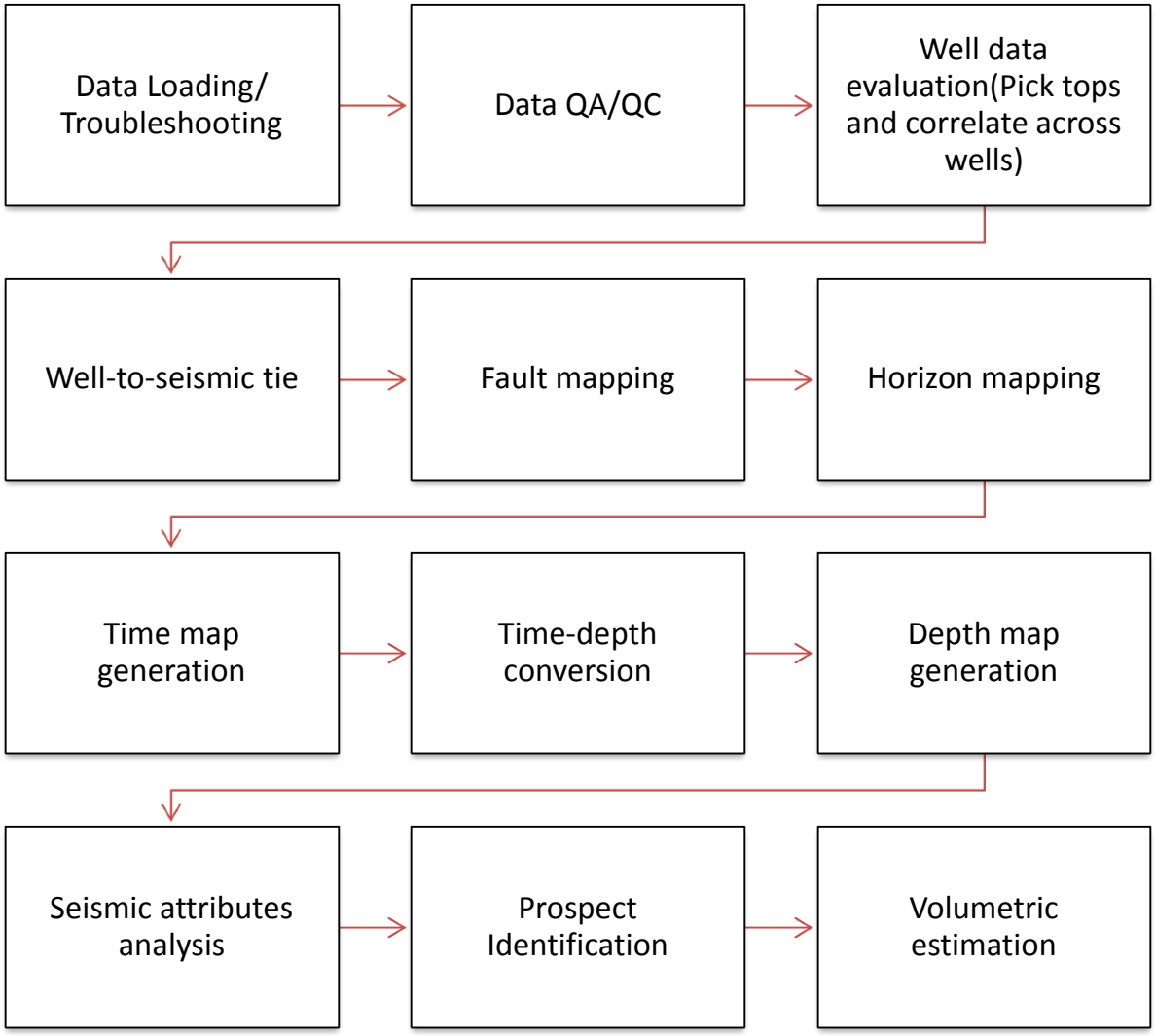

3.3.1 DATA LOADING

To begin this study, the available data set was loaded into the petrel software. This was done by first importing the seismic data which was in SGY format, then the wells were loaded one after the other. The well data were in LAS File. Directional data for the deviated wells (ASC File) were loaded thereafter. Checkshot data for the various wells were loaded then loaded. The checkshots format was in Text document.

3.3.2 DATA QA/QC

After data loading, data quality check was carried out. The assessment of the data was to know the quality of the data and to have knowledge of the availability of some data such as the well logs. This step gives the interpreter an idea of how to go about the interpretation.

3.3.3 WELL DATA EVALUATION

LITHOLOGY IDENTIFICATION AND CORRELATION

Reservoirs were identified and correlated across the six wells using the Gamma ray logs and Resistivity logs as seen in Figure 3.3. The lithologies penetrated by the wells were identified using the Gamma ray log. A shale base line was established. Deflection of the Gamma ray log signature to the right of the shale base line was interpreted as shale (non-reservoir lithology) and deflection of the Gamma ray log signature to the left side of the shale base line was interpreted as sand (reservoir lithology). For the resistivity log, deflections to the left were interpreted as low resistivity (high conductivity) and deflections to the right were identified as high resistivity (low conductivity). Hydrocarbon bearing reservoirs are characterized by high resistivity. After identifying the reservoirs, petrophysical parameters such as net reservoir thickness, gross reservoir thickness, porosity, water saturation and hydrocarbon saturations were calculated. A composite line was drawn across the base map which assisted in the order in which the wells were arranged.

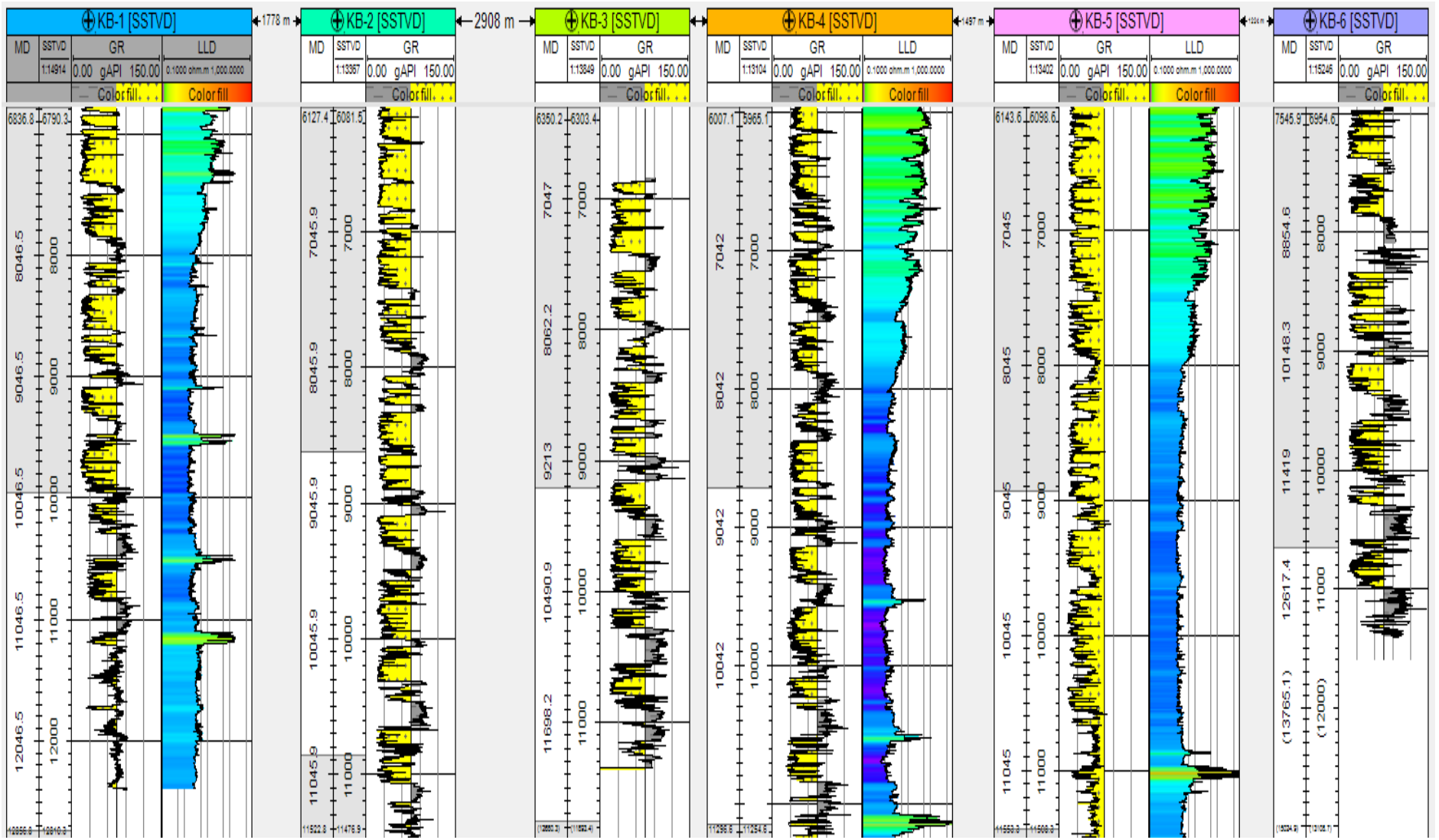

Figure 3.3: Diagram of the gamma ray logs and resistivity logs showing the lithology encountered across the various wells

IDENTIFICATION OF DEPOSITIONAL ENVIRONMENTS

The stacking patterns of the lithology signature from the logs play a vital role in predicting the environment in which sediments were deposited. In this study, due to the unavailability of core data, the interpretation of the environment of deposition was based on the shape of the gamma ray log only (figure 3.4). The principal shapes observed were the bell, the funnel and the cylinder (figure 3.4). The gamma ray log was used because of its ability to give greater variety of shapes, greater definition and has more 'character' than other logs.

Some of the environments investigated for in this study include:

1. **Deltaic-Fluvial Environments.**

   The Fluvial environments are mostly associated with a bell-shaped gamma ray log signature which indicates a fining upwards pattern of sediments deposition as seen in figure 3.5(a). The Deltaic environments are associated with a serrated funnel-shaped gamma ray log signature which indicates a coarsening upwards pattern of sediments deposition as seen in figure 3.5(a).

2. **Shallow marine environments.**

   The shallow marine environment is mostly associated with a bell-shaped gamma ray log signature which indicates a transgressive marine shelf as seen in figure 3.5(b) and a funnel-shaped gamma ray log signature which indicates a prograding marine shelf as seen in figure 3.5(b).

3. **Deep Marine Environments.**

   The deep marine environments includes the slope channel, the inner fan channel, the middle fan channel, the supra-fan channel and the basin plain as shown in figure 3.5(c).

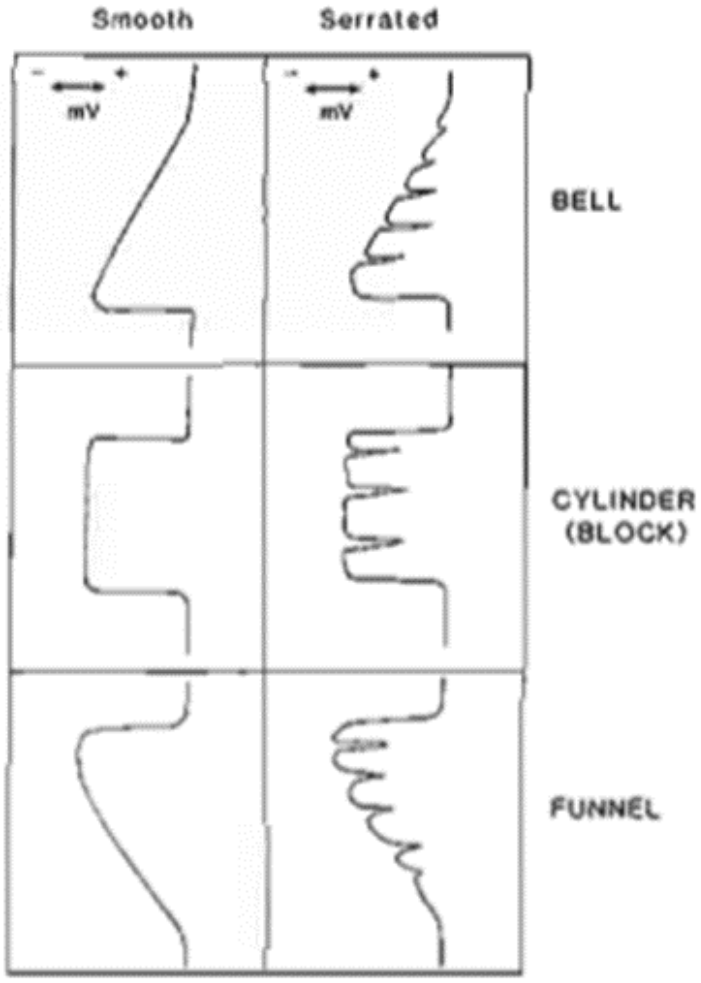

Figure 3.4: Log shape classification. The basic geometrical shapes and description used to analyze gamma ray log shapes (Rider, 2002).

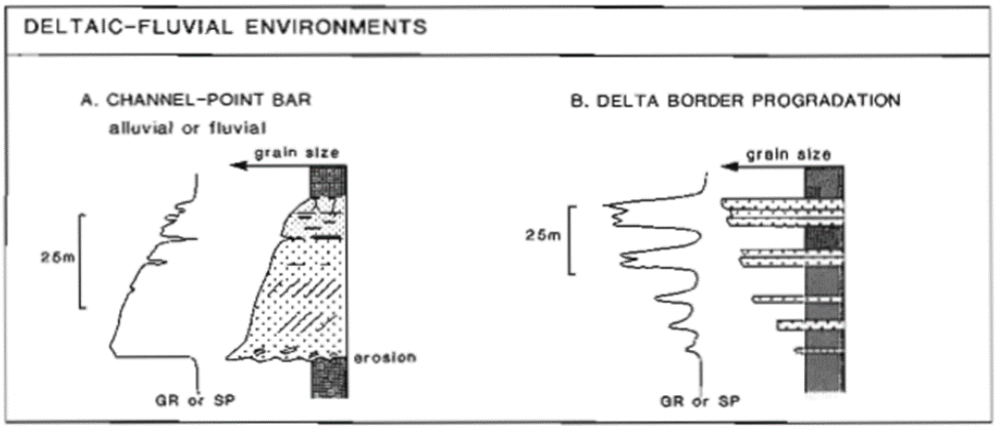

Figure 3.5(a): Gamma ray indication model from a Deltaic-Fluvial Environment (Rider, 2002).

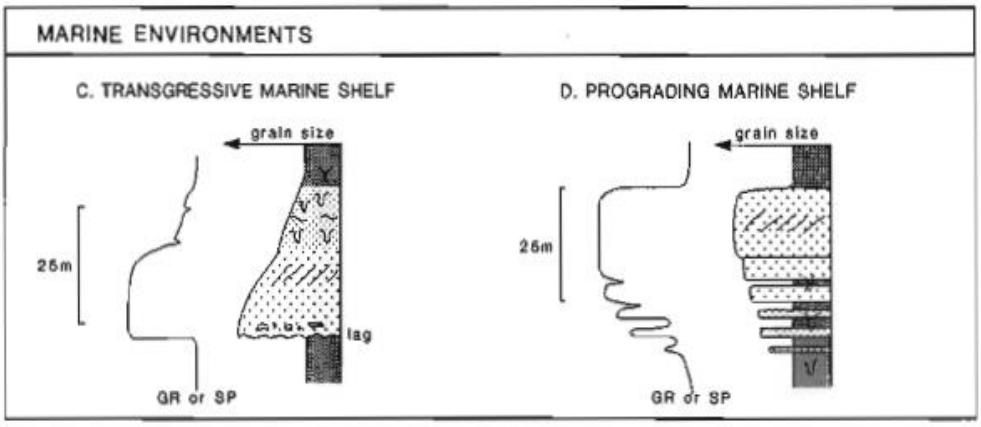

Figure 3.5(b): Gamma ray indication model from Marine Environments (Rider, 2002).

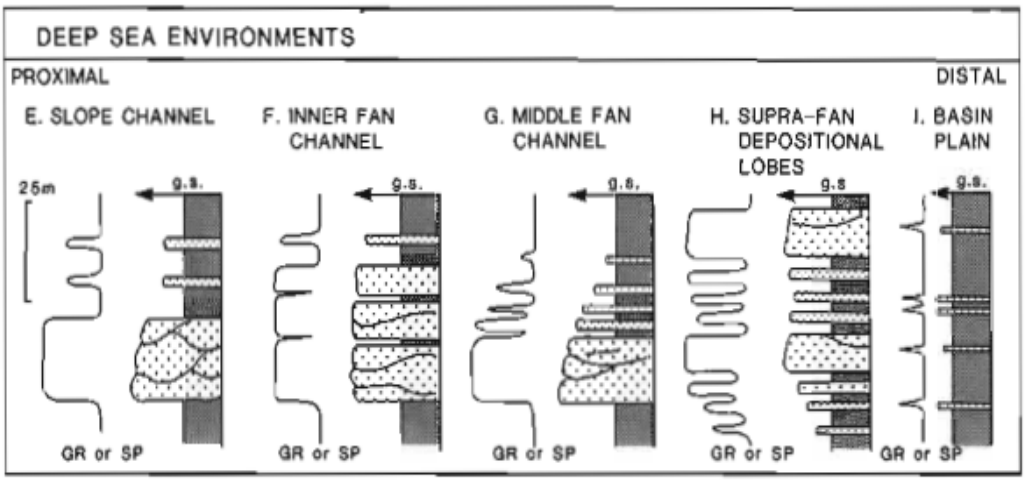

Figure 3.5(c): Gamma ray indication model from Deep Marine Environments (Rider, 2002).

PETROPHYSICS

In this study, petrophysics was carried out to have a better understanding of the reservoir, interconnection of the pore spaces and how they affect the migration and accumulation of hydrocarbons. The rock properties that were studied include lithology, porosity, water saturation, density and permeability. Well logs are often used to perform these measurements.

1. Shale Volume Estimation

Shale volume (Vsh) was calculated using the formula in equation (1) which uses values from the gamma ray (GR) in equation (2)

$$Vsh = 0.083^{(2(3.7\ x\ IGR\ )} - 1.0 \quad (1)$$

$$IGR = \frac{GR_{log} - GR_{min}}{GR_{max} - GR_{min}} \quad (2)$$

2. Porosity Determination

Porosity, ΦD is the percentage of voids to the total volume of rocks. This parameter was determined by substituting the bulk density readings obtained from the formation density log within each reservoir into equation (3)

$$\Phi_D = \frac{\rho_{ma} - \rho_b}{\rho_{ma} - \rho_f} - Vsh\ \frac{\rho_{ma} - \rho_b}{\rho_{ma} - \rho_f} \quad (3)$$

Where ρ_{ma}, ρ_b and ρ_f are matrix density, formation bulk density and fluid density respectively.

3. Water Saturation Calculation

For the calculation of water saturation, Sw of uninvaded zone, the water resistivity, Rw value at formation temperature from the porosity and resistivity logs within the clear water zone was used.

$$Rw = \frac{\Phi^m - R_o}{a} \quad (4)$$

Where RO and Φ are the deep resistivity and total porosity values in the water zone respectively. Turtuosity factor is represented as “a” and m is the cementation factor usually 2 for sands.

Water saturation was calculated using the Archie's method given by:

$$Sw = \left(\frac{R_w}{R_{wa}}\right)^{\frac{1}{n}} \quad (5)$$

Where n is the saturation exponent and Rwa is water resistivity in the zone of interest calculated in the same manner as Rw at formation temperature

4. **Hydrocarbon Saturation Calculation**

Hydrocarbon Saturation, Sh is the percentage of pore volume in a formation occupied by hydrocarbon. It was determined by the subtraction of the water saturation value from 100%

$$Sh = (100 - Sw)\ \% \quad (6)$$

5. **Permeability Calculation**

Permeability, K is the property of a rock to transmit fluids. It was calculated using equation (7)

$$K = \sqrt{\frac{250\ x\ \Phi^2}{S_{wirr}}} \quad (7)$$

Where Swirr is the irreducible water saturation

3.3.4 WELL-TO-SEISMIC TIE

Well-to-seismic tie is the process of tying your well to your seismic data with accurate synchronization of seismic horizons to well tops as seen in Figure 3.8. To perform the well-to-

seismic tie, a synthetic seismogram was generated and matched to a real seismic trace thereafter features from the well were then correlated to the seismic data. The procedures for this process are:

1. Editing and calibrating the sonic and density logs. This process is simply referred to as the sonic log calibration.
2. Construction of the synthetic seismogram from the calibrated well-logs by choosing the appropriate reflection series (usually p-waves) and constructing this series in two-way-time.
3. Performing the match. In doing this, the best match location is determined.
4. After the well-to-seismic tie is done, the quality of the tie can be adjusted by
   a. Experiment on the wavelet e.g. zero-phase, minimum-phase, ricker, etc
   b. Bulk shift
   c. Squeeze
   d. Stretch

SONIC LOG CALIBRATION

The sonic log calibration (Figure 3.6) is the process of bringing the sonic log into agreement with the seismic times. Practical and theoretical analysis of the factors that influence the accuracy of well ties shows that timing is paramount (White 1997). Timing errors in the synthetic seismogram are very unfavorable in estimating correctly the higher frequency components of the seismic wavelet. Well-log calibration establishes the timing of the synthetic seismogram. Sonic log calibration started with picking checkshot times. Thereafter knee points were chosen. Knee points have to be chosen at major jumps in the sonic log so as to avoid introducing artificial or abnormal reflection coefficients. Note that calibration points often show sudden bends at unconformities. Changes in character of the logs and knee points allow direct control of the calibration. Drift curve was applied to the sonic log.

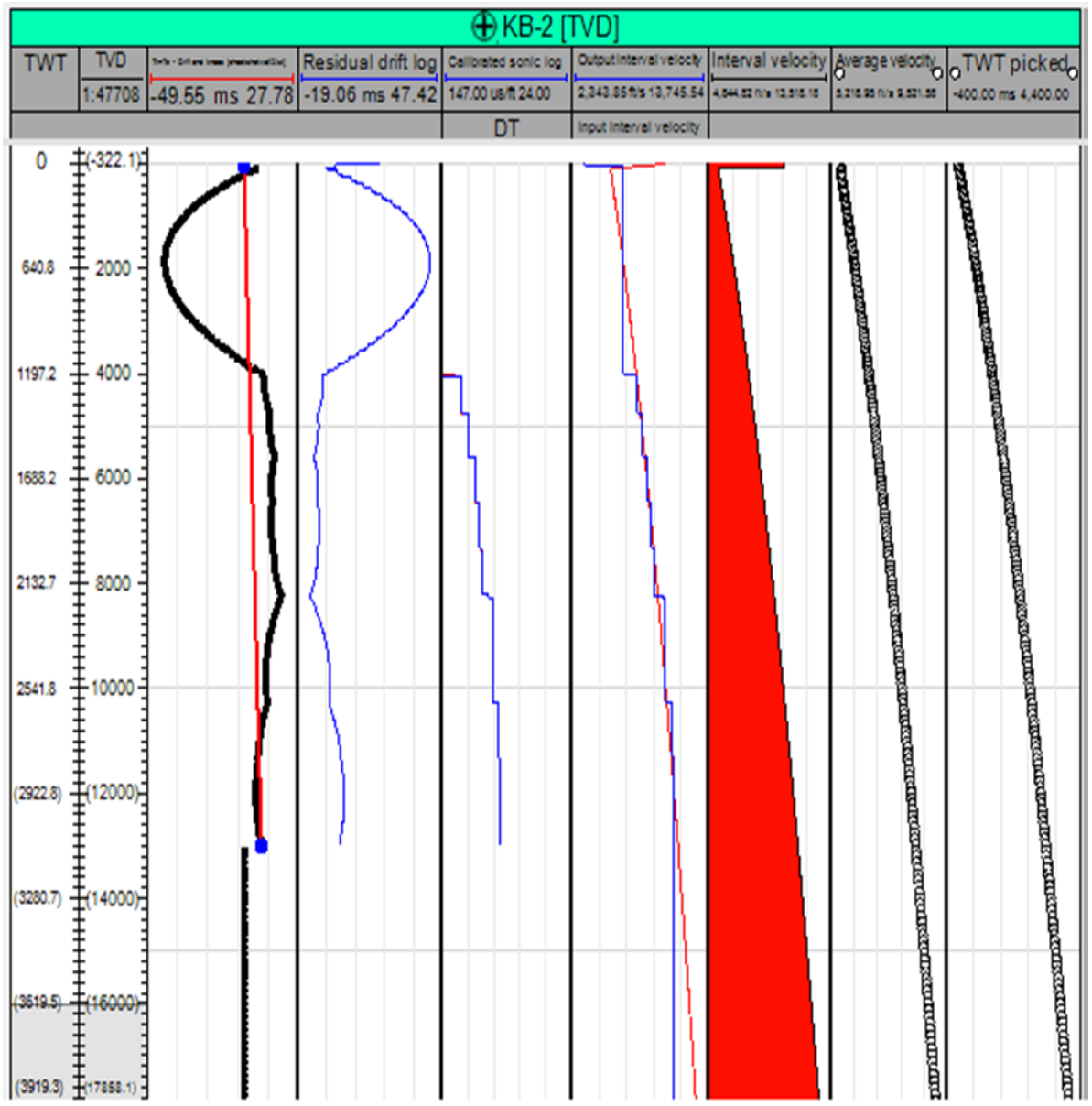

Figure 3.6: The Sonic log calibration of well KB-2.

SYNTHETIC GENERATION

At the start of every seismic interpretation, there must be an attempt to tie seismic reflectors to geologic units through synthetic seismograms. The first goal in seismic data interpretation is to ensure that the well seismic and the surface seismic at the well trajectory look as similar as possible. After this is done, events in the well log and on the surface seismic can be linked thereby subsequently correlating structures and evaluating properties between wells. Figure 3.7(a) and Figure 3.7(b) shows the synthetic seismogram generated in this study.

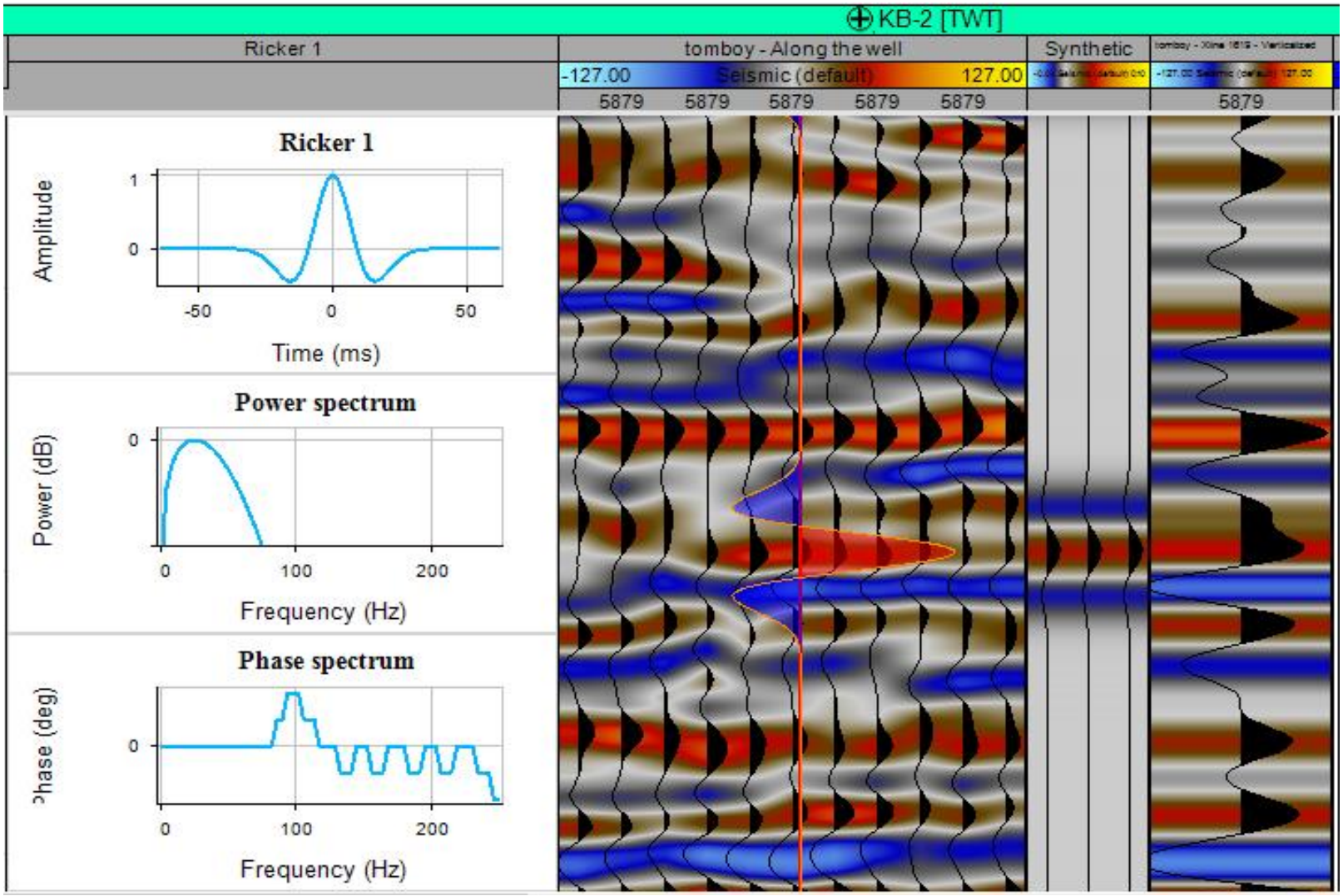

Figure 3.7(a): Synthetic seismogram from well KB-2.

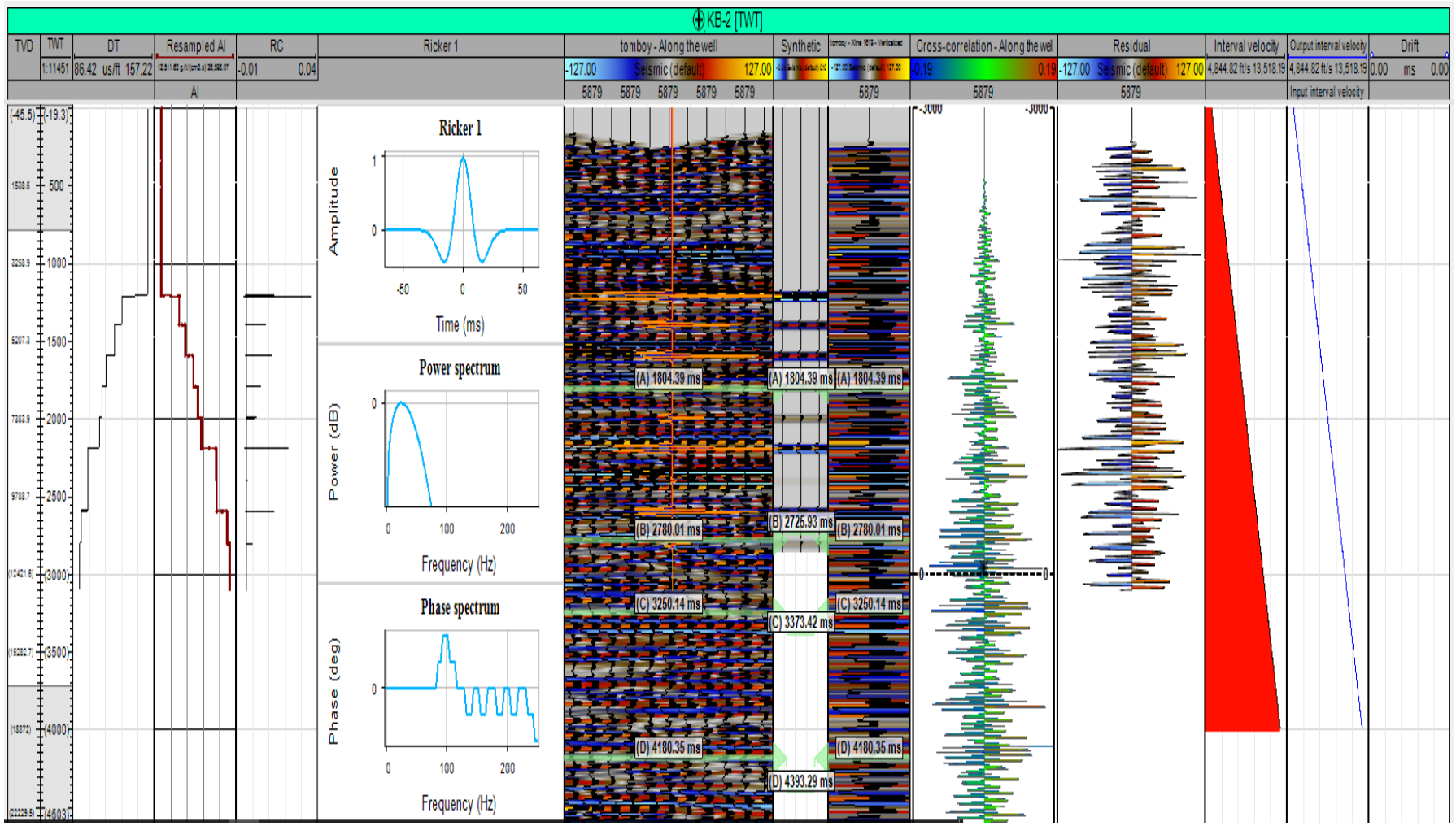

Figure 3.7(b): Synthetic seismogram from well KB-2.

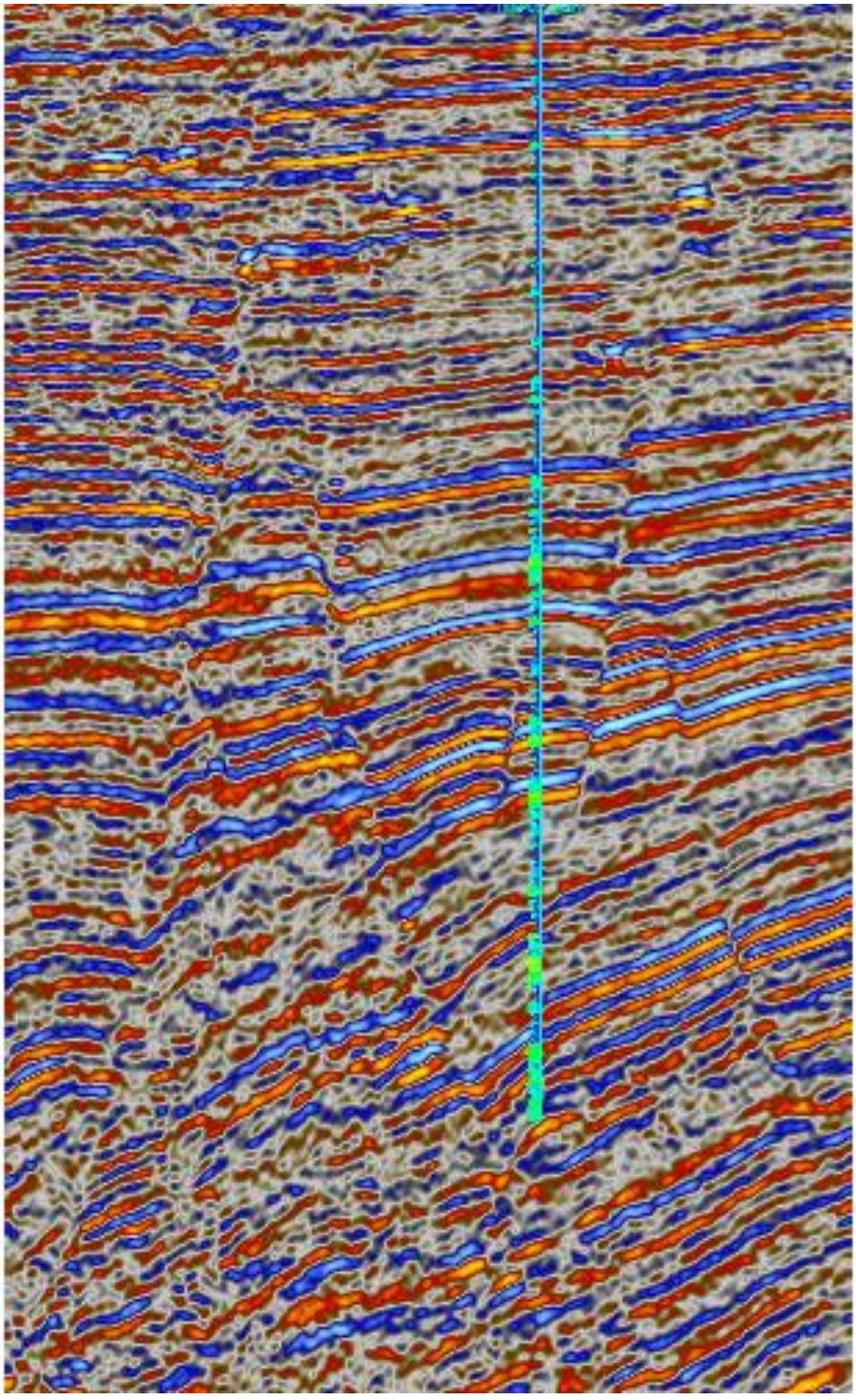

Figure 3.8: Well tied to the seismic data.

3.3.5 FAULT MAPPING

A fault is a discontinuity in a volume of rock across which there has been significant displacement resulting from the movements of rock-mass. Large faults in the Earth's crust are as a result of plate tectonic forces. In this study, it was essential to map out fault networks on the seismic data. Faults were mapped along the in-lines before been traced out on the cross-lines. The faults were mapped at a line spacing of 25m along the in-lines. Faults were identified on the seismic sections by observing the following seismic behaviors (Figure 3.9) which serve as an indication of faults:

1. Abrupt terminal of reflection events.
2. Abrupt change in dip along continuous reflections.
3. Obvious displacement along fault plane lines on the seismic section.
4. Breaks in reflection events.
5. Pattern change of reflection events across a fault.
6. Structural deformation in beds above the zone of faulting.

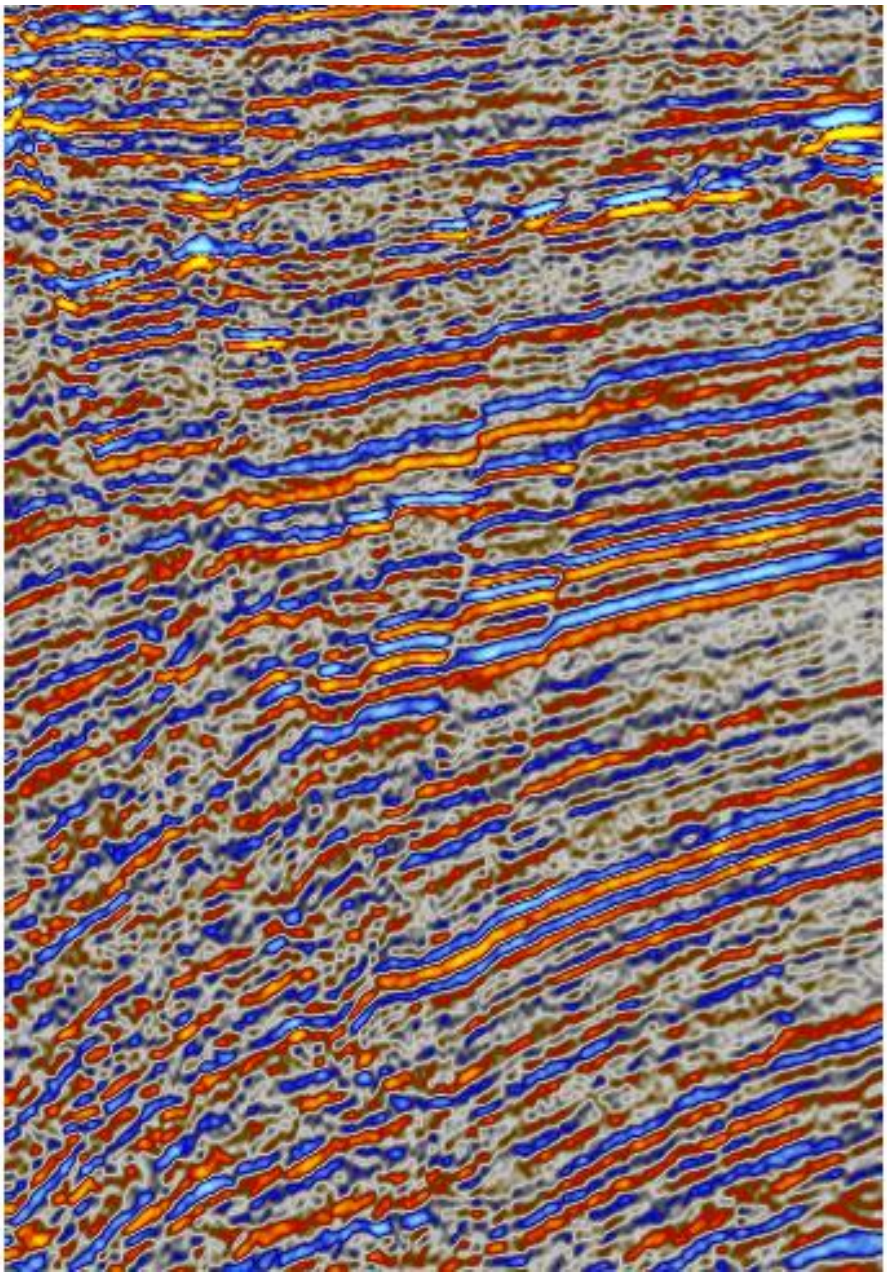

Figure 3.9: Seismic In-line data (Inline 5800) showing discontinuities in amplitude signal.

3.3.6 HORIZON MAPPING

The horizon mapping was done after the faults were mapped. Before mapping horizons, seismic-to-well tie must be carried out using the generated synthetic well log. This ensures accuracy in the picking of horizons.

3.3.7 TIME MAP GENERATION

After the mapping of the various horizons, the time map for each horizon was generated. The time map is characterized by contour lines which show points of equal elevation. Points of equal elevation are also characterized by the same colour.

3.2.8 TIME-DEPTH CONVERSION

The time-depth conversion was carried out using Microsoft Excel 2013. The Checkshot data was used. A Velocity model was plotted with depth (ft) against time (ms-1). Thereafter, a trendline was generated. Afterwards, a 2nd order polynomial equation for the trendline was generated which was used in the time map to depth map conversion. The relationship between time and depth is seen in equation (8)

$$V = \frac{\Delta y}{\Delta x} \qquad (8)$$

Where V is velocity, Δx is change in distance and Δt is change in time.

3.3.9 DEPTH MAP GENERATION

The depth map was generated using the 2nd order polynomial which was generated in the time-depth conversion. The depth map was used in prospects identification and evaluation. The depth map is characterized by contour lines which show points of equal elevations.

3.3.10 ISOPACH MAP GENERATION

Isopach maps were generated to show the thickness between each of the horizons that were interpreted. The isopach maps were characterized by contour lines joining areas of equal elevation and colours which show points of equal elevations.

3.2.11 SEISMIC ATTRIBUTES ANALYSIS

Seismic attributes is any measure of seismic data that helps in visualization of features of interpretation of interest (Marfurt, 2005). Attributes such as amplitude, phase, frequency, polarity and velocity are useful for hydrocarbon indication (Table 2). Attributes such as acoustic impedance, reflectivity and transmissitivity are useful for boundary conditions, hardness and nature of surface (Table 2). Anomalies due to variations in seismic attributes appear in seismic sections as velocity sags, bright spots and flat spots. Seismic attributes are useful in geological interpretations for defining lithological contrast, bed spacing and thickness, bedding continuity, depositional environment, gross porosity, fluid content, abnormal pressure, temperature and polarity of seismic. Sheriff (1980), Chambers and Yarus (2002).

The seismic attributes analyzed in this study includes RMS Amplitude, sum of amplitudes, sum of energy and average instantaneous phase.

Table 2 shows the geological significance of the various seismic attributes that were analyzed.

Seismic attributes	Geological significance
Amplitude	Lithological contrast Bedding continuity Bed spacing Gross porosity Fluid content
Average instantaneous frequency	Bed thickness Lithological contrast Fluid content
Reflection strength	Lithological contrast Bedding continuity Bed spacing Gross porosity
Average instantaneous phase	Bedding continuity

Geological significance of seismic attributes (Schlumberger, 2009)

3.2.12 PROSPECT IDENTIFICATION

Identification of hydrocarbon can be done by locating areas of reducing contour values and deciding its configuration, whether a four way closure, fault assisted or fault dependent. Identification of prospects can be supported using seismic attributes.

3.3.13 VOLUMETRIC ESTIMATIONS

The volumetric estimation requires the volume of the reservoir to be calculated using the maps and the petrophysical parameters of the particular reservoir. Volumetric estimated was carried out to find the Oil originally in place (OOIP), original gas in place (OGIP) and Stock tank oil initially in place (STOIIP).

$$STOIIP = GRV * NTG * Porosity * (1-Sw)/FVF \quad (9)$$

CHAPTER FOUR

RESULTS AND DISCUSSION

4.1 INTRODUCTION

In this chapter, the reservoirs observed in the various wells, their depositional environments, geological and geophysical properties are presented and discussed. The geological and geophysical properties of the field are presented including the various maps and models. All the maps are presented, tested and prospects are identified and reservoir volumes are estimated in this chapter.

4.2 WELL CORRELATION AND EVALUATION

4.2.1 WELL CORRELATION

A lithostratigraphic correlation was carried out across all the wells as seen in Figure 4.1(b) which was done by mapping out the top and base of each reservoir unit. 8 reservoirs units were correlated which includes Sand A, Sand B, Sand C, Sand D, Sand E, Sand F, Sand G and Sand H. The direction of correlation was determined by drawing a composite line from west to east linking close wells together as seen in Figure 4.1(a). The correlation is flattened on the base of the continental Benin Formation. The correlated stratigraphy shows almost uniform layer thicknesses across the field for most of the levels. However, sand F indicates marked variation in thicknesses with the thickness part centred around KB-5 (well 5). The thickest part of sand F is interpreted as channel or the deeper part of a channel. Such a layering scheme shown in this correlation depicts a coastal to shoreface depositional environment. A discontinuity of sand G was observed in well KB-5 which is suspected to be due to erosion of layer.

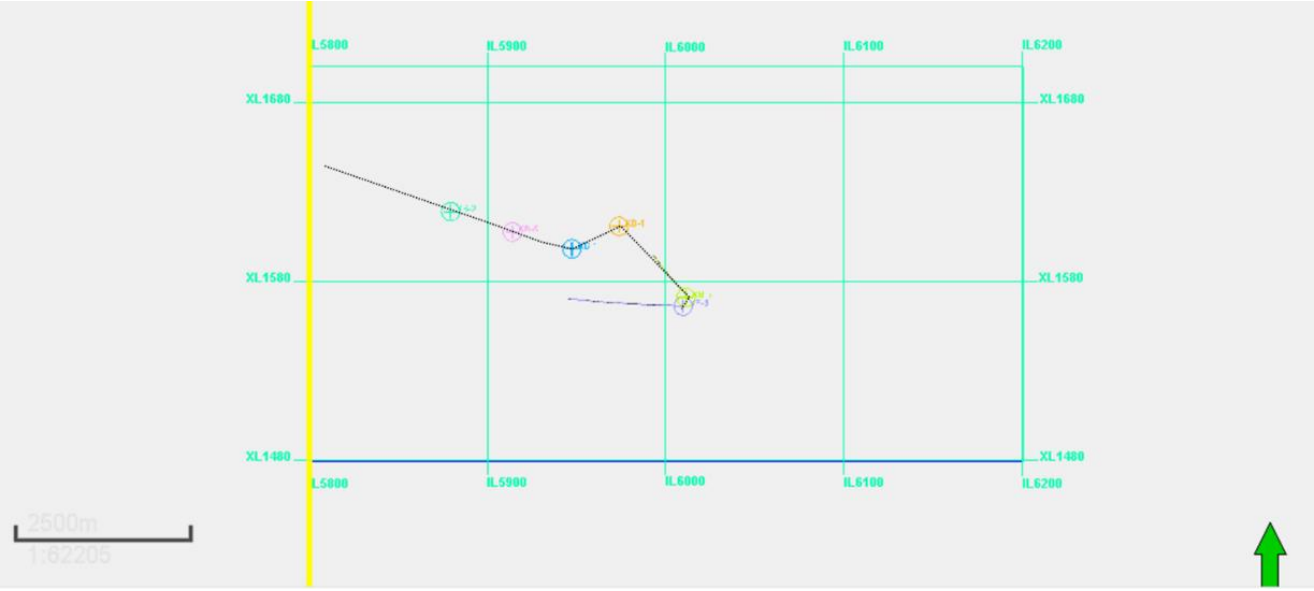

Figure 4.1(a): Composite line drawn across the various wells showing the direction in which the correlation was carried out.

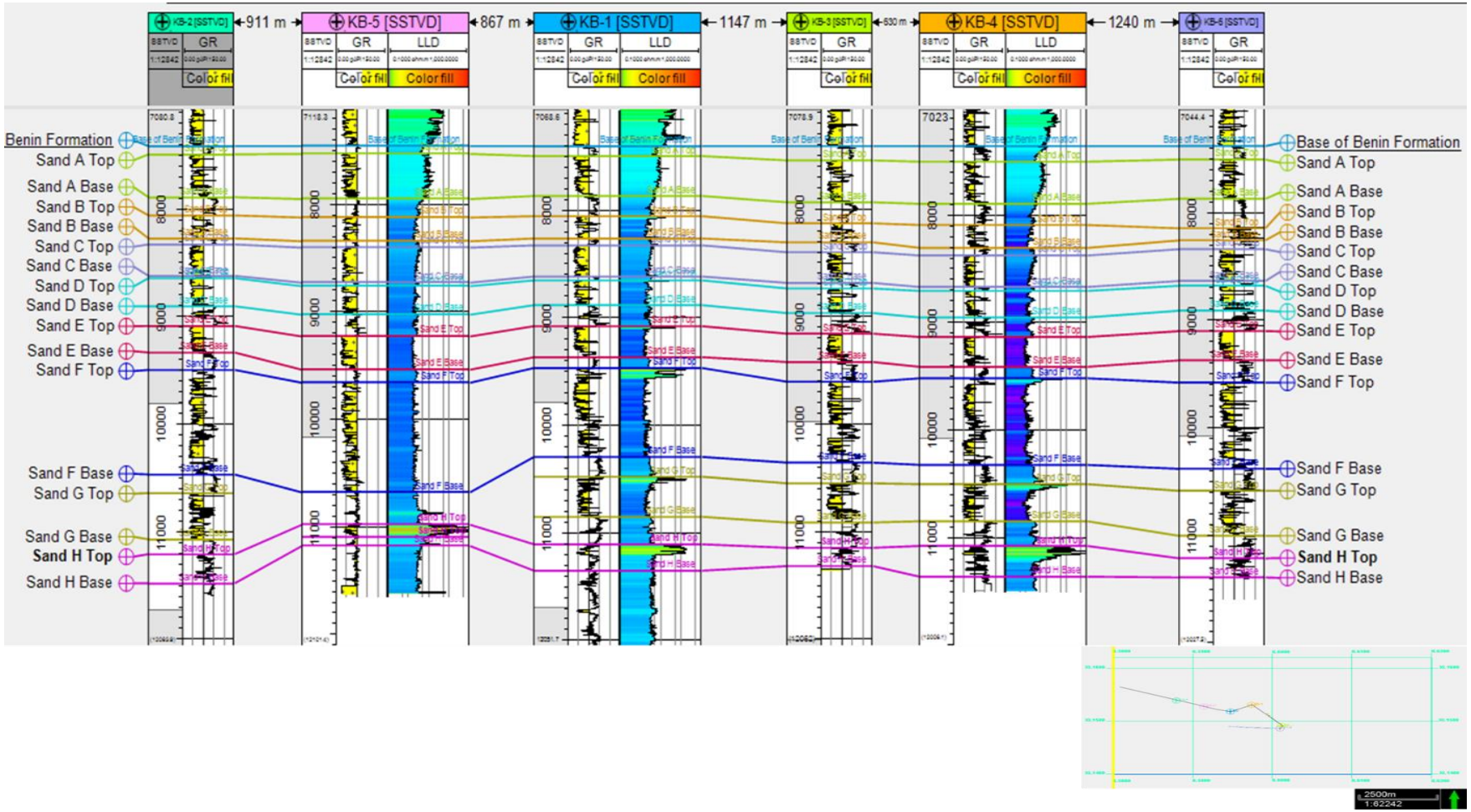

Figure 4.1(b): Lithostratigraphic correlation across all wells showing the top and base of the reservoirs correlated and a diagram showing the direction in which the correlation was done.

4.2.2 DEPOSITIONAL ENVIRONMENTS

The depositional environments for all the sands were investigated and the results are presented below. A summary of the results obtained is presented in Table 3.

Sand A

Sand A has an average thickness of about 400ft across all wells. The gamma ray signature in figure shows a funnel shape succession as shown in Figure 4.2(a). The funnel shape indicates coarsening upwards of sediments and is most likely associated with a channel-fill. Sand A represents a period of high energy deposition.

Sand B

Sand B has an average thickness about 200ft across all wells. The gamma ray log indicates a blocky non-serrated profile as shown in Figure 4.2(b). This profile indicates an aggradational stacking pattern, and probably deposited in a channel.

Sand C

Sand C has an average thickness of about 290ft across all wells. The gamma ray log indicates a blocky, slightly serrated profile indicating an aggradational stacking pattern as shown in Figure 4.2(c). This stacking pattern is most likely associated with a coastal environment such as a channel-fill.

Sand D

Sand D has an average thickness of about 260ft across all wells. The gamma ray log indicates a blocky slightly serrated profile as shown in Figure 4.2(d). This profile indicates an aggradational stacking pattern which is associated with a channel-fill. The top of sand D indicates a flooding surface.

Sand E

Sand E has an average thickness of about 300ft across all wells. The gamma ray log indicates a funnel-shaped succession as shown in Figure 4.2(e). The funnel shape indicates a coarsening upwards of sediments with increasing energy of deposition and can be classified as a prograding marine shelf environment.

Sand F

Sand F has an average thickness of about 1000ft across all wells. The gamma ray log indicates a blocky, highly serrated profile as shown in Figure 4.2(f). This indicates an aggradational stacking pattern. This stacking pattern is most likely associated with a channel-fill.

Sand G

Sand G has an average thickness of about 400ft across all wells. There is a discontinuity of Sand G in well TMB-05. This can be due to faulting. The gamma ray response shows a funnel-shaped succession which is very serrated as shown in Figure 4.2(g). The funnel-shaped response indicates coarsening upwards of shallow sediments with increasing energy of deposition and can be termed as a prograding marine shelf environment.

Sand H

Sand H has an average thickness of about 190ft across all wells. The gamma ray log indicates a funnel- shaped succession which is highly serrated as shown in Figure 4.2(h). The funnel-shaped response indicates coarsening upwards of shallow sediments with increasing energy of deposition and can be inferred to as a prograding delta border.

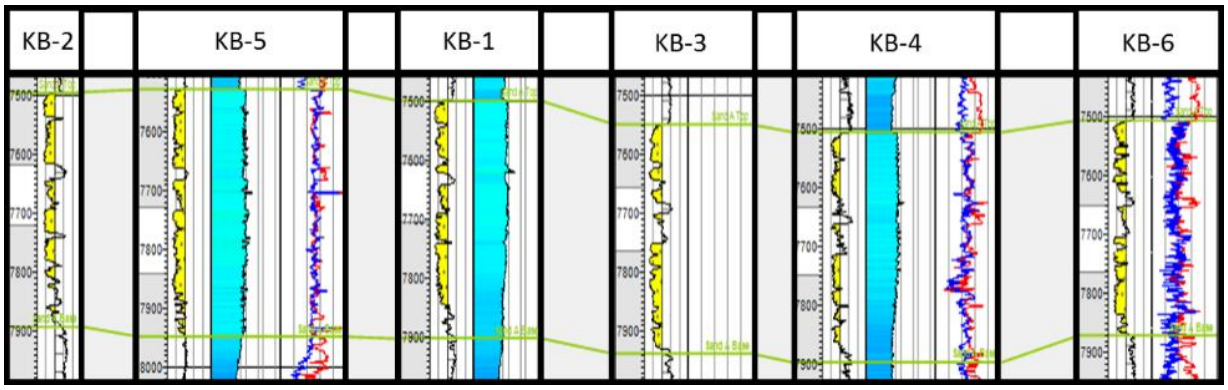

Figure 4.2(a): Correlation of sand A across all wells.

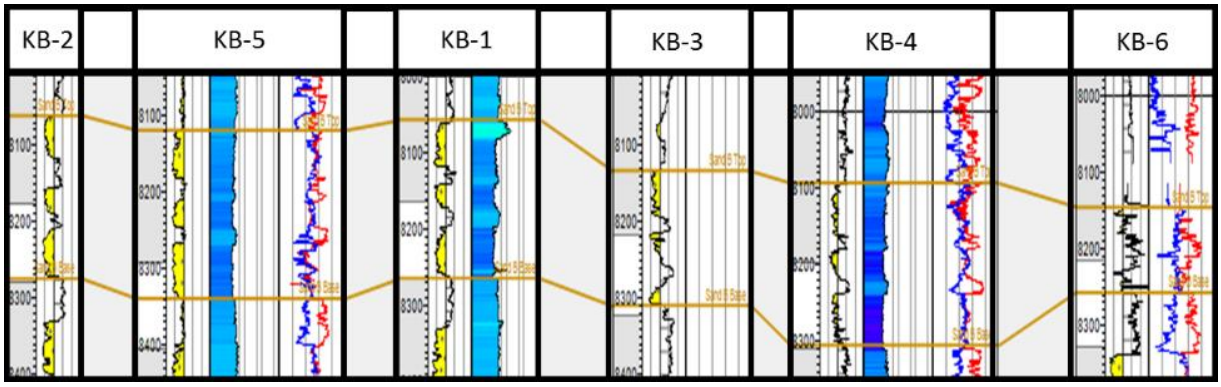

Figure 4.2(b): Correlation of sand B across all wells.

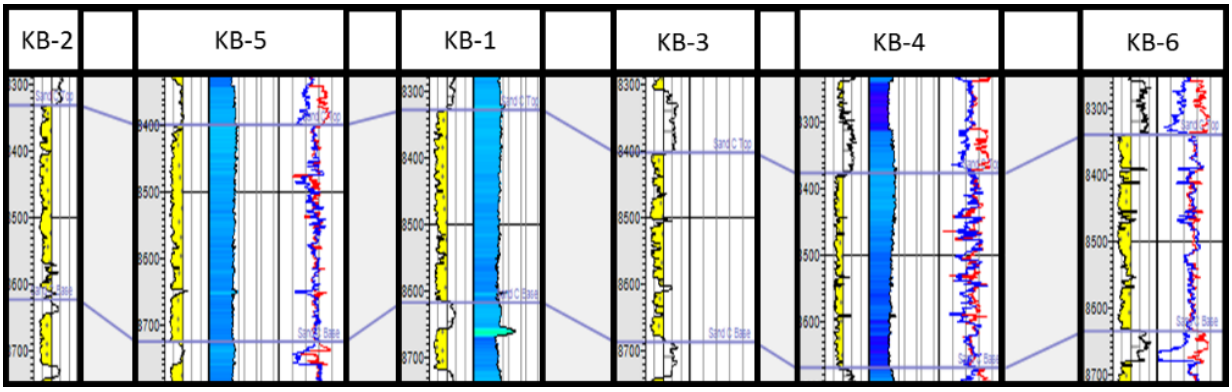

Figure 4.2(c): Correlation of sand C across all wells.

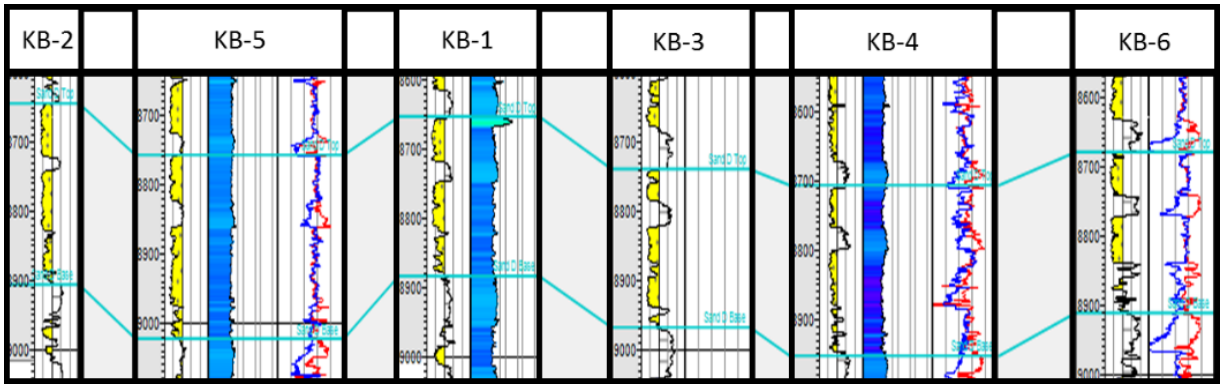

Figure 4.2(d): Correlation of sand D across all wells.

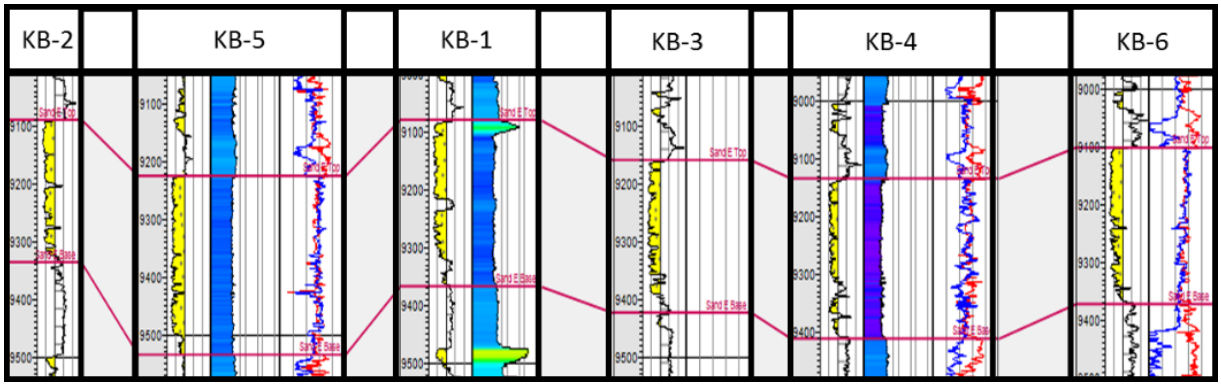

Figure 4.2(e): Correlation of sand E across all wells.

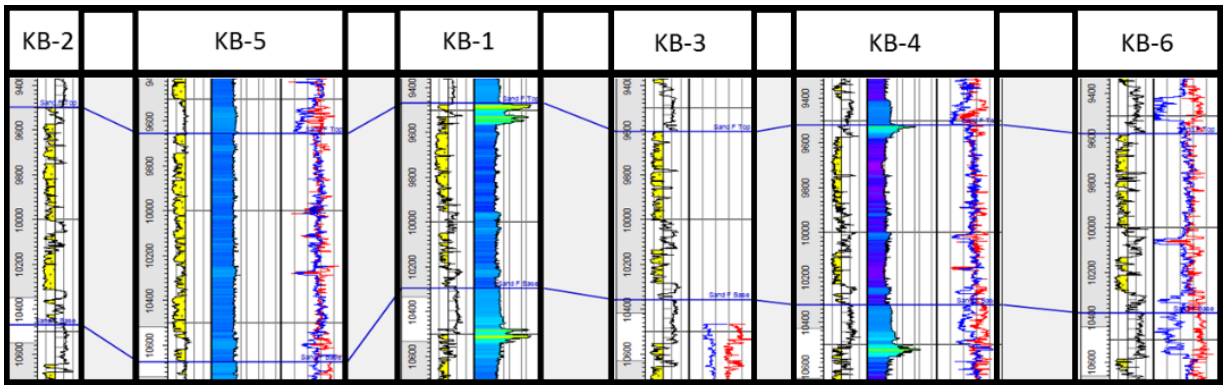

Figure 4.2(f): Correlation of sand F across all wells.

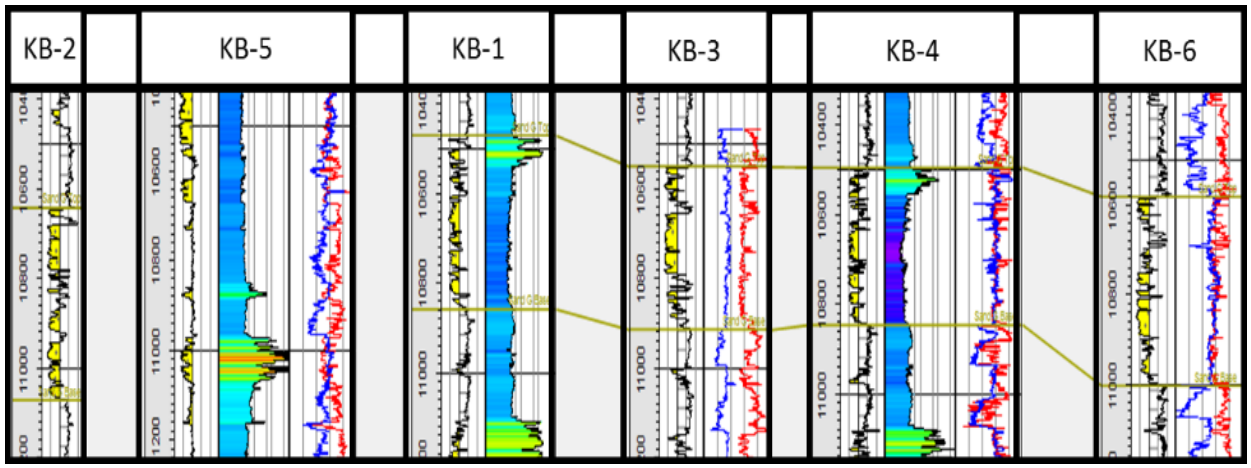

Figure 4.2(g): Correlation of sand G across all wells.

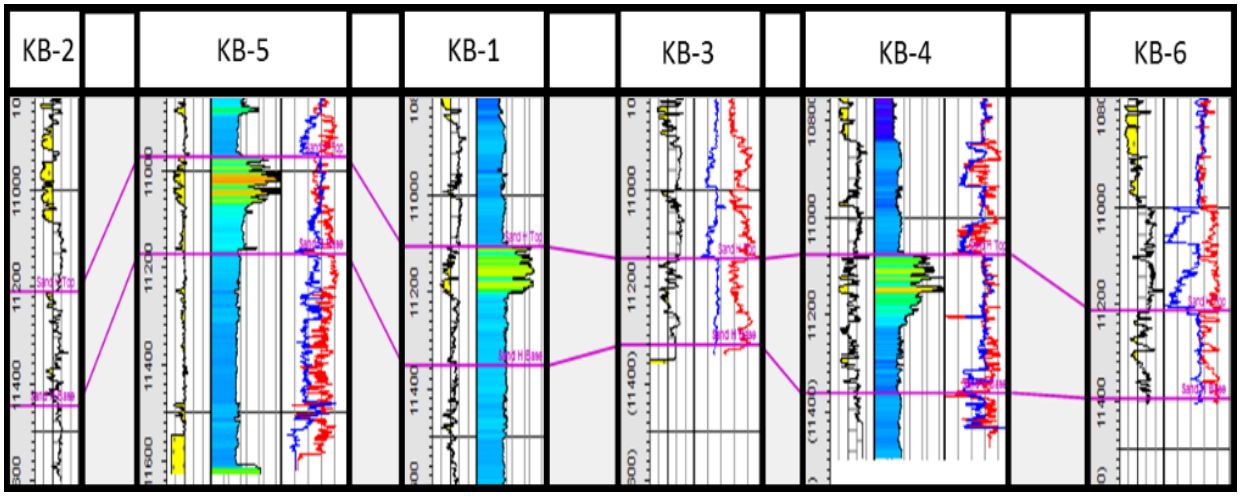

Figure 4.2(h): Correlation of sand H across all wells.

Table 3: Summary of the sands correlated showing their gamma ray log from well TMB-01, their stacking pattern and their depositional environments.

SAND	GAMMA RAY LOG	PATTERN	DEPOSITIONAL ENVIRONMENT
SAND A	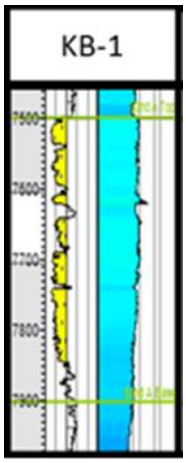	Coarsening upwards	Coastal Environment
SAND B	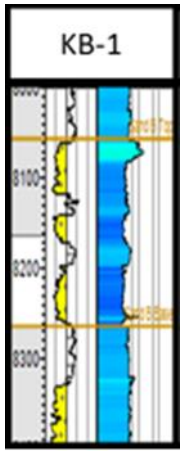	Aggradational stacking pattern	Coastal Environment

SAND C	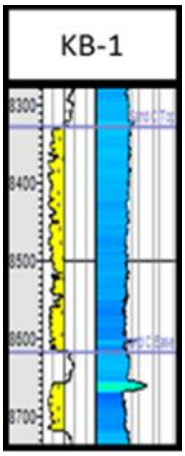	Aggradational stacking pattern with flooding surface.	Coastal Environment
SAND D	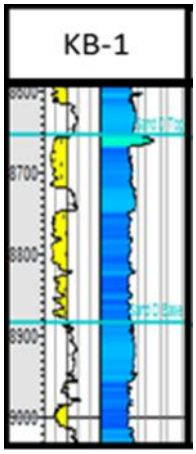	Aggradational stacking pattern with flooding surface.	Coastal Environment
SAND E	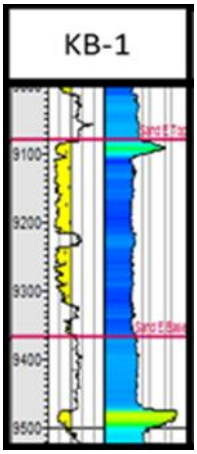	Coarsening upwards	Marine Environment

SAND F	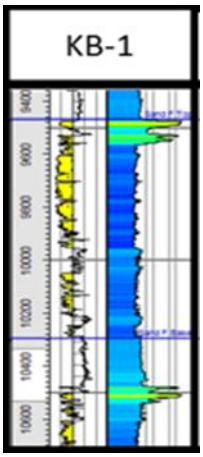	Aggradational stacking pattern	Coastal Environment
SAND G	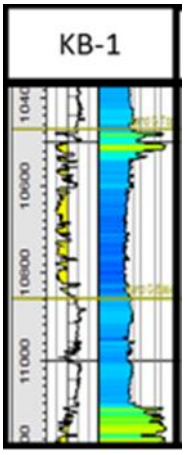	Coarsening upwards	Marine Environment
SAND H	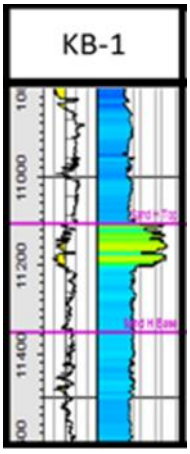	Coarsening upwards	Coastal Environment

4.3 FAULT INTERPRETATION

The faults were mapped on every 16 seismic section. Faults were noticeable mostly on the in-line because they were acquired in a direction that is perpendicular to the regional fault trend. Figure 4.3(a) shows the un-interpreted seismic section while Figures 4.3(b), 4.3(c), 4.3(d) and 4.3(e) show the interpreted faults. 10 faults denoted as F1, F2, F3, F4, F5, F6, F7, F8, F9 and F10 were interpreted from the seismic data (Table 4). Faults F1 and F4 are major faults extending across the whole field known as major regional growth faults, and they are interpreted to be the major faults that bounds the coastal swamp depo-belts from the offshore and central swamp depo-belts (Doust and Omatsola, 1990). Synthetic and antithetic faults were also interpreted from the seismic section.

Table 4: Faults interpreted showing the type of fault, direction of dip and extent across field.

FAULTS	DIRECTION OF DIP	INLINE COVERED	FAULT TYPE
F1	South	5800-6200	Regional growth fault
F2	South	5800-5896	Synthetic fault
F3	North	5800-5944	Antithetic fault
F4	South	5800-6200	Regional growth fault
F5	North	5800-5960	Antithetic fault
F6	South	6020-6200	Synthetic fault
F7	South	5800-5820	Synthetic fault
F8	North	6160-6200	Antithetic fault
F9	South	5800-5820	Synthetic fault
F10	North	5800-5860	Antithetic fault

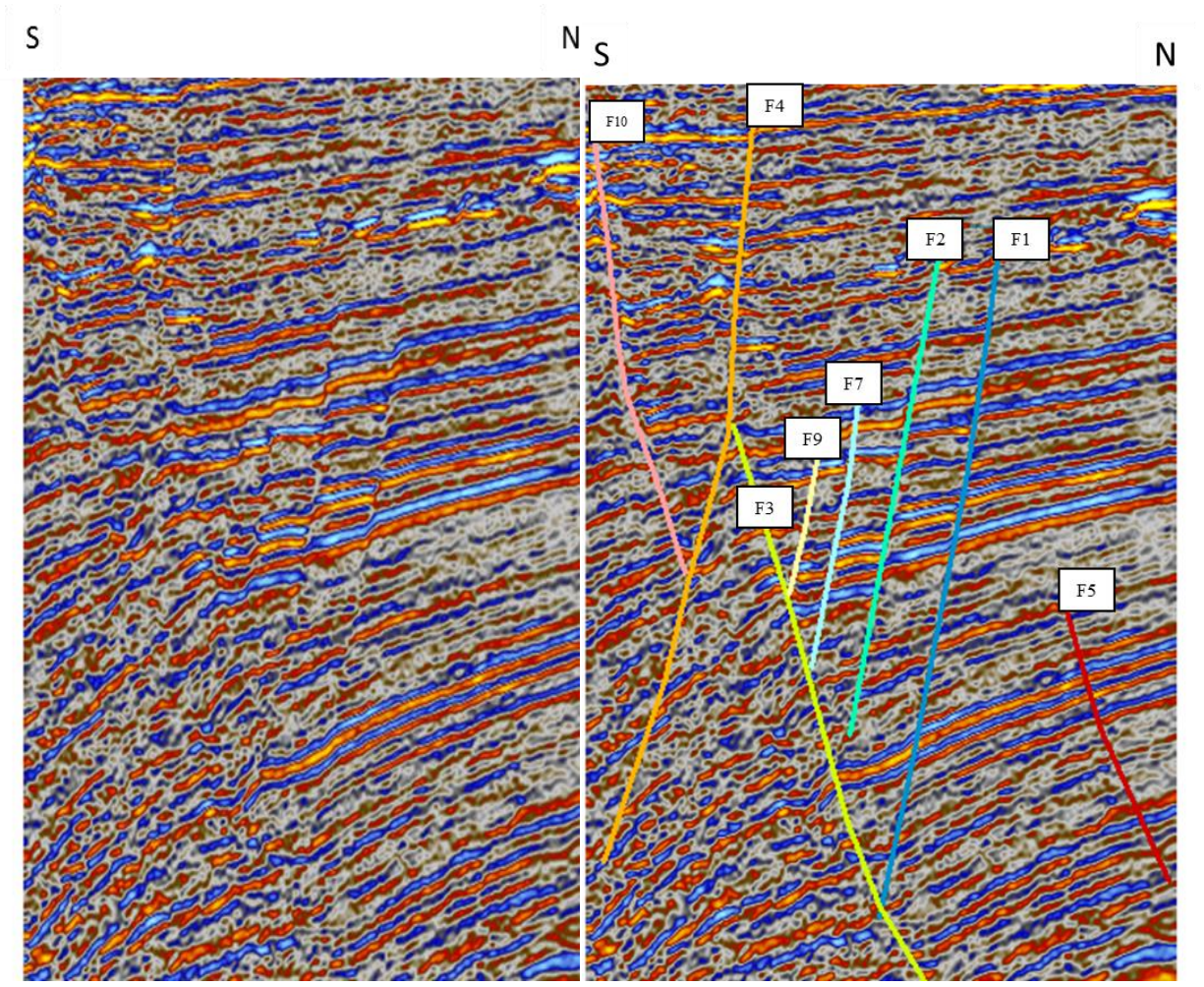

(a) **(b)**

Figure 4.3(a) Un-interpreted Seismic section (Inline 5800) and Figure 4.3(b) Interpreted Seismic section (Inline 5800) showing the faults interpreted.

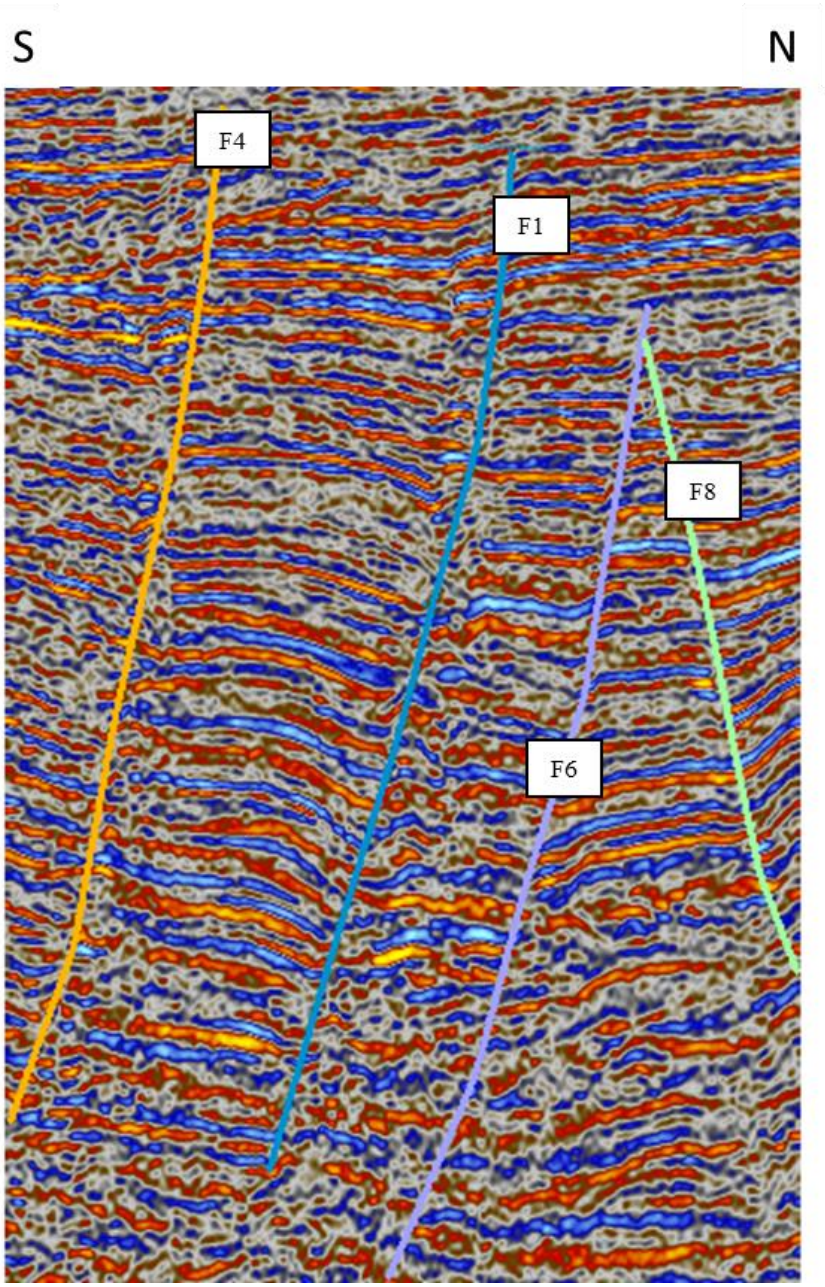

(c)

Figure 4.3(c): Interpreted Seismic section (Inline 6200) showing the faults interpreted.

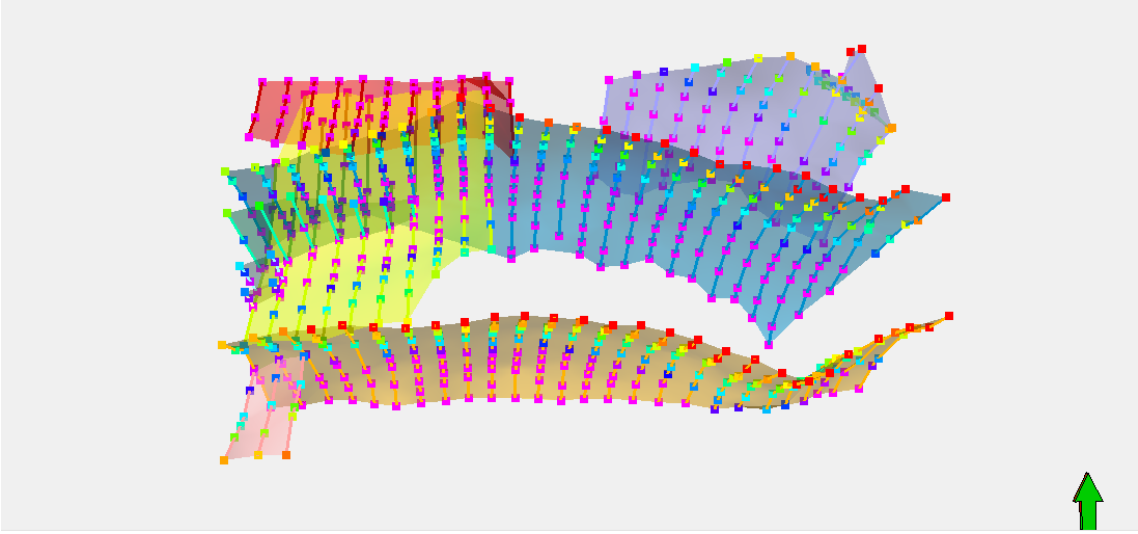

Figure 4.3(d): Interpreted fault sticks in 3D view.

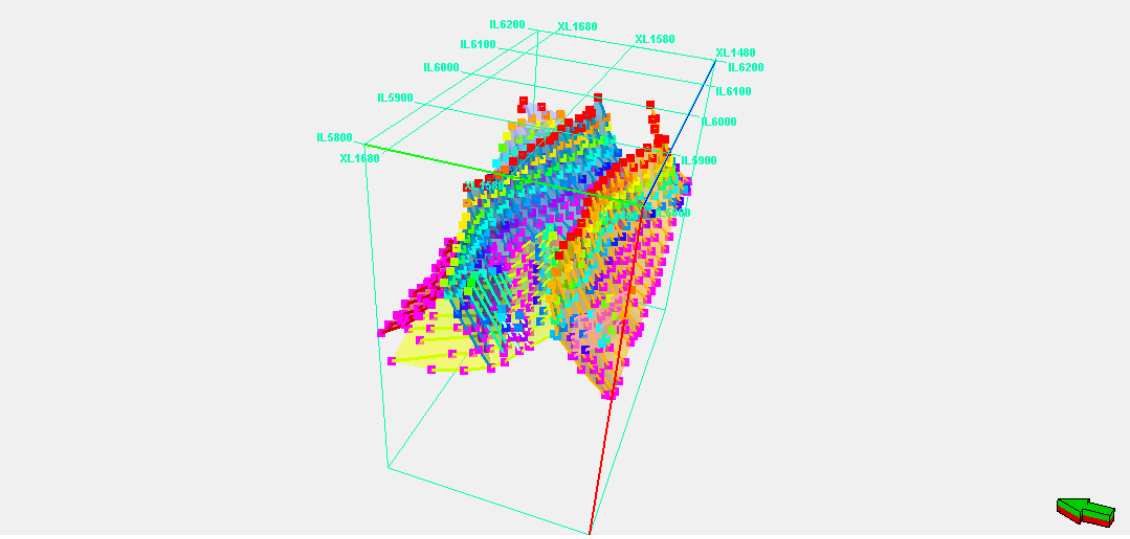

Figure 4.3(e): Interpreted fault sticks in 3D view showing their positions in the survey area.

4.4 HORIZON INTERPRETATION

Six Horizons were interpreted across the field which includes sand A, sand B, sand E, sand F, sand G and sand H as shown in Figure 4.4. Time maps, depths maps and seismic attributes maps such as RMS amplitude, sum of amplitudes, sum of energies and average instantaneous phase were generated for each of these horizons.

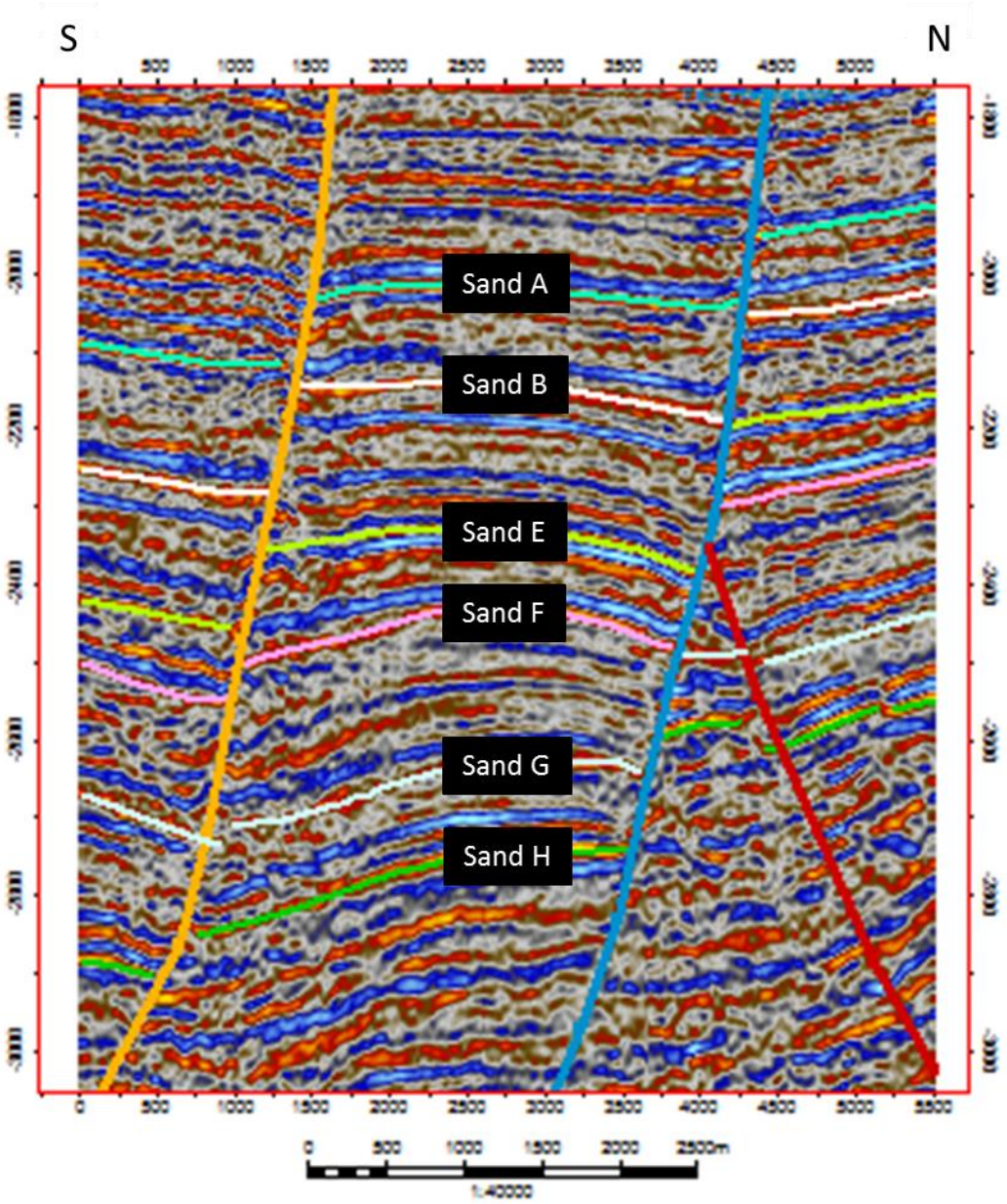

Figure 4.4: Seismic section showing the 6 interpreted horizons including the faults F1, F4 and F5.

4.5 TIME MAPS

4.5.1 SAND A STRUCTURAL TIME MAP

The structural time map for sand A as shown in Figure 4.5(a) is characterized with a contour interval of 5ft. The colors show difference in elevation of the horizon. Four faults (F1, F3, F4 and F6) cut through this horizon.

4.5.2 SAND B STRUCTURAL TIME MAP

The structural time map for sand B as shown in Figure 4.5(b) is characterized with a contour interval of 5ft. The colors show difference in elevation of the horizon. Four faults (F1, F3, F4 and F6) cut through this horizon.

4.5.3 SAND E STRUCTURAL TIME MAP

The structural time map for sand E as shown in Figure 4.5(c) is characterized with a contour interval of 10ft. The colors show difference in elevation of the horizon. Four faults (F1, F3, F4 and F6) cut through this horizon.

4.5.4 SAND F STRUCTURAL TIME MAP

The structural time map for sand F as shown in Figure 4.5(d) is characterized with a contour interval of 10ft. The colors show difference in elevation of the horizon. Four faults (F1, F3, F4 and F6) cut through this horizon.

4.5.5 SAND G STRUCTURAL TIME MAP

The structural time map for sand G as shown in Figure 4.5(e) is characterized with a contour interval of 10ft. The colors show difference in elevation of the horizon. Four faults (F1, F3, F4 and F6) cut through this horizon.

4.5.6 SAND H STRUCTURAL TIME MAP

The structural time map for sand H as shown in Figure 4.5(f) is characterized with a contour interval of 10ft. The colors show difference in elevation of the horizon. Four faults (F1, F3, F4 and F6) cut through this horizon.

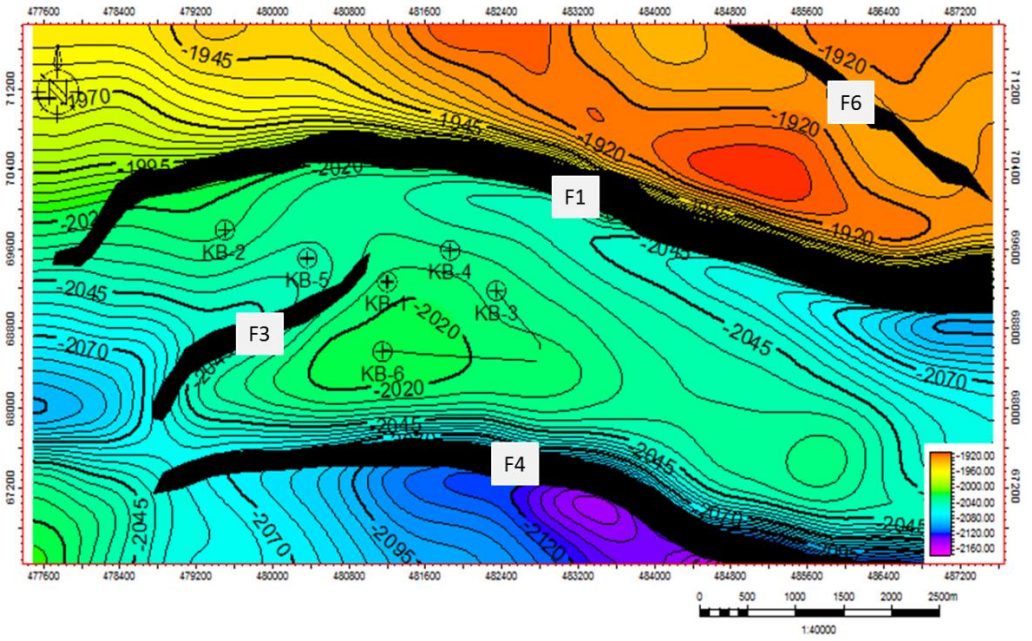

Figure 4.5(a): Structural Time Map for sand A showing the location of all wells and the faults encountered.

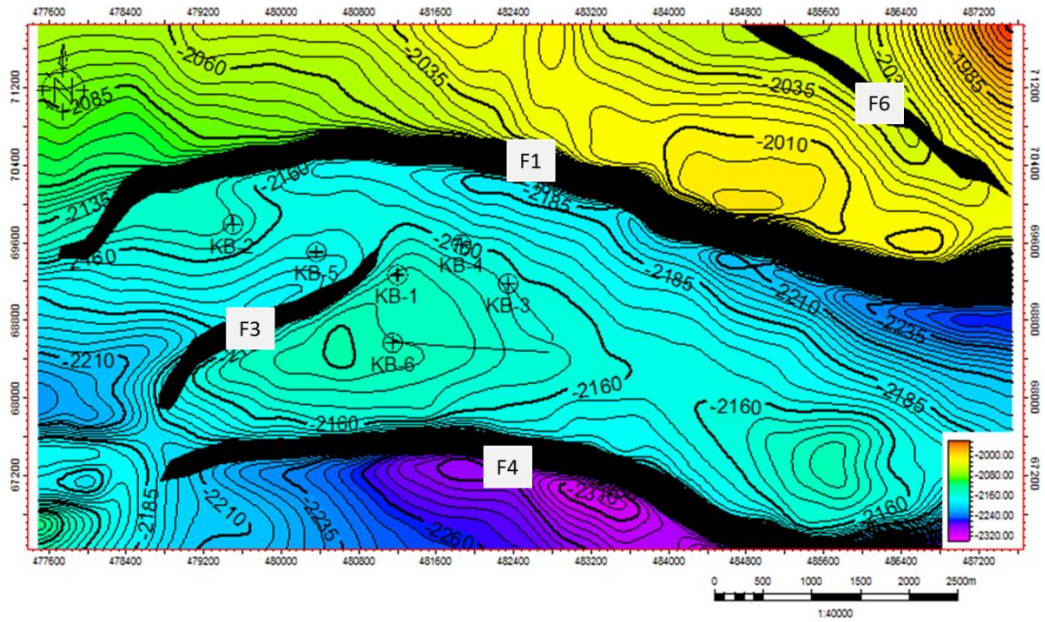

Figure 4.5(b): Structural time map for sand B showing the location of all wells and the faults encountered.

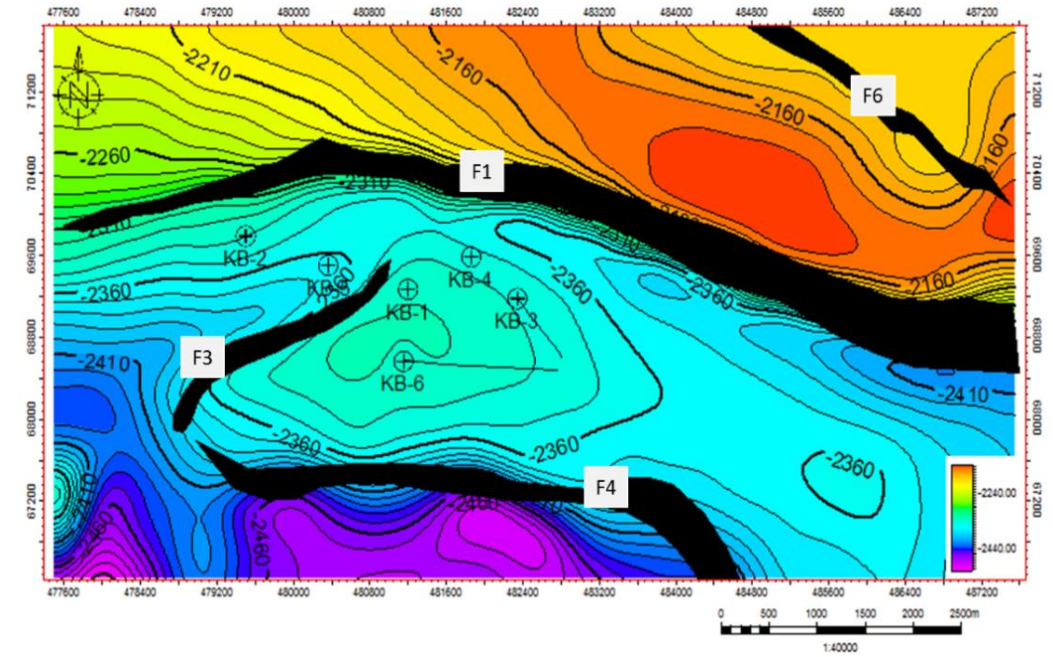

Figure 4.5(c): Structural time map for sand E showing the location of all wells and the faults encountered.

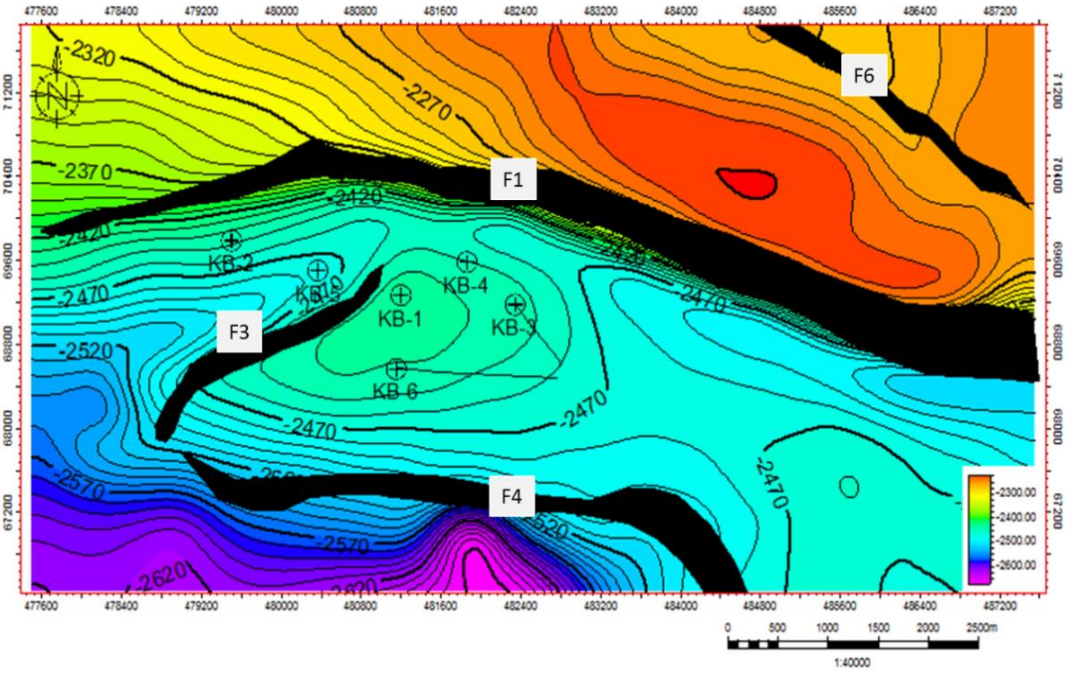

Figure 4.5(d): Structural time map for sand F showing the location of all wells and the faults encountered

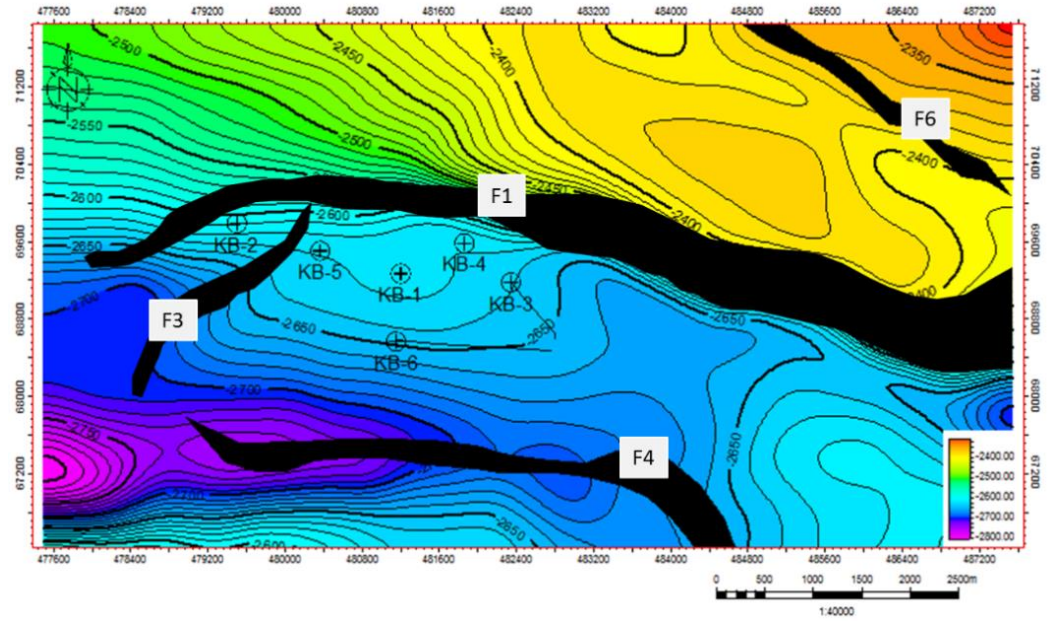

Figure 4.5(e): Structural time map for sand G showing the location of all wells and the faults encountered.

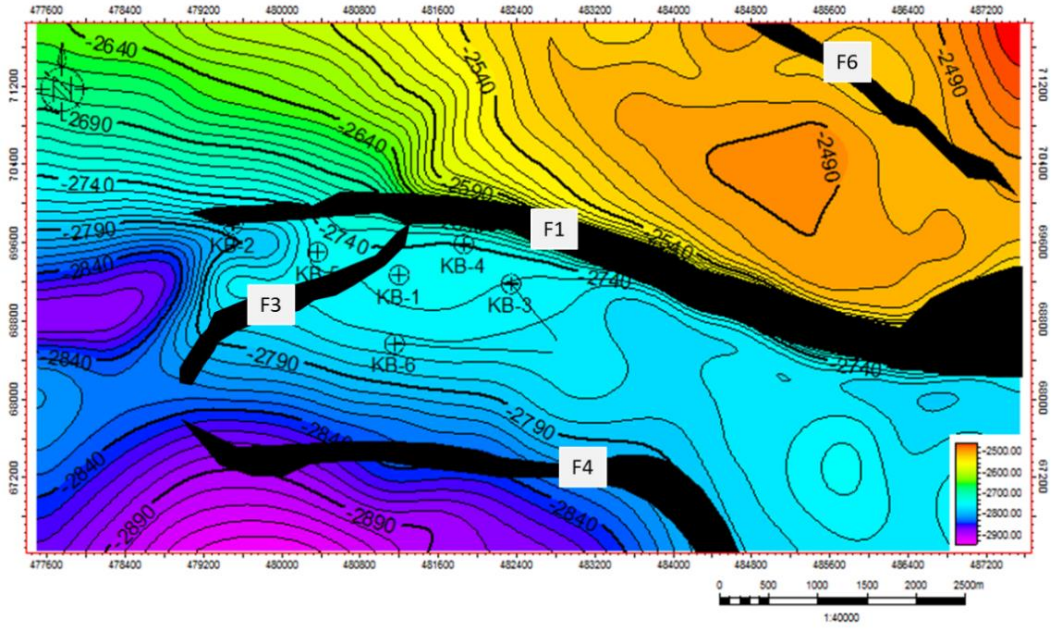

Figure 4.5(f): Structural time map for sand H showing the location of all wells and the faults encountered.

4.6 TIME-DEPTH CONVERSION

Time-depth plot of checkshot data is shown in Figure 4.6. The second order polynomial "y=$0.0005x^2$ + $2.6331x$ + 154.07" was generated from the time-depth plot. It was used for the time-depth conversion, where y=depth from the well data and x=time information from the checkshot data.

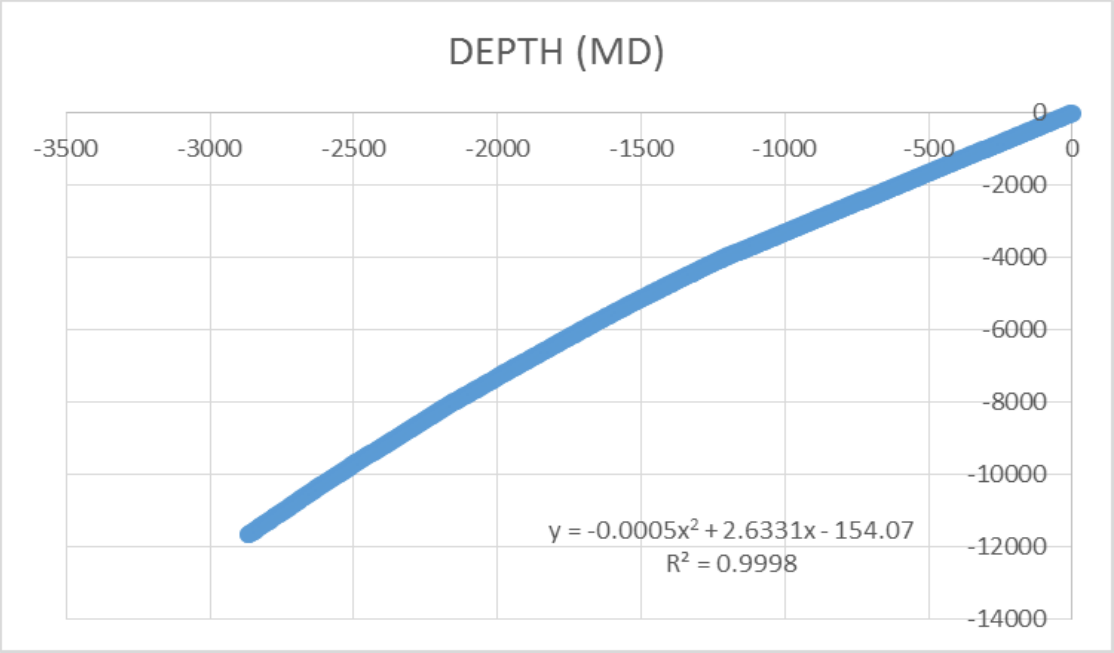

Figure 4.6: Time-depth plot of checkshot data

4.7 STRUCTURAL DEPTH MAPS

4.7.1 SAND A STRUCTURAL DEPTH MAP

The structural depth map for sand A as shown in Figure 4.7(a) is characterized with a contour interval of 20ft. The colors show difference in elevation of the horizon. Four faults (F1, F3, F4 and F6) cut through this horizon. A drilled and tested area is identified on the map alongside two undrilled and prospect areas. The tested area is seen to be a fault assisted closure being assisted by fault F3. The undrilled and prospect areas are both 4-way closures. Figure 4.7(b) shows the sand A structural depth map in 3D view.

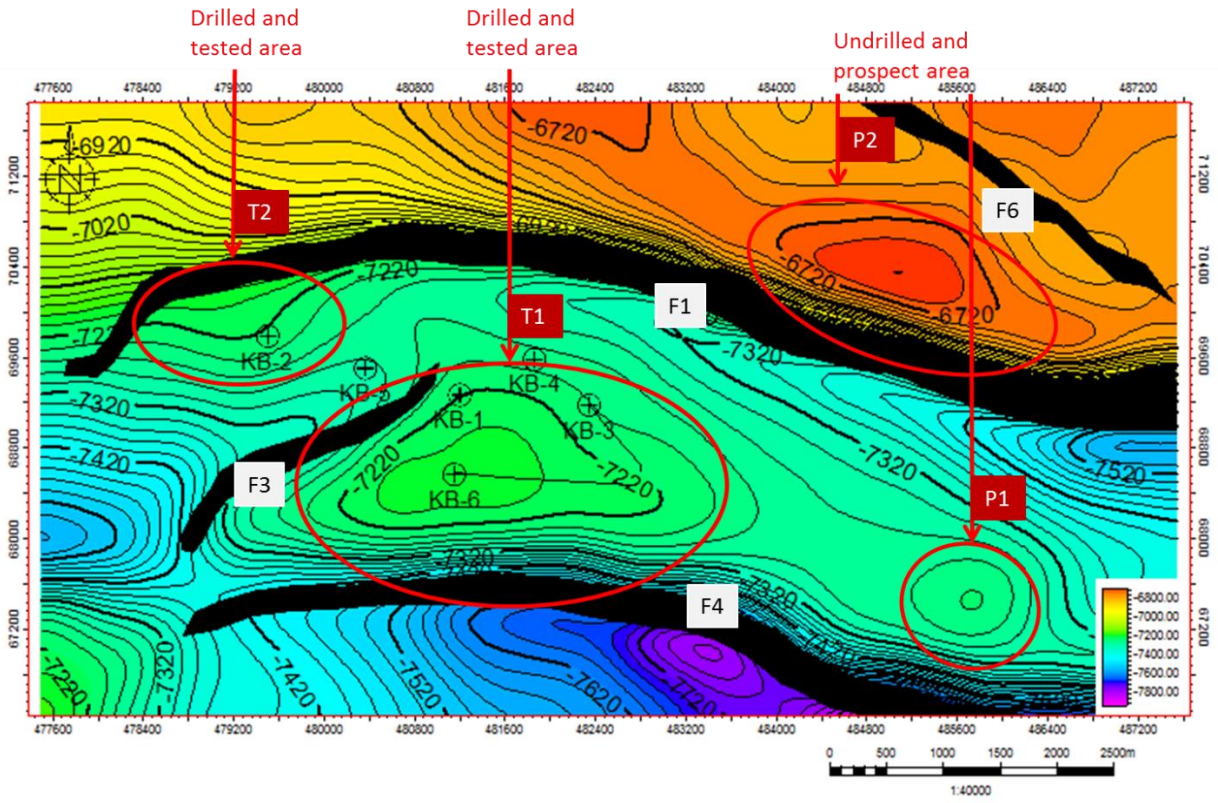

Figure 4.7(a): Structural depth map for sand A showing the tested area and prospect area.

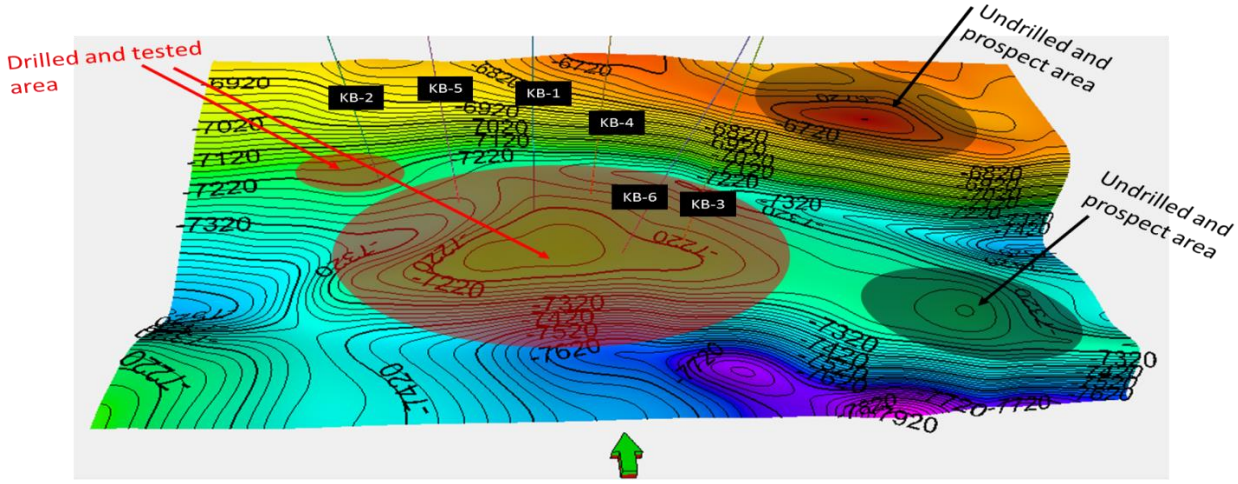

Figure 4.7(b): 3D view of structural depth maps for sand A showing the tested area and prospect area.

4.7.2 SAND B STRUCTURAL DEPTH MAP

The structural depth map for sand B as shown in Figure 4.8(a) is characterized with a contour interval of 20ft. The colors show difference in elevation of the horizon. Four faults (F1, F3, F4 and F6) cut through this horizon. A drilled and tested area is identified on the map alongside two undrilled and prospect areas. The tested area is seen to be a fault assisted closure being assisted by fault F3. The undrilled and prospect areas are both 4-way closures. Figure 4.8(b) shows the sand B structural depth map in 3D view.

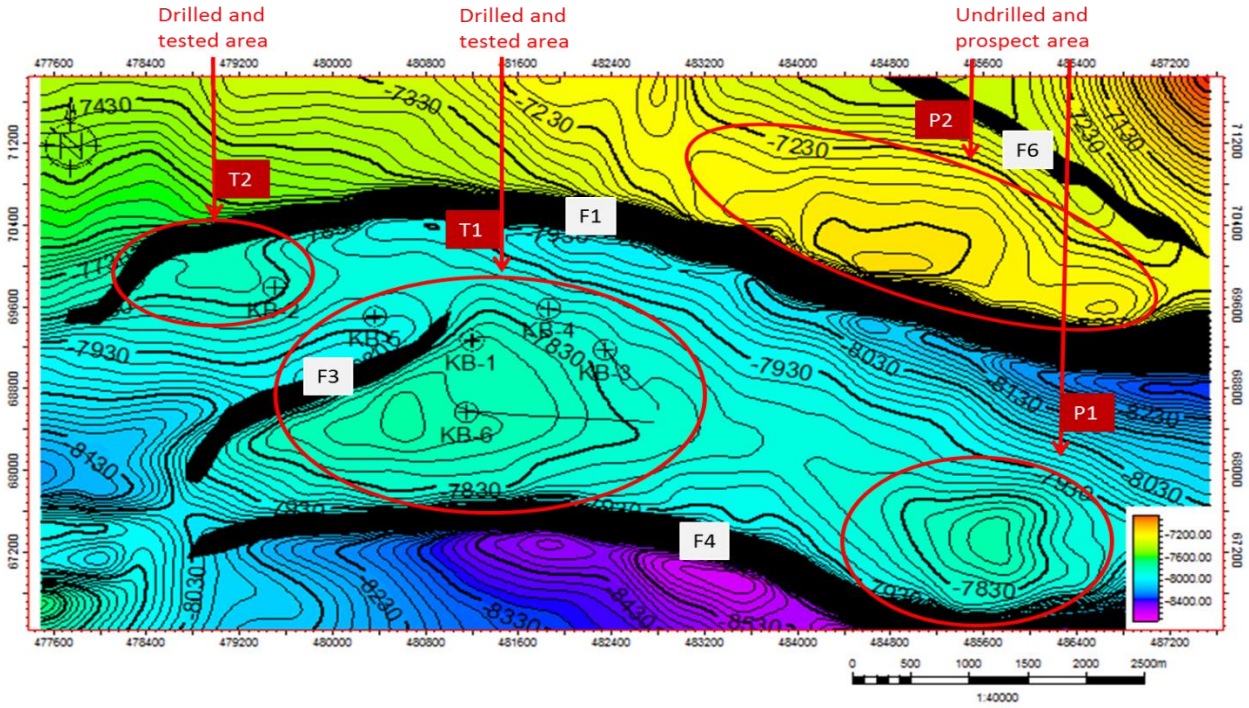

Figure 4.8(a): Structural depth map for sand B showing the tested area and prospect area.

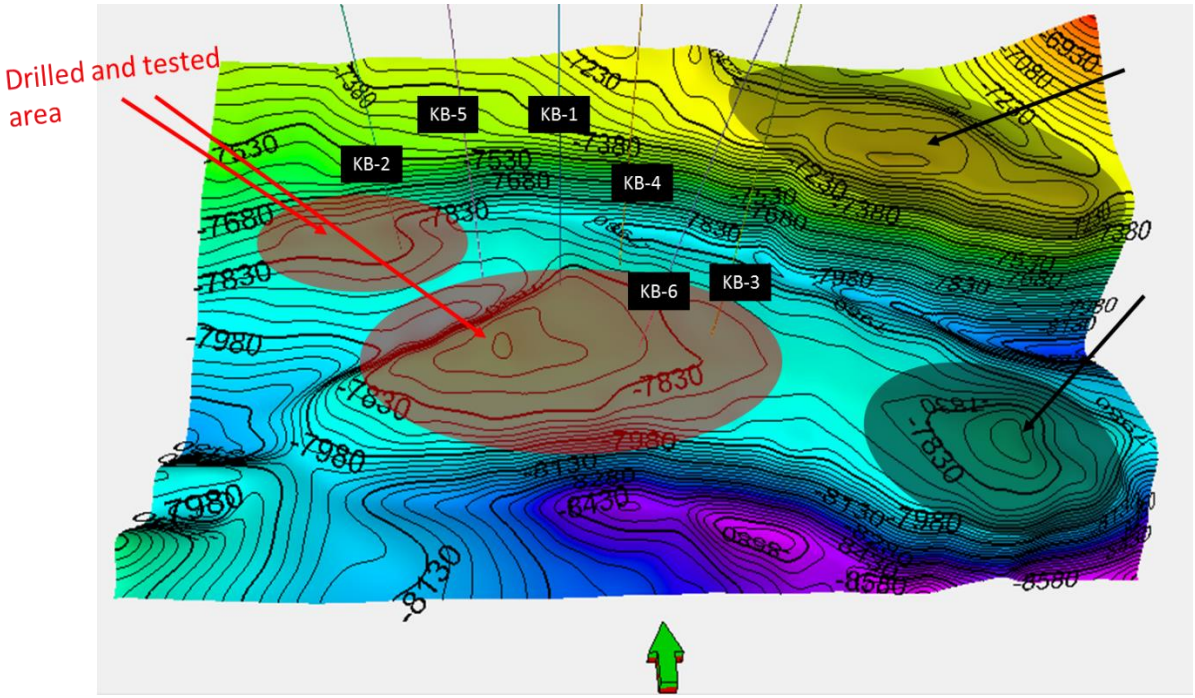

Figure 4.8(b): 3D view of structural depth maps for sand B showing the tested area and prospect area.

4.7.3 SAND E DEPTH MAP

The structural depth map for sand E as shown in Figure 4.9(a) is characterized with a contour interval of 50ft. The colors show difference in elevation of the horizon. Four faults (F1, F3, F4 and F6) cut through this horizon. A drilled and tested area is identified on the map alongside two undrilled and prospect areas. The tested area is seen to be a fault assisted closure being assisted by fault F3. The undrilled and prospect areas are both 4-way closures. Figure 4.9(b) shows the sand E structural depth map in 3D view.

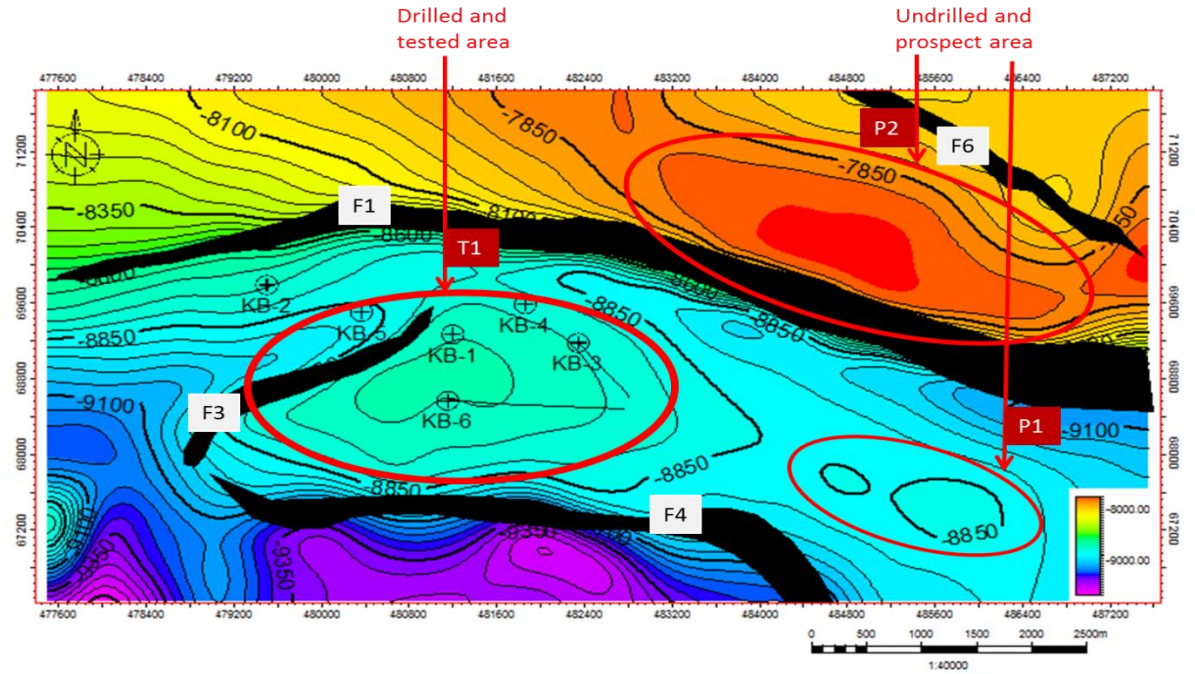

Figure 4.9(a): Structural depth map for sand E showing the tested area and prospect area

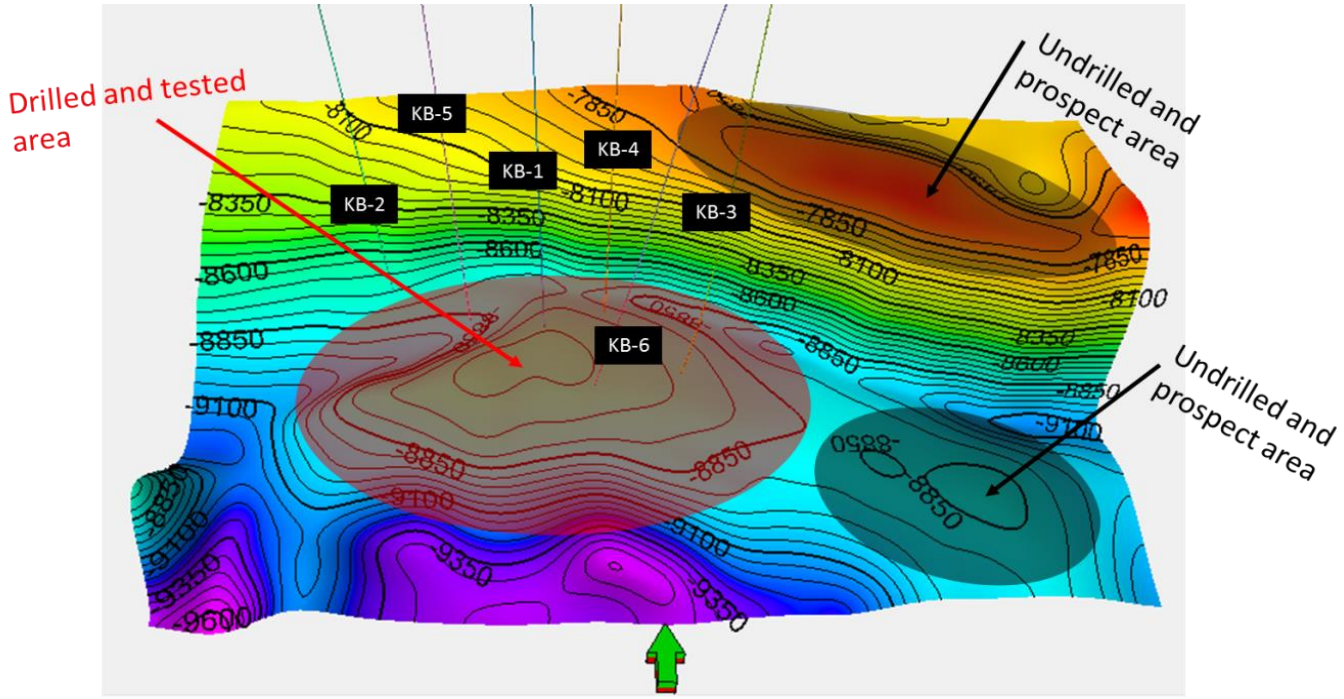

Figure 4.9(b): 3D view of structural depth maps for sand E showing the tested area and prospect area

4.7.4 SAND F DEPTH MAP

The structural depth map for sand F as shown in Figure 4.10(a) is characterized with a contour interval of 50ft. The colors show difference in elevation of the horizon. Four faults (F1, F3, F4 and F6) cut through this horizon. A drilled and tested area is identified on the map alongside two undrilled and prospect areas. The tested area is seen to be a fault assisted closure being assisted by fault F3. The undrilled and prospect areas are both 4-way closures. Figure 4.10(b) shows the sand F structural depth map in 3D view.

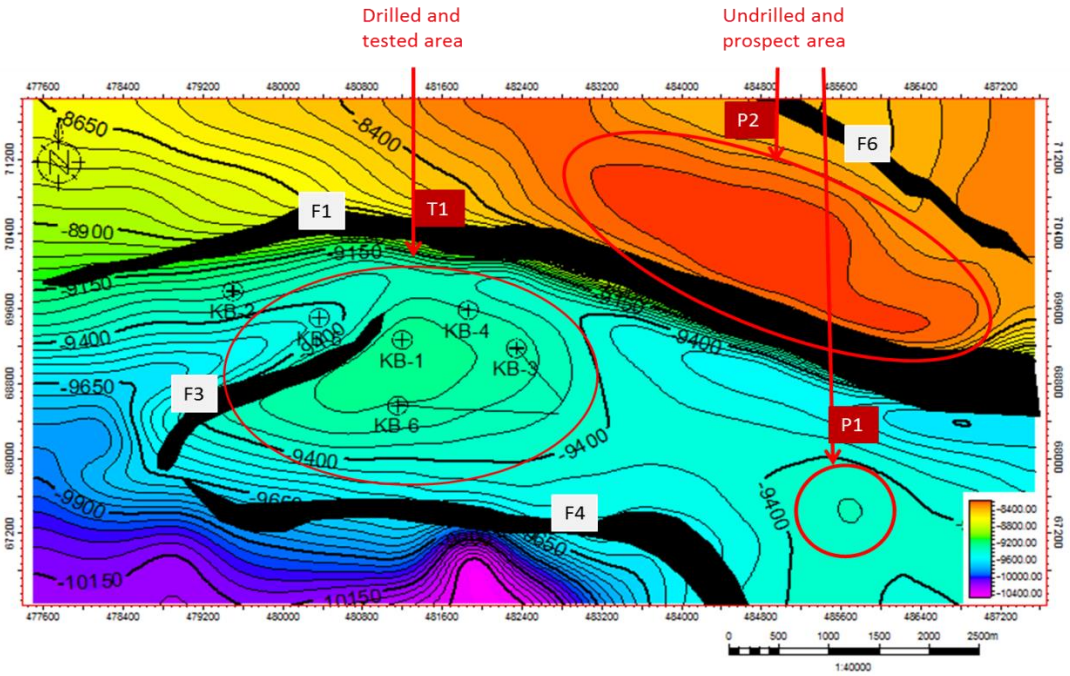

Figure 4.10(a): Structural depth map for sand F showing the tested area and prospect area

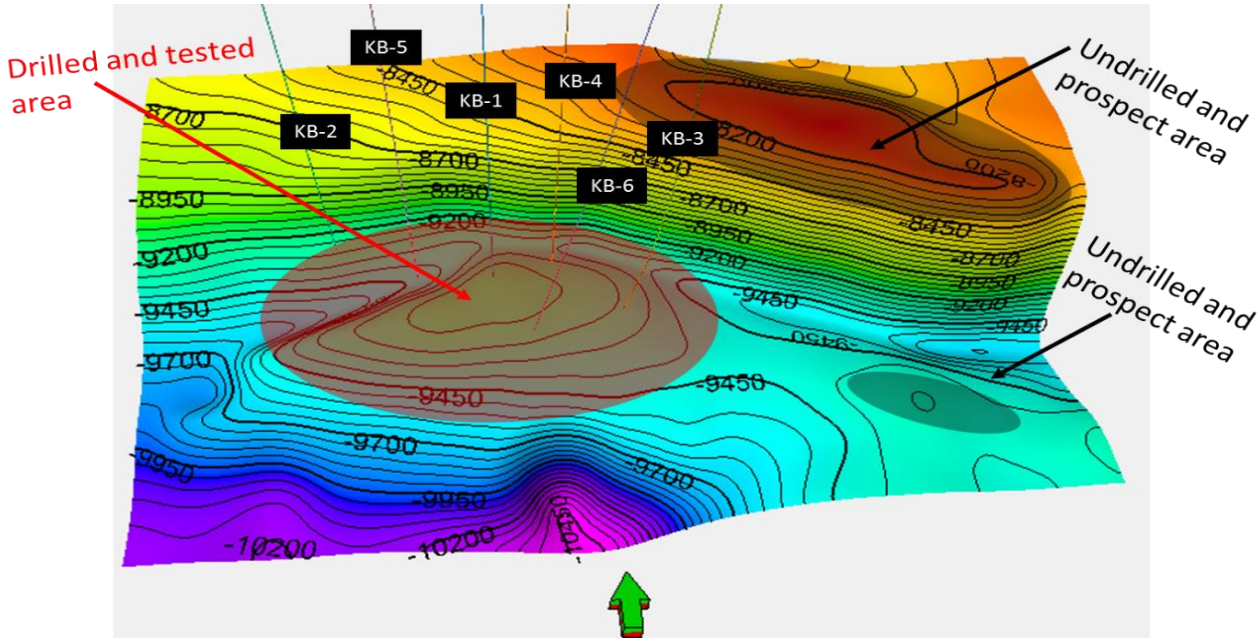

Figure 4.10(b): 3D view of structural depth maps for sand F showing the tested area and prospect area

4.7.5 SAND G DEPTH MAP

The structural depth map for sand G as shown in Figure 4.11(a) is characterized with a contour interval of 50ft. The colors show difference in elevation of the horizon. Four faults (F1, F3, F4 and F6) cut through this horizon. A drilled and tested area is identified on the map alongside two undrilled and prospect areas. The tested area is seen to be a fault assisted closure being assisted by fault F3. The undrilled and prospect areas are both 4-way closures. Figure 4.11(b) shows the sand G structural depth map in 3D view.

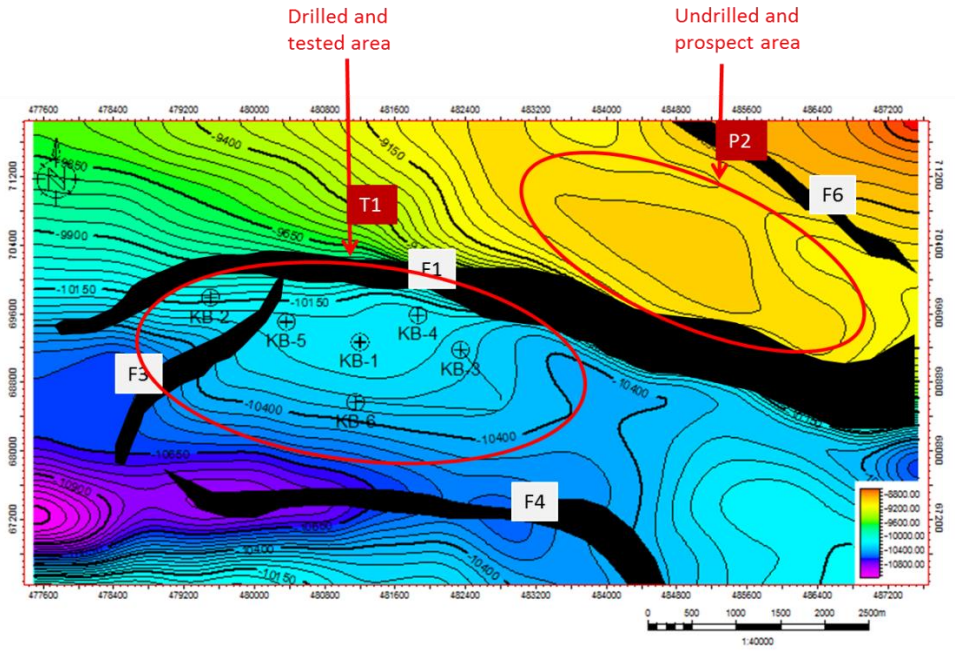

Figure 4.11(a): Structural depth map for sand G showing the tested area and prospect area

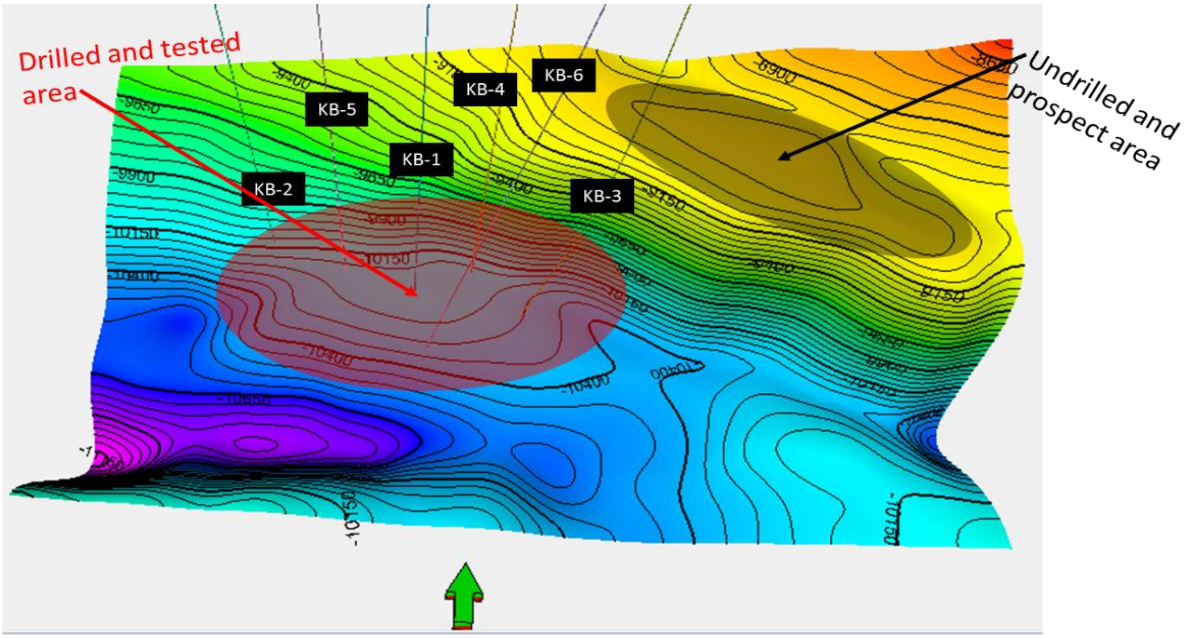

Figure 4.11(b): 3D view of structural depth maps for sand G showing the tested area and prospect area

4.7.6 SAND H DEPTH MAP

The structural depth map for sand H as shown in Figure 4.12(a) is characterized with a contour interval of 50ft. The colors show difference in elevation of the horizon. Four faults (F1, F3, F4 and F6) cut through this horizon. A drilled and tested area is identified on the map alongside two undrilled and prospect areas. The tested area is seen to be a fault assisted closure being assisted by fault F3. The undrilled and prospect areas are both 4-way closures. Figure 4.12(b) shows the sand H structural depth map in 3D view.

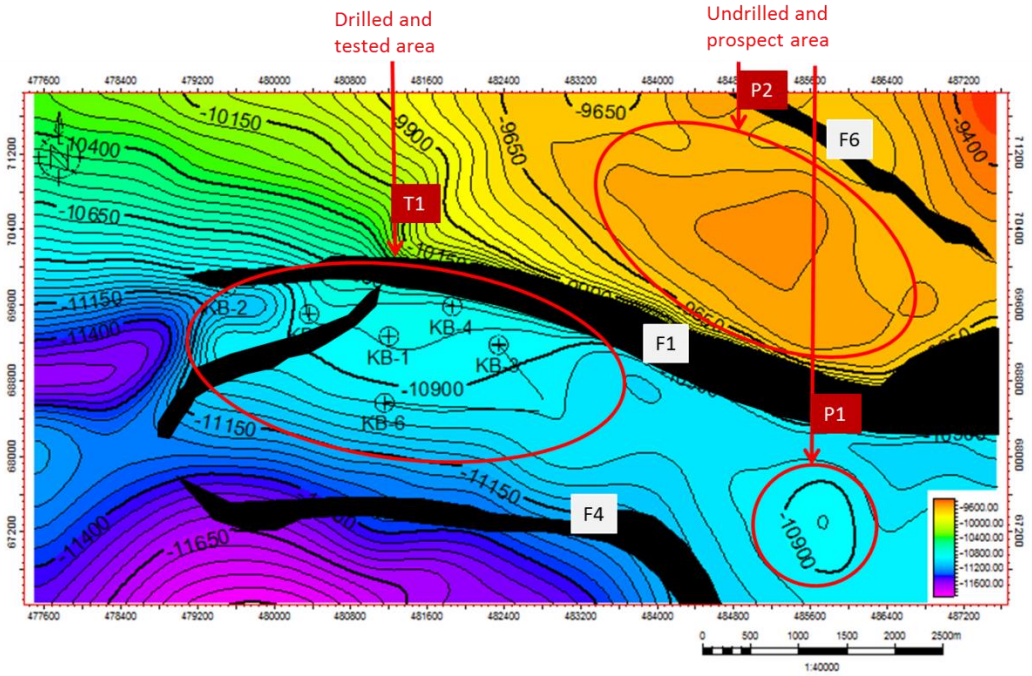

Figure 4.12(a): Structural depth map for sand H showing the tested area and prospect area

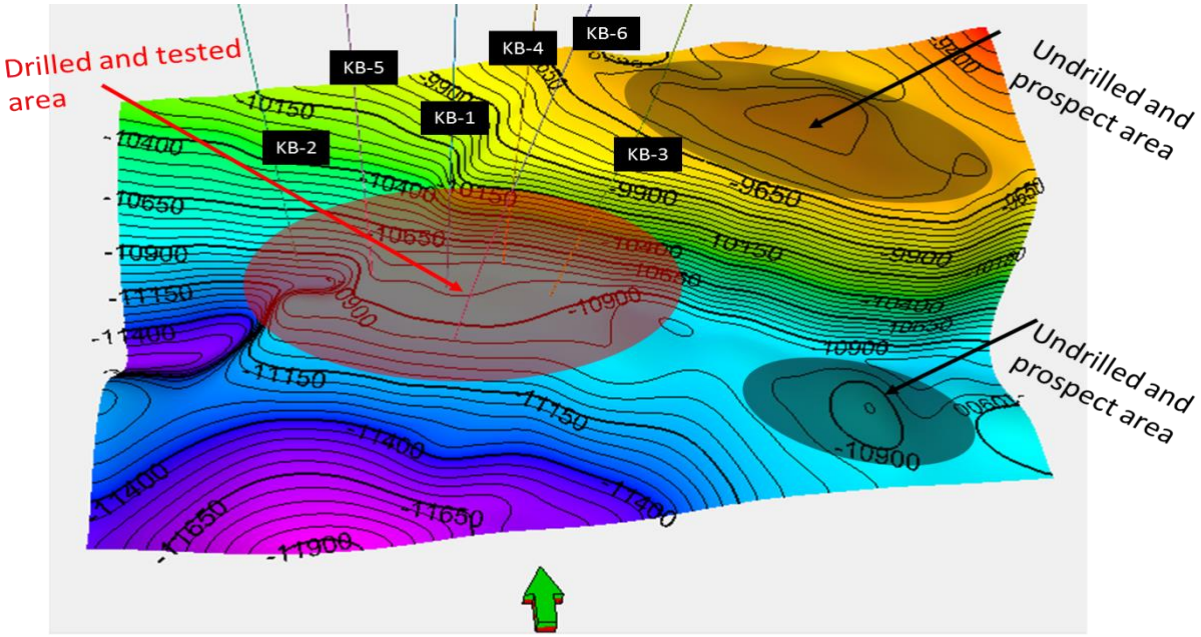

Figure 4.12(b): 3D view of structural depth maps for sand H showing the tested area and prospect area

4.8 ISOPACH MAPS

4.8.1 SAND A – SAND B

Isopach map showing variation in thickness between sand A and Sand B as seen in Figure 4.13(a). It is characterized with contour lines and colors which show differences in thickness. The zones of drastic changes in thickness indicated by the red arrows both of which are trending E-W are most likely associated with faults. The range of thickness in the map below is from about 500ft to about 800ft.

4.8.2 SAND B – SAND E

Isopach map showing variation in thickness between sand B and Sand E as seen in Figure 4.13(b). It is characterized with contour lines and colors which show differences in thickness. There are two areas of drastic changes in thickness in the map presented below as indicated by the red arrows both of which are trending E-W and are most likely to be as a result of faulting. The range of thickness is from about 750ft to about 1200ft.

4.8.3 SAND E – SAND F

Isopach map showing variation in thickness between sand E and Sand F as seen in Figure 4.13(c). It is characterized with contour lines and colors which show differences in thickness. Drastic changes of thickness which are trending E-W are most likely associated with faulting of horizon. The range of thickness of the map presented below is from about 350ft to about 950ft.

4.8.4 SAND F – SAND G

Isopach map showing variation in thickness between sand F and Sand G as seen in Figure 4.13(d). It is characterized with contour lines and colors which show differences in thickness. There are two zones of drastic changes in thickness which are denoted by the red arrows. This variation in thickness is most likely due to the presence of faults in the horizon. The range of thickness of the map is from about 100ft to about 1000ft.

4.8.4 SAND G – SAND H

Isopach map showing variation in thickness between sand G and Sand H as seen in Figure 4.13(e). It is characterized with contour lines and colors which show differences in thickness. There are two zones of drastic changes in thickness which are denoted by the red arrows. This variations in thickness is most likely due to the presence of faults in the horizon. The range of thickness of the map is from about 100ft to about 1500ft.

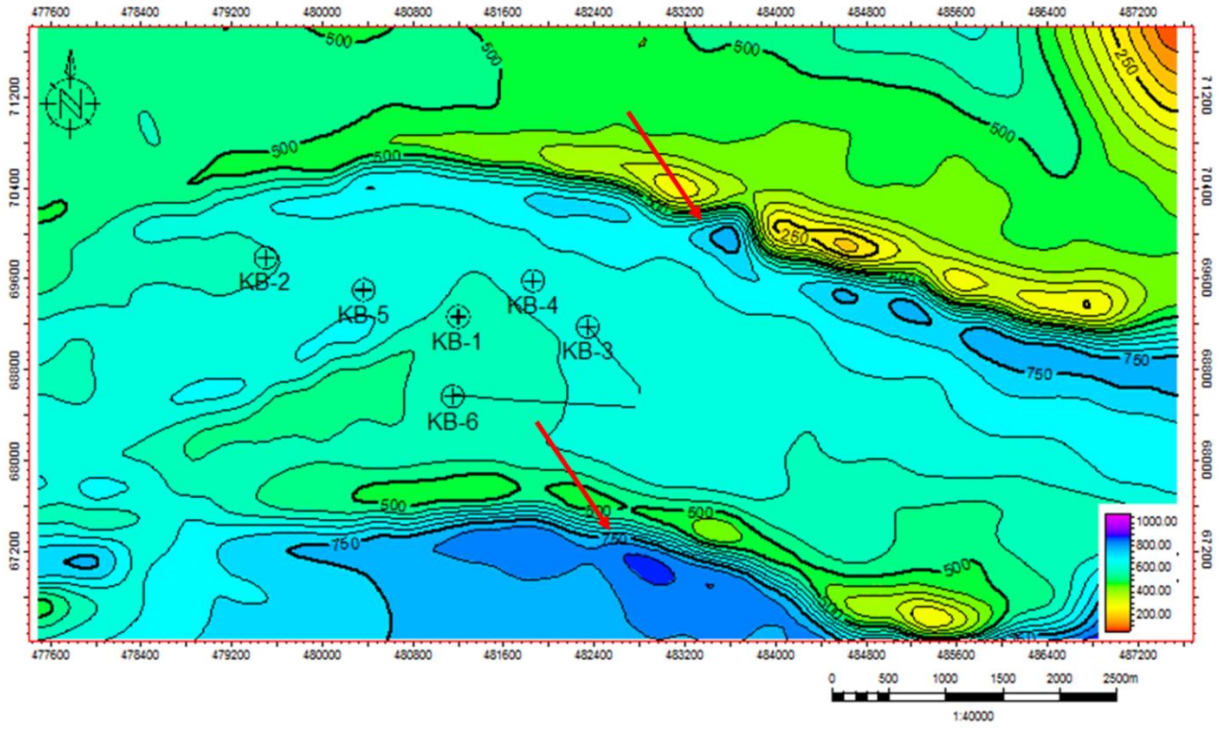

Figure 4.13(a): Isopach map of thickness between sand A and sand B.

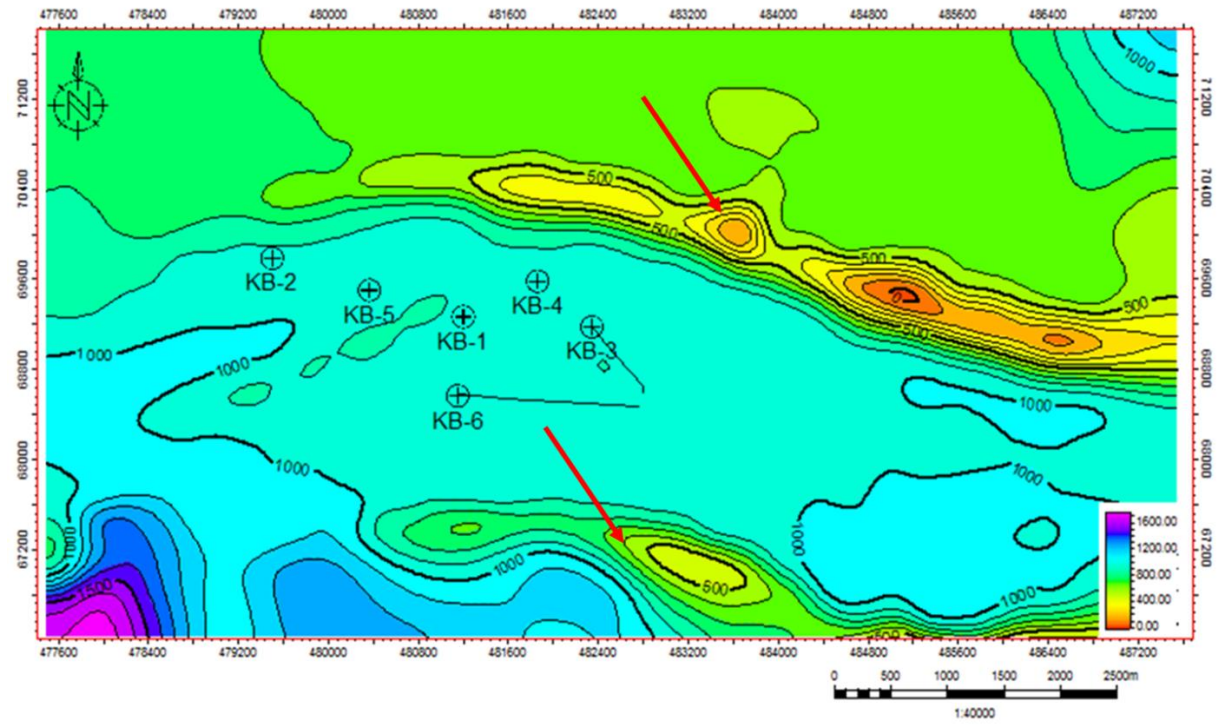

Figure 4.13(b): Isopach map of thickness between sand B and sand E.

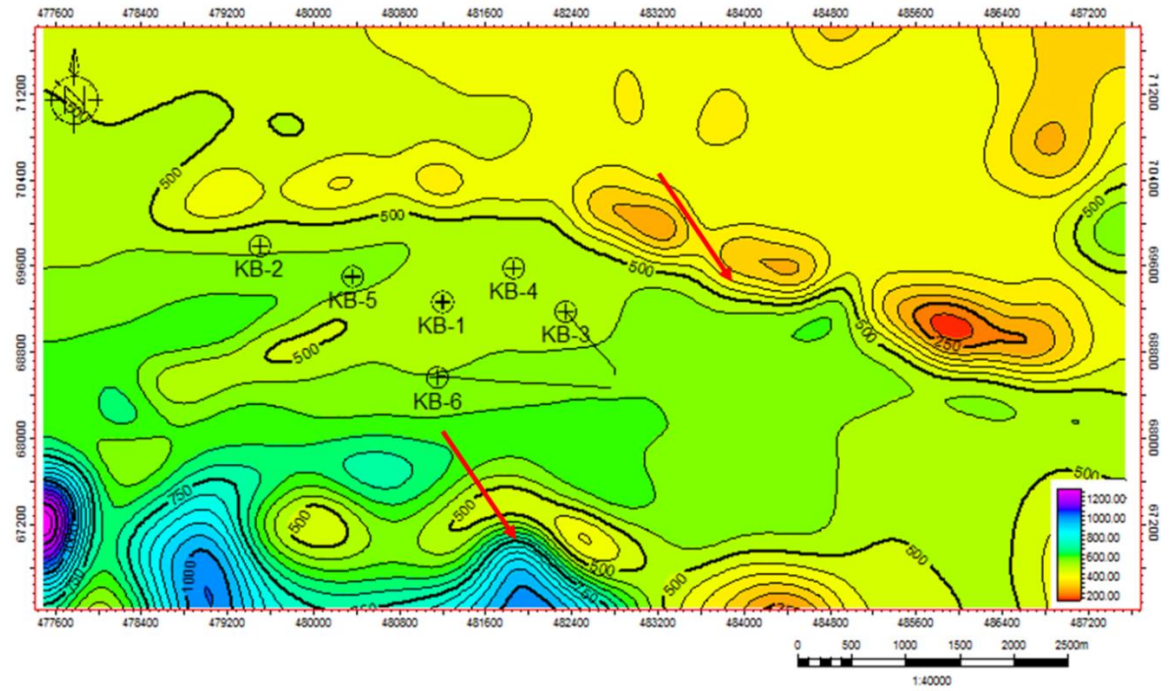

Figure 4.13(c): Isopach map of thickness between sand E and sand F.

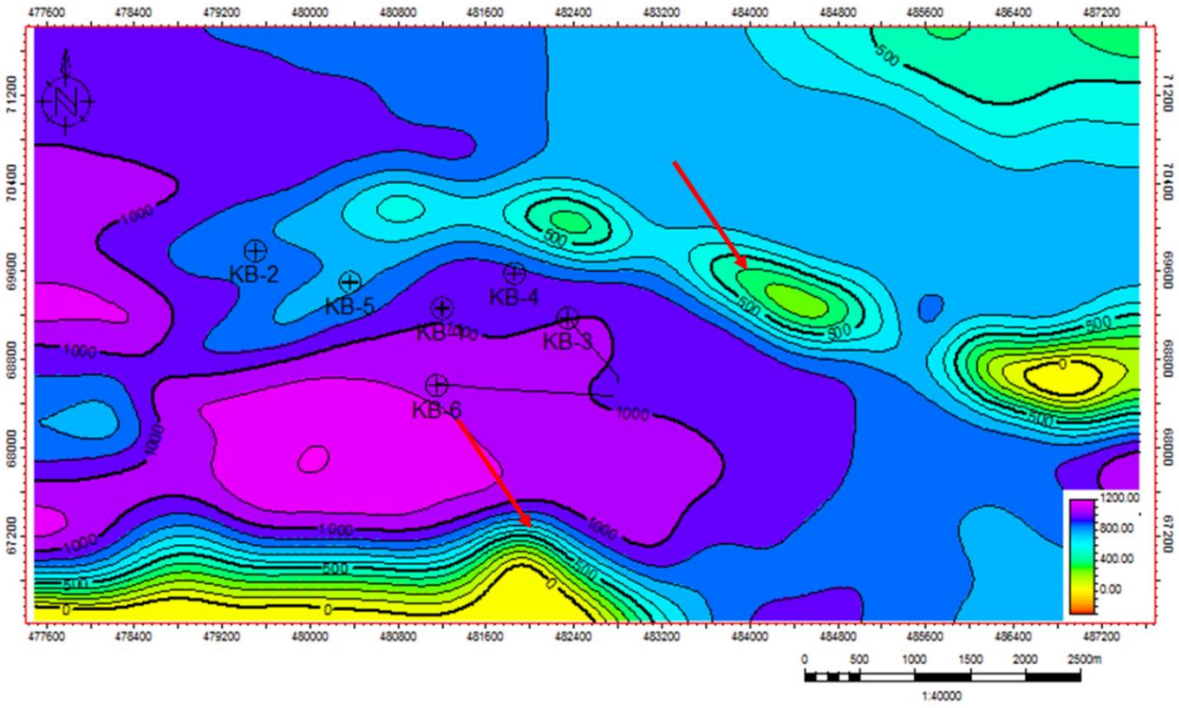

Figure 4.13(d): Isopach map of thickness between sand F and sand G

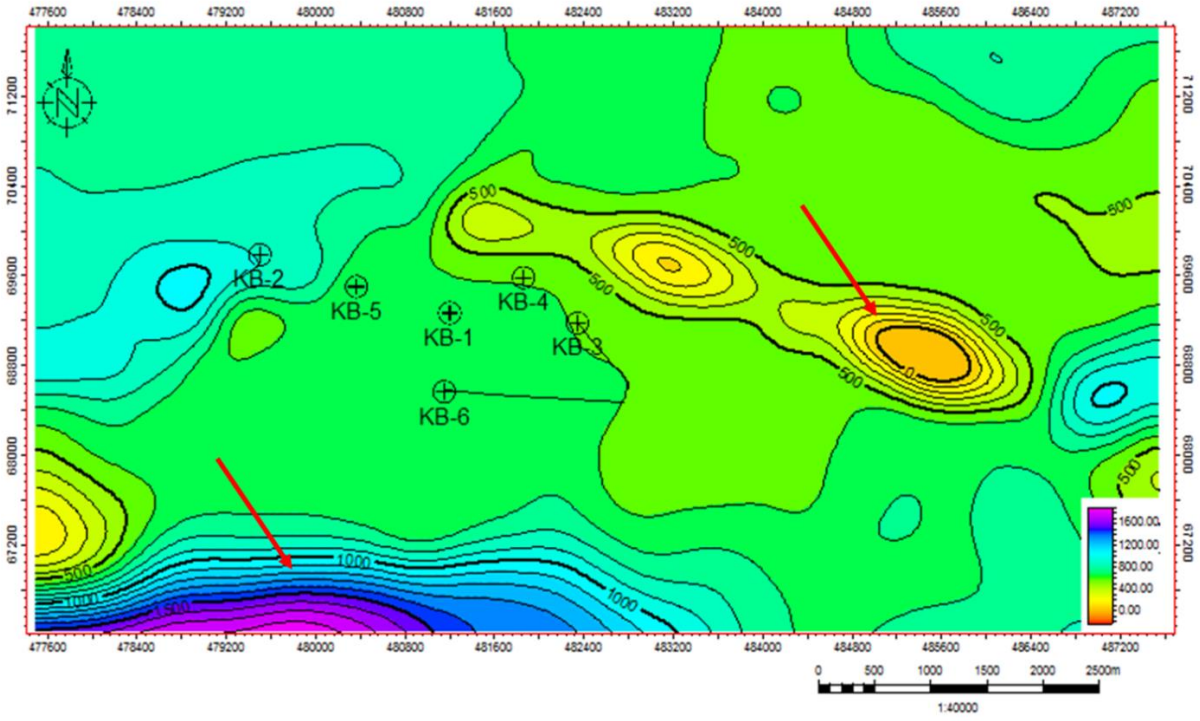

Figure 4.13(e): Isopach map of thickness between sand G and sand H.

4.9 SEISMIC ATTRIBUTES MAPS

4.9.1 SAND A

The positive attribute in the tested area shows that drilling was successful. The undrilled area has the same potential since the positive attribute cuts across both areas (Figure 4.14). A variation in color is observed in tested region from the RMS amplitude map, sum of amplitudes map and sum of energies map is most likely showing the presence of fluid as these amplitudes most times act as direct hydrocarbon indicators. Also in the prospect areas there are slight variations in color from the maps although not very precise

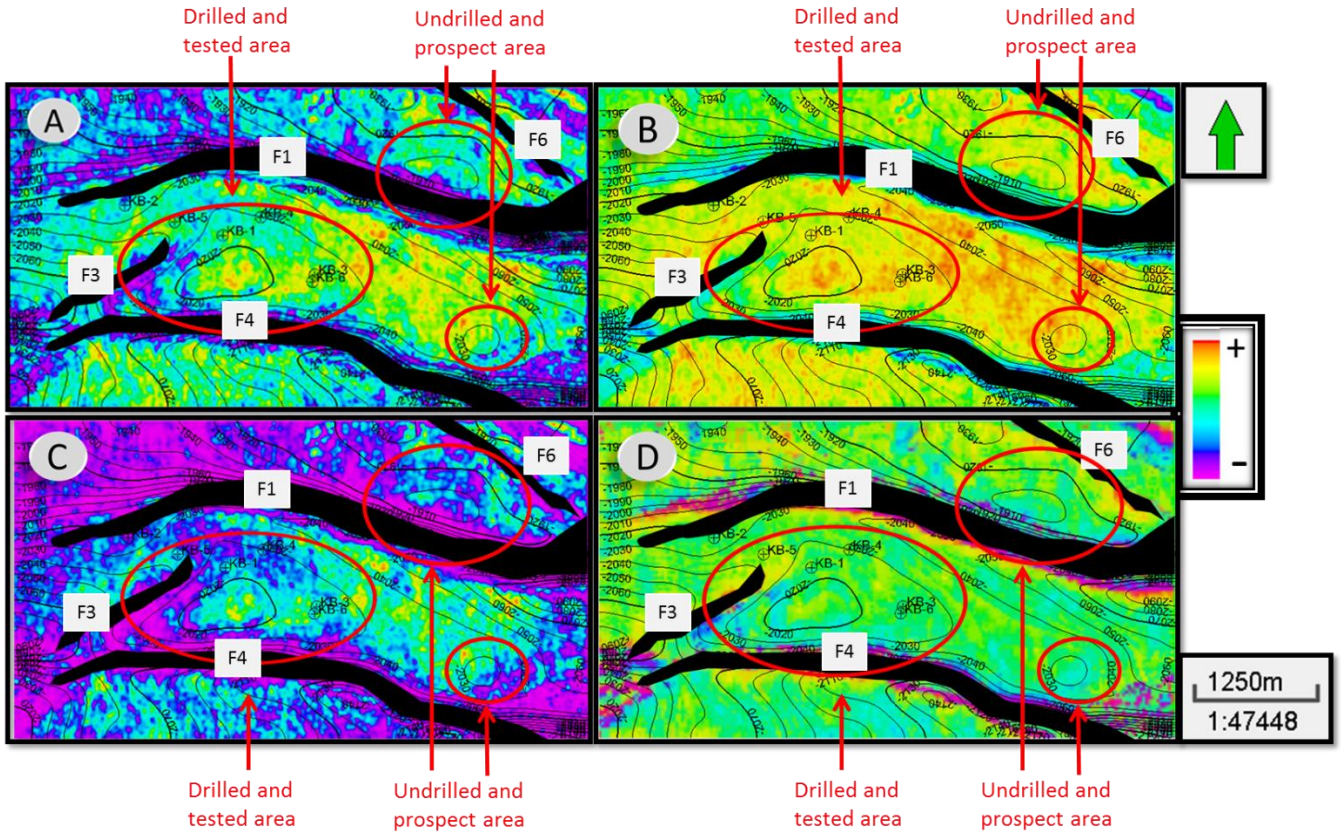

Figure 4.14: Seismic attributes of sand A characterized with high amplitude in the tested area and the prospect area. (A) RMS amplitude; (B) Sum of amplitudes; (C) Sum of energies; (D) Average Instantaneous phase.

4.9.2 SAND B

The positive attribute in the tested area shows that drilling was successful as seen in Figure 4.15. The variation in color in tested region from the RMS amplitude map, sum of amplitudes map and sum of energies map is most likely showing the presence of fluid as these amplitudes most times act as direct hydrocarbon indicators. The prospect areas in this horizon are not supported by the attributes analysis.

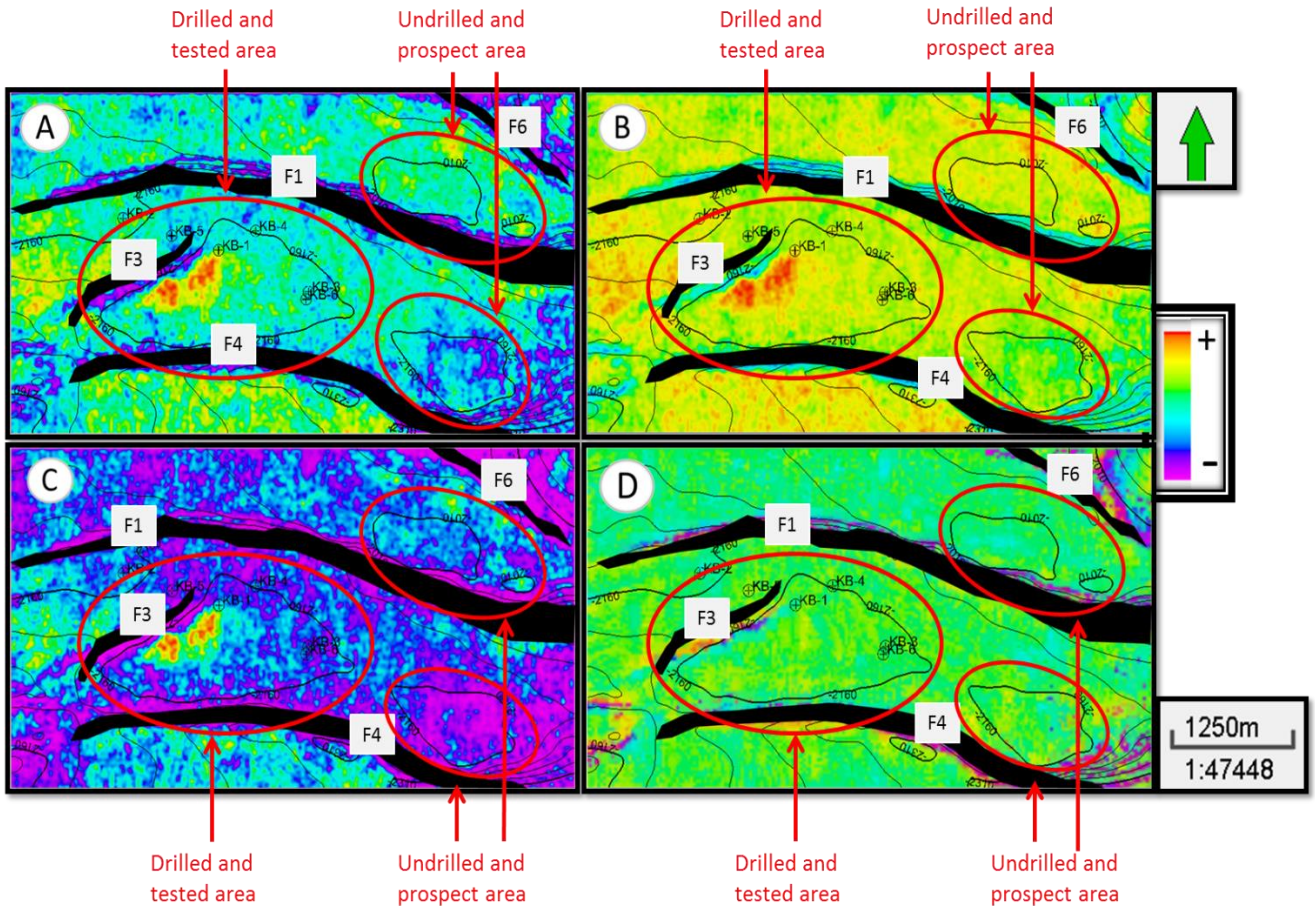

Figure 4.15: Seismic attributes of sand B characterized with high amplitude in the tested area (A) RMS amplitude; (B) Sum of amplitudes; (C) Sum of energies; (D) Average Instantaneous phase.

4.9.3 SAND E

The positive attribute in the tested area shows that drilling was successful as shown in Figure 4.16. Variations in amplitudes observed by the variations in color in the tested area of this horizon from the attribute maps presented is most likely an indication of the possible presence of fluid in the sand.

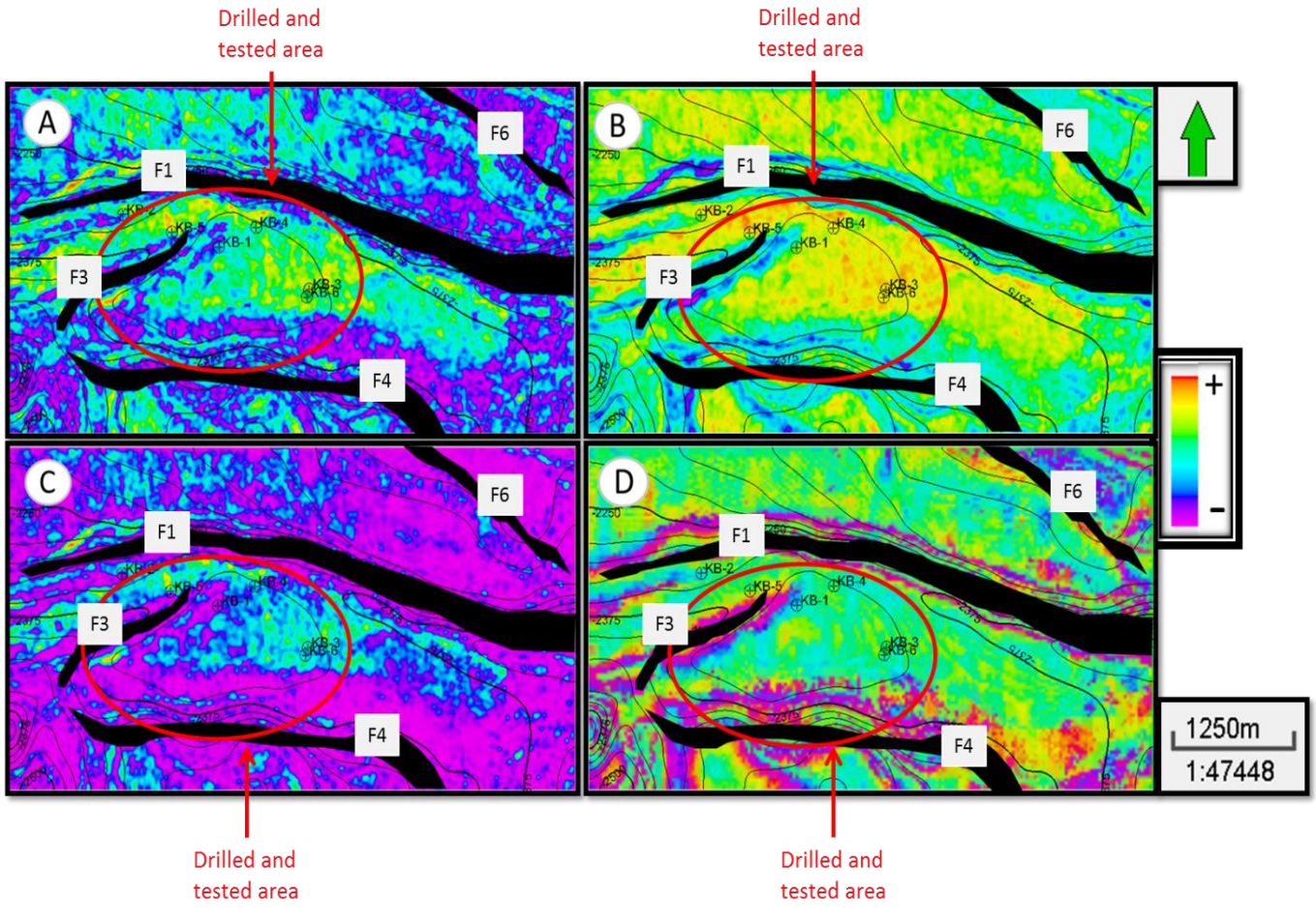

Figure 4.16: Seismic attributes of sand E characterized with high amplitude in the tested area. (A) RMS amplitude; (B) Sum of amplitudes; (C) Sum of energies; (D) Average Instantaneous phase.

4.9.4 SAND F

The positive attribute in the tested area shows that drilling was successful. As shown in Figure 4.17. Variations in amplitudes shown in the maps below in the tested area of the study area show the possible presence of fluid in the zone although the attributes maps do not support the prospect area.

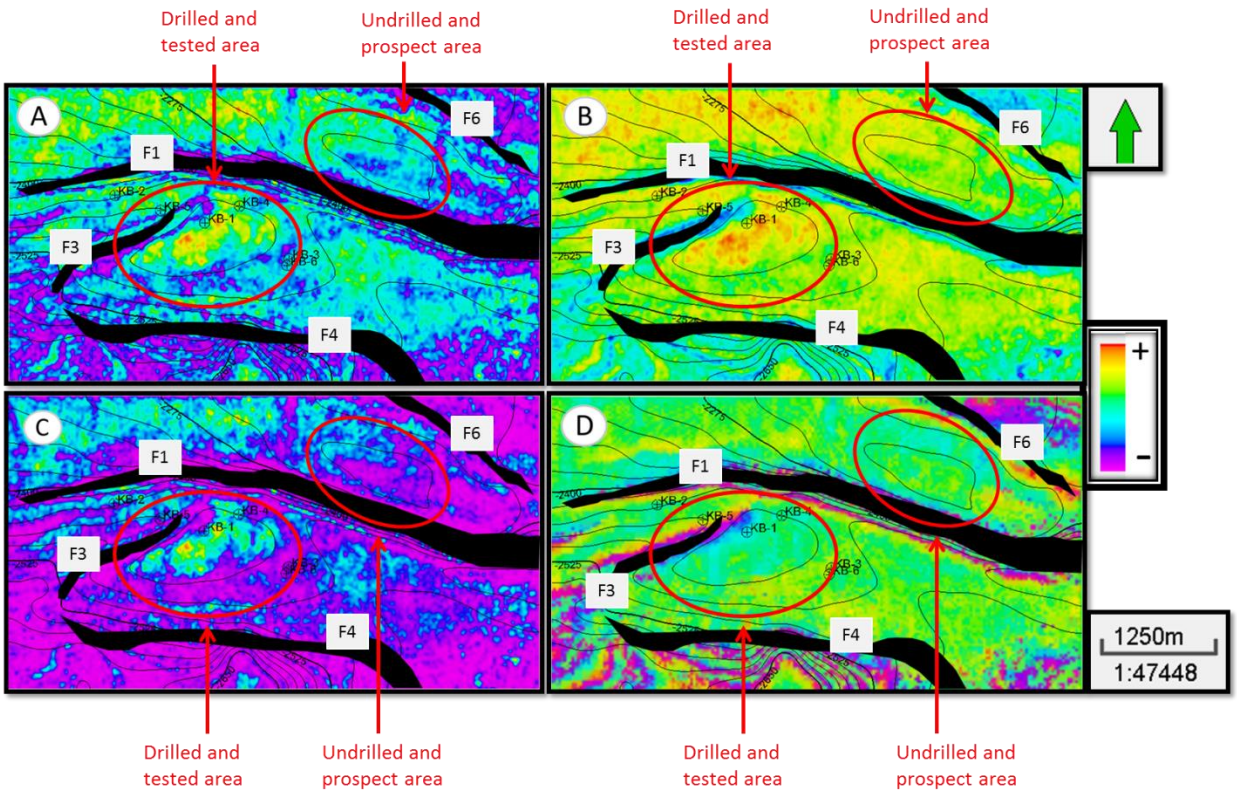

Figure 4.17: Seismic attributes of sand F characterized with high amplitude in the tested area. (A) RMS amplitude; (B) Sum of amplitudes; (C) Sum of energies; (D) Average Instantaneous phase.

4.9.5 SAND G

The positive attribute in the tested area shows that drilling was successful. The undrilled area has the same potential since the positive attribute cuts across both areas (Figure 4.18). Variations in amplitudes in the tested and prospect area are showing possible presence of fluid as these seismic attributes serve as hydrocarbon indicators.

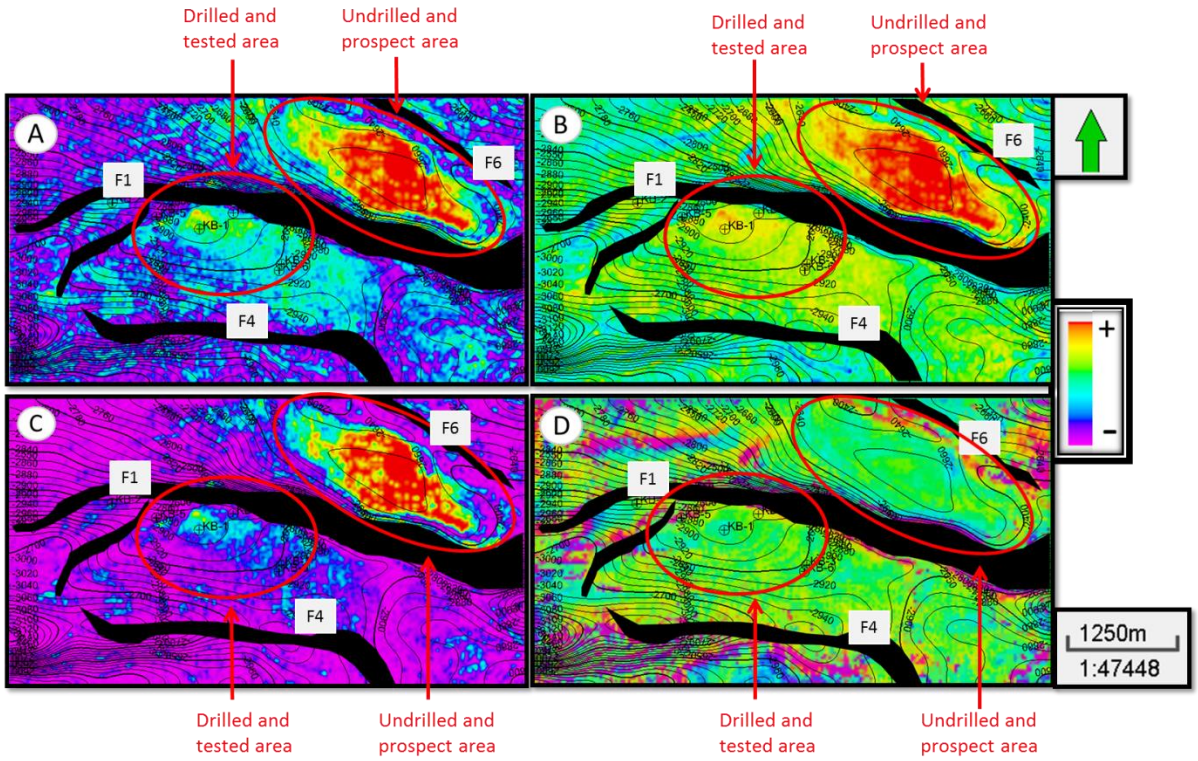

Figure 4.18: Seismic attributes of sand G characterized with high amplitude in the tested area. (A) RMS amplitude; (B) Sum of amplitudes; (C) Sum of energies; (D) Average Instantaneous phase.

4.9.6 SAND H

The positive attribute in the tested area shows that drilling was successful. The undrilled area has the same potential since the positive attribute cuts across both areas (Figure 4.19). The very high variation in amplitude in the tested and prospect area of the horizon presented below is an indicator of possible presence of fluid.

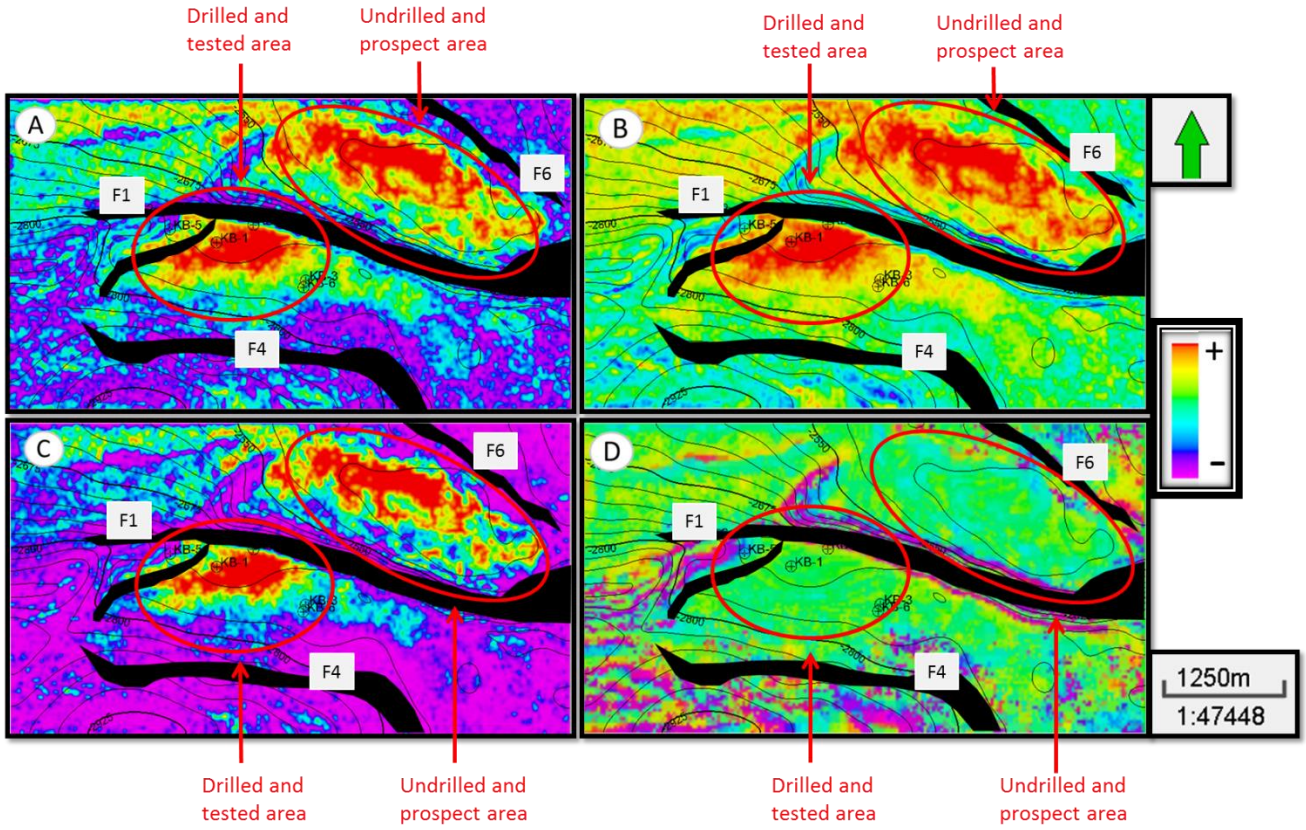

Figure 4.19: Seismic attributes of sand H characterized with high amplitude in the tested area and prospect area. (A) RMS amplitude; (B) Sum of amplitudes; (C) Sum of energies; (D) Average Instantaneous phase.

4.10 PETROPHYSICAL EVALUATION

The petrophysical paramaters were calculated for each reservoir that contains hydrocarbon (Table 5). The results are presented and discussed below.

For Well KB-4, Sand F is seen to be a hydrocarbon-filled reservoir through the deflection of the resistivity log signature to the right as seen in Figure 4.20(a). The reservoir has a top of 9,567.23ft and the base of 10,350.59ft. The Net to Gross of the reservoir was estimated to be 0.68. The volume of shale of the reservoir was estimated to be 0.27. The total porosity and effective porosity of the reservoir was calculated to be 0.25 and 0.19 respectively. The water saturation was estimated to be 0.47.

For Well KB-4, Sand G is seen to be a hydrocarbon-filled reservoir through the deflection of the resistivity log signature to the right as seen in Figure 4.20(b). The reservoir has a top of 10,580.49ft and the base of 10,881.96ft. The Net to Gross of the reservoir was estimated to be 0.74. The volume of shale of the reservoir was estimated to be 0.27. The total porosity and effective porosity of the reservoir was calculated to be 0.23 and 0.17 respectively. The water saturation was estimated to be 0.57.

For Well KB-4, Sand H is seen to be a hydrocarbon-filled reservoir through the deflection of the resistivity log signature to the right as seen in Figure 4.21(a). The reservoir has a top of 11,126.21ft and the base of 11,383.98ft. The Net to Gross of the reservoir was estimated to be 0.3. The volume of shale of the reservoir was estimated to be 0.44. The total porosity and effective porosity of the reservoir was calculated to be 0.23 and 0.14 respectively. The water saturation was estimated to be 0.71.

For Well KB-5, Sand H is seen to be a hydrocarbon-filled reservoir through the deflection of the resistivity log signature to the right as seen in Figure 4.21(b). The reservoir has a top of 10,971.63ft and the base of 11,164.91ft. The Net to Gross of the reservoir was estimated to be 0.9. The volume of shale of the reservoir was estimated to be 0.57. The total porosity and effective porosity of the reservoir was calculated to be 0.23 and 0.12 respectively. The water saturation was estimated to be 0.53.

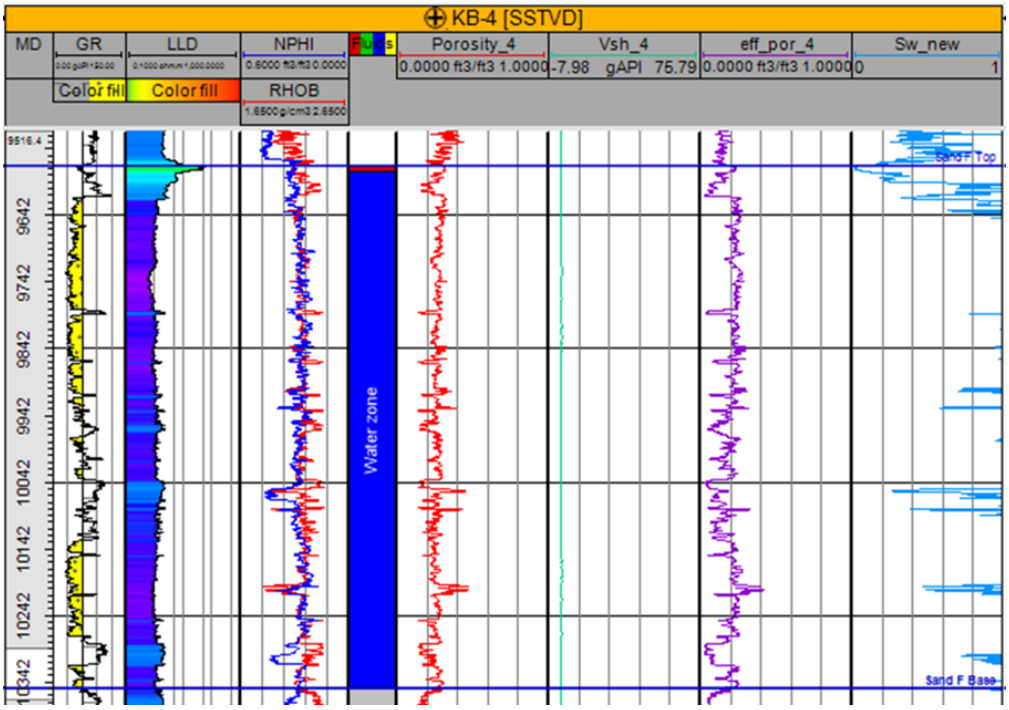

Figure 4.20(a): Well KB-4 showing the petrophysical parameters of sand F.

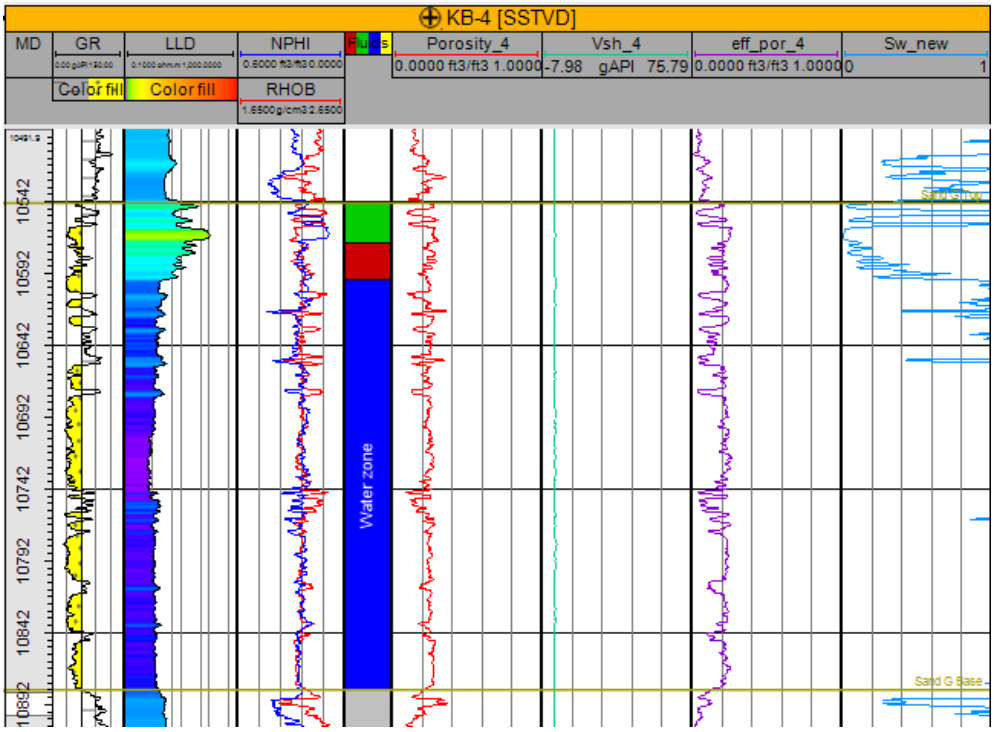

Figure 4.20(b): Well KB-4 showing the petrophysical parameters of sand G.

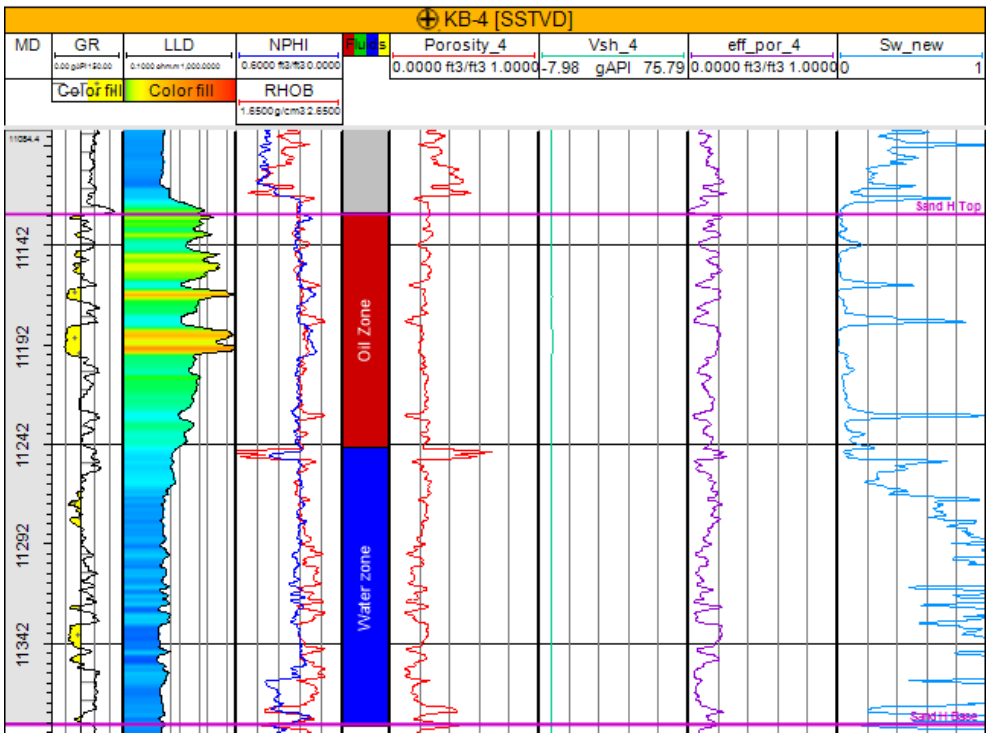

Figure 4.21(a): Well KB-4 showing the petrophysical parameters of sand H.

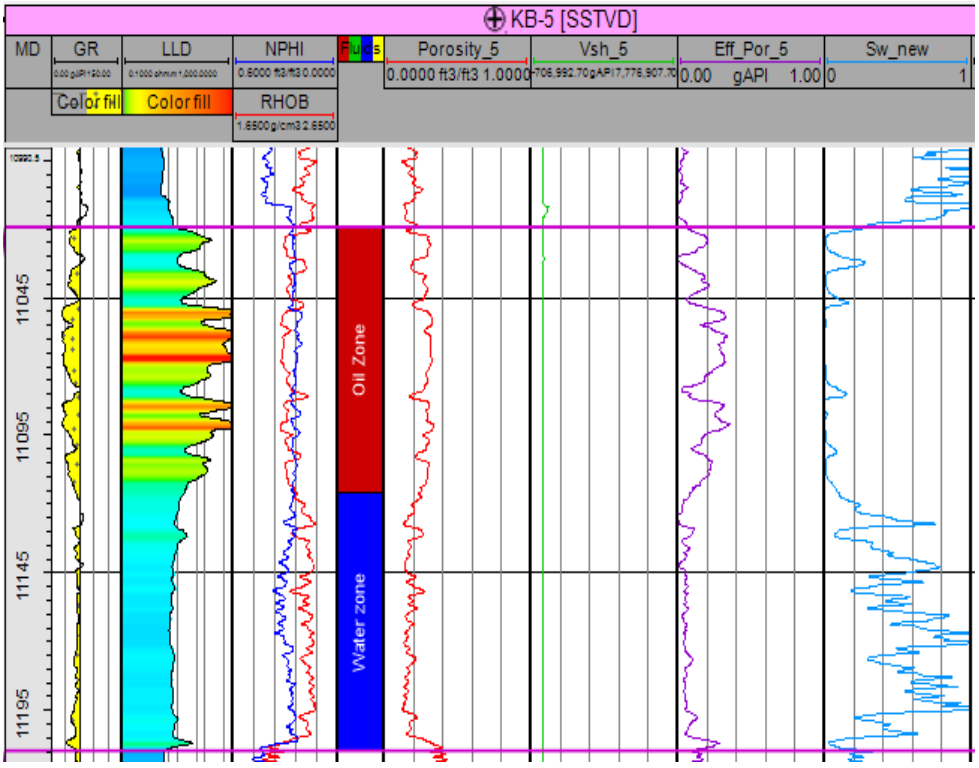

Figure 4.21(b): Well KB-5 showing the petrophysical parameters of sand H.

Table 5 showing the petrophysical parameters of all reservoirs containing hydrocarbon and their various wells

WELL NAME	KB-4						
RESERVOIR NAME	SAND F						
	SAND TOP (ft)	SAND BASE (ft)	NTG	VOLUME OF SHALE (Vsh)	TOTAL POROSITY (Φ)	EFFECTIVE POROSITY (Φe)	WATER SATURATION (Sw)
	9,567.23	10,350.59	0.68	0.27	0.25	0.19	0.47
RESERVOIR NAME	SANG G						
	SAND TOP (ft)	SAND BASE (ft)	NTG	VOLUME OF SHALE (Vsh)	TOTAL POROSITY (Φ)	EFFECTIVE POROSITY (Φe)	WATER SATURATION (Sw)
	10,580.49	10,881.96	0.74	0.27	0.23	0.17	0.57
RESERVOIR NAME	SAND H						
	SAND TOP (ft)	SAND BASE (ft)	NTG	VOLUME OF SHALE (Vsh)	TOTAL POROSITY (Φ)	EFFECTIVE POROSITY (Φe)	WATER SATURATION (Sw)
	11,126.21	11,383.98	0.3	0.44	0.23	0.14	0.71
WELL NAME	KBI-5						
RESERVOIR NAME	SAND H						
	SAND TOP (ft)	SAND BASE (ft)	NTG	VOLUME OF SHALE (Vsh)	TOTAL POROSITY (Φ)	EFFECTIVE POROSITY (Φe)	WATER SATURATION (Sw)
	11,019.16	11,209.60	0.9	0.57	0.23	0.13	0.53

4.11 VOLUMETRIC ESTIMATIONS

The volumes of hydrocarbon in the hydrocarbon-bearing reservoirs of the mapped sands were estimated and the results are shown below

Sand F from well KB-4 has a top of 9,567.23ft and a base of 10,350.59ft. It has an oil-water-contact (OWC) of 9576.77ft. The tested zone has a gross rock volume (GRV) of 1.74E+9ft^3while prospects 1 and 2 have gross rock volumes of 1.31E+8ft^3 and 6.39E+8ft^3 respectively. The Oil originally in place (OOIP) for the tested area, prospect 1 and prospect 2 were estimated to be 27.9mmBBL, 2.1MMbbl and 10.3MMbbl respectively. The stock tank oil initially in place (STOIIP) for the tested area, prospect 1 and prospect 2 were estimated to be 21.5MMbbl, 1.6MMbbl and 7.9MMbbl respectively.

Sand G from well KB-4 has a top of 10,580.49ft and a base of 10,881.96ft. It has a gas-oil-contact (GOC) of 10,608.04ft and an oil-water-contact (OWC) of 10,633.82ft. For the tested zone, the area containing gas has a gross rock volume (GRV) of 1.4E+9ft^3 while the area containing oil has a gross rock volume (GRV) of 1.31E+9ft^3. For the prospect, the area containing gas has a gross rock volume (GRV) of 5.04E+8ft^3 while the area containing gas has a gross rock volume (GRV) of 4.72E+8ft^3. The original gas in place (OGIP) for the tested area and prospect were estimated to be 102.5MMscf and 36.8MMscf while the Oil originally in place (OOIP) for the tested area and prospect were estimated to be 16.9mmBBL and 6.2MMbbl. The stock tank oil initially in place (STOIIP) for the tested area and prospect were estimated to be 17.3MMbbl and 4.7MMbbl.

Sand H from well KB-4 has a top of 11,126.21ft and a base of 11,383.98ft. It has an oil-water-contact (OWC) of 11,244.06ft. The tested zone has a gross rock volume (GRV) of 3.44E+9ft^3while prospects 1 and 2 have gross rock volumes of 4.18E+8ft^3 and 1.65E+8ft^3 respectively. The Oil originally in place (OOIP) for the tested area, prospect 1 and prospect 2 were estimated to be 52.5mmBBL, 6.4MMbbl and 25.2MMbbl respectively. The stock tank oil initially in place (STOIIP) for the tested area, prospect 1 and prospect 2 were estimated to be 40.4MMbbl, 4.9MMbbl and 19.4MMbbl respectively.

The results for the volumetric estimations are presented in table 6.

Table 6 Volumetric estimations of hydrocarbon-bearing reservoirs mapped.

RESERVOIR NAME		TESTED	PROSPECT 1	PROSPECT 2
Sand F	Area (ft2)	33,850,799	8,790,362.80	26,953,424
	OOIP (bbl)	27,945,454	2,103,939	10,262,727
	STOIIP (bbl)	21,496,435	1,618,415	7,894,406
Sand G	Area (ft2)	50,900,716	-	18,293,303
	OGIP (scf)	102,460,400	-	36,812,558
	OOIP (bbl)	16,959,323	-	6,152,338
	STOIIP (bbl)	17,293,048	-	4,732,568
Sand H	Area (ft2)	45,150,330	13,327,889	46,891,914
	OOIP (bbl)	52,464,598	6,375,059	25,164,706
	STOIIP (bbl)	40,357,384	4,903,891	19,357,466

CHAPTER FIVE

CONCLUSION AND RECOMMENDATIONS

5.1 CONCLUSION

3D seismic interpretation was carried out on the KB Field using well logs and Seismic data volume. The six wells used in this study were correlated and eight sand bodies (Sand A, B, C, D, E, F, G and H) were interpreted using their gamma ray logs and resistivity logs. The sand bodies B, C, D and F show a blocky gamma ray log motif thus displaying an aggradational stacking pattern indicating a channel-fill. Funnel-shaped successions noticed in Sands A, E, G and H are due to coarsening or cleaning upwards of shallow sediments with increasing energy of deposition which has been interpreted as a prograding marine shelf environment.

Ten faults were interpreted from the seismic inlines denoted F1, F2, F3, F4, F5, F6, F7, F8, F9 and F10. All interpreted faults are normal faults – growth faults (F1 and F4), synthetic faults (F2, F6, F7 and F9) and antithetic faults (F3, F5, F8 and F10). Within the study area, there are neither thrust nor strike-slip faults. North dipping antithetic fault F3 is a very important fault as it is responsible for trapping hydrocarbons in wells KB-1, KB-3, KB4 and KB-6. Structural highs such as rollover anticlines were interpreted to be part of the geology of the study area.

Five selected horizons were mapped out which include; H1, H2, H3, H4 and H5. These horizons were used for the location of the hydrocarbon zones in the field. From the structural maps, it was observed that the hydrocarbon accumulations are associated with anticlines, fault assisted closures and fault dependent closures.

The tested areas from all sands were supported by the seismic attributes maps that were analyzed. Only prospects in sand A, sand G and sand H were supported by the seismic attributes maps.

The petrophysical values which include the porosity, Net to Gross, Water saturation, hydrocarbon saturation have values that are almost ideal for the Niger Delta reservoir sands with average porosity value of 0.24, water saturation of 0.52 and average Net to gross value of 0.6. The lower the water saturation, the higher the hydrocarbon saturation in the reservoir sand.

From the volumetric estimations, sand G is seen to have the largest hydrocarbon zone while Sand F is seen to have the smallest hydrocarbon zone.

5.2 RECOMMENDATIONS

I recommend that the prospects should be tested to improve the viability of the field especially the prospects that supported by seismic attributes. I as recommended that this study should be extended to reservoir modelling to ascertain the 3D distribution of stratigraphic units and for improved resource assessment.

REFERENCES

Abam T.K.S (2016). Engineering Geology of the Niger Delta, Journal of Earth Sciences and Geotechnical Engineering, vol.6, no. 3, 2016, 65-89**.**

Adegoke O.S., Oyebamiji A.S., Edet J.J., Osterloff P.L., Ulu O.K., (2017). Cenozoic Foraminifera and calcareous Nannofossil Biostratigraphy of the Niger Delta, Pages 25-66.

Aminzadeh F. and Dasgupta S.N., (2013). Fundamentals of petroleum geophysics, developments in petroleum science, volume 60, pages 37-92.

Ayolabi E.A and Adigun A.O., (2013). The use of seismic attributes to enhance structural interpretation of Z-field, Onshore, Niger delta. Earth science research, 2(2).

Chambers, R. L. and Yarus, J. M., (2002). Quantitative Use of Seismic Attributes for Reservoir Characterization. CSEG Recorder, pp. 14 – 25

Corridor F., Shaw J.H. and Bilotti F., (2005). Structural styles in the deep-water fold and thrust belts of the Niger delta. AAPG Bulletin, 89, 753-780.

Davarpanah M. and Akhlaghi J., (2017). 3D seismic interpretation and structural analysis of Z Field, eastern Persian Gulf. Article in the Leading Edge 2017.

Doust, H. and Omatsola, E. (1990) Niger-Delta. In: Edwards, J.D. and Santogrossi, P.A., Eds., Divergent/Passive Margin Basins, AAPG Memoir 48, American Association of Petroleum Geologists, Tulsa, 239-248.

Ebun D.O (2017). Three dimensional seismic, well log and structural analysis of Igbobi Field, offshore, Niger delta. PET Coal, 59(5), page 620-640.

Edwin A.N.,Agyingyi C.M., Nton M.E. and Oladunjoye M.A., (2018). Seismic Stratigraphic and Petrophysical Characterization of Reservoirs of the Agbada Formation in the Vicinity of 'Well M', Offshore Eastern Niger Delta Basin, Nigeria, Journal of Geology & Geophysics**.**

Ejedavwe J., Fatumbi A., Ladipo K. and Stone K., (2002). Pan-Nigeria exploration well look-back (post-drill well analysis). Shell Petroleum Development Company of Nigeria Exploration Report.

Etuk N.O., Aka M.U., Agbasi O.E. and Ibuot J.C., (2020). Evaluation of seismic attributes for reservoir characterization over Edi field, Niger delta, Nigeria using 3d seismic data, International Journal of Advanced Geosciences, 8 (2) 168-172.

Fajana A.O., Ayuk M.A., Enikanselu P.A. and Oyebamiji A.R., (2018). Seismic interpretation and petrophysical analysis for hydrocarbon resource evaluation of 'Pennay' field, Niger Delta. Journal of Petroleum Exploration and Production Technology.

Fatoke O.A.,(2010). Sequence Stratigraphy of the Pliocene-Pleistocene strata and shelf-margin Deltas of the Eastern Niger Delta, Nigeria.

Helander D.P. (1983). Fundamentals of formation evaluation, OGCI publications.

Herrmann F. and Gorman G., (2017). Rapid development of seismic imaging applications using symbolic mathematics.

Jackson U.P., Ayodele Moses C.A., (2018). Reservoir studies and paleoenvironmental studies of the Fagba sand, 'FAGBA' Field, Niger delta, Nigeria, International Journal of Research In Earth & Environmental Sciences, Vol. 11. No.1 ISSN 2311-2484.

Kukreja N., Lange M., Louboutin M., Luporini F., Hueckelheim J., Witte P., Yount C.,

Lutgens F.K., Tarbuck E.J. and Tasa D., (2012). Essentials of geology, 11th edition, Boston: Prentice Hall, page 32.

Marfurt, K., (2005). 3D Seismic Attributes for Prospect Identification and Reservoir Characterization.

Nyeneime O. E., Mfoniso U. A., Okechukwu E. A. and Johnson C. I., (2020). Evaluation of seismic attributes for reservoir characterization over Edi field, Niger delta, Nigeria using 3D Seismic Data, International Journal of Advanced Geosciences, 8 (2) (2020) 168-172.

Obaje S.O. and Okosun E.A., (2013). Paleoenvironmental Interpretation of Tomboy Field, Offshore Western Niger Delta, Nigeria, International Journal of Science and Technology Volume 2 No. 9.

Okeke H.C., Okoro A.U., Ezediegwu P.C., Chinwuko A.I., Onuigbo E.N. and Omeokachie A.I., (2018). Evaluation of hydrocarbon prospect of Tomboy CFielcd offshore Niger delta Nigeria, Journal of Basic Physical Research Vol.8, No.2 pp. 65- 78.

Olatunbosun L.G. (2015). 3D Seismic Reflection Data Analysis in Part of Niger-Delta, Environmental and Ecology Research 3(6): 178-184.

Ologe O., Buraimo O.A., Bankole S.A., (2013). 3D Seismic structural interpretation of a part of Aloo-Field, southwestern Niger Delta, Nigeria, IOSR Journal of Applied Geology and Geophysics.

Onayemi J. and Oladele S., (2017). Reconstruction of the Subsurface Depositional History of Onshore Niger Delta Basin, Search and Discovery Article.

Opara A.I., Anyiam U.O. and Nduka A.V.,(2011). 3D Seismic Interpretation and Structural Analysis of Ossu Oil Field, Northern Depobelt, Onshore Niger Delta, Nigeria.

Reynolds J.W. (2011), "An introduction to Applied and Environmental Geophysics", Second Edition, Page 217.

Rider M. (2002). The geological interpretation of well logs, 2nd Edition, Page 226-229

Saeland G.T. and Simpson G.S., (1982). Interpretation of 3D data in delineating a sub-unconformity trap in Block 34/10, Norwegian North sea, American association of petroleum geologists, Tulsa, pages 217-236.

Satti I.A., Deva Ghosh and Wan Yusoff W.I., (2014). Integrated Seismic Interpretation, Offshore Peninsular Malaysia, Research gate conference paper January 2014.

Sheriff, R. E., (1980). Seismic Stratigraphy. International Human Resources Development Corporation (IHRDC), Boston, page 227.

Short K.C., Stauble A.J.,(1967). Outline of Geology of Niger Delta, AAPG Bulletin 51(5): 761-779.

Tuttle M.L.W, Brownfield M.E., Charpentier R.R., (1999)[a]. Tertiary Niger Delta (Akata-Agbada) Petroleum System, Niger Delta Province, Nigeria, Cameroon and Equatorial Guinea, Africa.

Tuttle M.L.W, Brownfield M.E., Charpentier R.R., (1999)[b]. The Niger Delta Petroleum System: Niger Delta province, Nigeria, Cameroon, and Equatorial Guinea, Africa.